The effects of microwave irradiation on kimberlite and associated rocks: Basis for the development of microwave-assisted rock breakage technology

by:

Samir M. Deyab

Department of Mining and Materials Engineering

McGill University, Montreal, Quebec, Canada

September 2022

A Thesis Submitted to McGill University in Partial Fulfillment of the Requirement for the Degree of Doctor of Philosophy

Abstract

Finding an efficient non-explosive rock breakage method is an ongoing challenge in mining and civil engineering applications and is required for hard rock underground excavation. The explosive/ blasting techniques employed over many years have caused numerous problems, including excessive noise, dust, pollution, vibrations, and potential damage to nearby structures. As the future of underground hard rock mining is continuous mining techniques, drill-and-blast have the disadvantage of time for the fumed gasses to be cleared. Continuous mechanical excavation in hard rocks has low production rates and high operating costs, and field trials have shown that the lifespan of the cutting tools is short, reducing the efficiency of the operation. New approaches are needed to consider safety, efficiency, and economics.

This thesis is part of an overall research project which has been ongoing for the past several years in the Geomechanics Laboratory at McGill University on the application of microwave irradiation to facilitate rock breakage for excavations and mineral processing. It tackles the problem of rock breaking by exploring how hard rocks might be preconditioned and weakened prior to impact by a mechanical excavator. This project investigates the effect of microwave irradiation on the mechanical strength of specific rock samples such as kimberlite, and associated rocks such as granite, limestone and basalt for comparison. Given the lack or limited knowledge on kimberlite as well as its effect under microwave irradiation.,different properties of these rock samples, such as dielectric properties, physical properties (i.e., mineral composition, rock quality designation, specific gravity, porosity, specific heat capacity and moisture content), abrasivity, were measured during the project to evaluate the heating behaviors, as well as mechanical properties of rocks subjected to microwave irradiation, were investigated. Mechanical strength tests were conducted to evaluate the effect of microwave irradiations on the strength of rock samples. The rock samples for the first time were treated

for 4–360s in a multi-mode and single-mode microwave cavity at power levels from 2 to 15 kW. Also, in this study, calorimetry is performed to measure and analyze heat absorption, and thermal images are studied to determine the temperature contour on the sample surface.

The unconfined compressive strength (UCS) and Brazilian tensile strength (BTS) were significantly reduced by microwave irradiation. The tests showed that Cerchar Abrasivity Index (CAI) was not affected by microwave irradiation. Furthermore, the Percentage of the change of Pulse sound velocity (PSV) increased with microwave power level and exposure time as a result of the microcracks within the samples. The mode I fracture toughness (K_{IC}) test results showed that K_{IC} decreases when exposure time increases and when the samples are cut prior to treatment. It was also observed in the study that energy absorption by the samples was more when the samples were close to the horn of the microwave. Microwave treatment is found to be a promising strategy that combines microwave irradiation and mechanical techniques. The aim of potentially implementing microwave-based methods is to facilitate continuous mining and to improve the production rate while reducing the costs of fracture.

Résumé

Trouver une méthode efficace et non explosive pour briser les roches est un défi permanent dans les applications minières et de génie civil et est nécessaire pour l'excavation souterraine de roches dures. Les techniques d'abattage à l'explosif utilisées depuis de nombreuses années ont causé de nombreux problèmes, notamment un bruit excessif, de la poussière, de la pollution, des vibrations et des dommages potentiels aux structures voisines. Comme l'avenir de l'exploitation souterraine des roches dures passe par des techniques d'exploitation en continu, le forage et le dynamitage présentent l'inconvénient de laisser le temps aux gaz fumigènes de s'évacuer. L'excavation mécanique continue dans les roches dures a des taux de production faibles et des coûts d'exploitation élevés, et les essais sur le terrain ont montré que la durée de vie des outils de coupe est courte, ce qui réduit l'efficacité de l'opération. De nouvelles approches sont nécessaires pour prendre en compte la sécurité, l'efficacité et l'économie.

Cette thèse fait partie d'un projet de recherche global qui se poursuit depuis plusieurs années au Laboratoire de géomécanique de l'Université McGill sur l'application de l'irradiation par micro-ondes pour faciliter le bris des roches pour les excavations et le traitement des minéraux. Ce projet s'attaque au problème de la rupture des roches en explorant comment les roches dures peuvent être préconditionnées et affaiblies avant l'impact d'une excavatrice mécanique. Ce projet étudie l'effet de l'irradiation par micro-ondes sur la résistance mécanique d'échantillons de roches spécifiques, comme la kimberlite, et de roches associées, comme le granite, le calcaire et le basalte, à titre de comparaison. Étant donné le manque ou la limitation des connaissances sur la kimberlite ainsi que sur son effet sous irradiation par micro-ondes, différentes propriétés de ces échantillons de roche, telles que les propriétés diélectriques, les propriétés physiques (c'est-à-dire la composition minérale, la désignation de la qualité de la

roche, la gravité spécifique, la porosité, la capacité thermique spécifique et la teneur en humidité), l'abrasivité, ont été mesurées au cours du projet pour évaluer les comportements de chauffage, ainsi que les propriétés mécaniques des roches soumises à l'irradiation par micro-ondes. Des tests de résistance mécanique ont été effectués pour évaluer l'effet des irradiations par micro-ondes sur la résistance des échantillons de roche. Les échantillons de roche ont été traités pour la première fois pendant 4-360s dans une cavité micro-ondes multimode et monomode à des niveaux de puissance de 2 à 15 kW. De plus, dans cette étude, une calorimétrie est effectuée pour mesurer et analyser l'absorption de chaleur, et des images thermiques sont étudiées pour déterminer le contour de la température à la surface de l'échantillon.

La résistance à la compression non confinée (UCS) et la résistance à la traction brésilienne (BTS) ont été considérablement réduites par l'irradiation aux micro-ondes. Les tests ont montré que l'indice d'abrasivité du Cerchar (CAI) n'était pas affecté par l'irradiation aux micro-ondes. En outre, le pourcentage de changement de la vitesse du son pulsé (PSV) a augmenté avec le niveau de puissance des micro-ondes et le temps d'exposition, en raison des microfissures présentes dans les échantillons. Les résultats de l'essai de ténacité à la rupture en mode I (KIC) ont montré que la KIC diminue lorsque le temps d'exposition augmente et lorsque les échantillons sont coupés avant le traitement. Il a également été observé dans l'étude que l'absorption d'énergie par les échantillons était plus importante lorsque les échantillons étaient proches de la corne des micro-ondes. Le traitement par micro-ondes s'avère être une stratégie prometteuse qui combine l'irradiation par micro-ondes et les techniques mécaniques. L'objectif de la mise en œuvre éventuelle de méthodes basées sur les micro-ondes est de faciliter l'exploitation minière continue et d'améliorer le taux de production tout en réduisant les coûts de fracture.

Acknowledgments

Contribution to Original Knowledge

This thesis considers the previous research work made in the field of impacts of single-mode and multi-mode microwave irradiation on various rock types with several experimental tests and by different rock characterization methods. In addition, and for the first time, this thesis highlights a comprehensive investigation of the physical and mechanical properties of Kimberlite and the effects of microwave irradiation on Canadian Kimberlites and their associated rocks to determine how and what extent microwave irradiation impacts their mechanical properties without affecting the integrity of the enclosed diamonds during the process. Important physical properties, mineral composition and dielectric properties of the kimberlite rock samples were measured. Moreover, for the first time, the overall energy efficiency was investigated to evaluate the energy efficiency of microwave-assisted rock fragmentation. A calorimeter was used to determine the exact amount of energy absorbed by the samples. As the calorimetric study of microwave-treated samples enhances the precision of

the energy analysis by taking all of the losses into account, this method was employed to portray a better picture of how microwave energy is converted into heat within the material. An advantage of the calorimetric method used in the present thesis is that it enables us to precisely define the ramp-up time which has been commonly neglected by the majority of research in the literature. Having developed suitable (calorimetric) tools, new parameters were introduced by our research team at McGill University in collaboration with the University of British Columbia which is called "Heat over Microwave Efficiency (HOME)". By definition, HOME is defined as the ratio of heat absorbed to microwave energy. The other parameter was defined as Weakening over Microwave Energy (WOME), as a novel index. In definition, WOME is % of strength reduction achieved per microwave energy input(kWhr/t).

Contribution of Authors

In accordance with the guidelines on the traditional monograph style thesis preparation provided by the office of Graduate and Postdoctoral Studies (GPS) at McGill University, an overview of my contributions and the help of Prof. Hassani, Dr. Mehrdad Kermani and Dr. Hamed Rafezi is provided as
follows.

I, Samir M deyab, am the author of all the chapters presented in this dissertation. I took the lead in

- Preparing the samples in the laboratory

- Conducting the experimental work in the laboratory

- Conducting formal analysis and data curation; and

- Writing all chapters of this dissertation

This work benefited from the invaluable support of Prof. Ferri Hassani (Thesis supervisor), Dr. Mehrdad Kermani and Dr. Hamed Rafezi

Prof. Ferri Hassani supported me in formulating the research problem for my thesis, supervised the research, acquired the funding, administered the project and assisted with the review and editing of all the chapters in this dissertation.

For chapter 3, Dr. Mehrdad Kermani helped me in conducting the UCS test after microwave treatment. and

For chapter 4, Dr. Hamed Rafezi helped me in reviewing the K_{IC} results of kimberlite rocks.

List of publications

- Deyab, S.M., Rafezi, H., Hassani, F., Kermani, M., Sasmito, A.P. Experimental investigation on the effects of microwave irradiation on kimberlite and granite rocks. Journal of Rock Mechanics and Geotechnical Engineering 2021, 13(2); 267-274.

- Deyab, S.M., Rafezi, H., Hassani, F., Sasmito, A.P., Kermani, M. The Effect of Microwave Irradiation on the Mechanical Properties of Kimberlite and Limestone. Selçuk-Teknik Dergisi. 2020 Dec 22;19(4); 97-109.

- Rafezi, H., Deyab, S.M., Hassani, F., Ghoreishi-Madiseh, S. A. A comparative study of the cooling-rate effect on rock strength reduction after microwave irradiation. Experimental Results 2020,1.

- Hassani, F., Rafezi, H., Deyab, S.M., A Review of Explosive-Free Rock Breakage (EFRB) Technologies in Mining Industry. Selçuk-Teknik Dergisi. 2020 Dec 22;19(4):84-96.

Statement of originality

I declare that the texts and the work presented in my thesis are original and that there are no sources other than those mentioned in the texts and the references have been used in creating them.

Table of contents

List of Figures

List of Tables

Nomenclature

α	Attenuation coefficient (unitless)
γ	Is the fracture surface energy (J/m^2)
δ	Distance from the horn antenna (mm)
δ_c	Unconfined compressive strength (MPa)
δ_f	Is the stress at fracture (MN/m^2)
Δt	Exposure time in the microwave (s)
ε	Complex permittivity (unitless)
ε_r	Complex relative permittivity (unitless)
ε_0	Dielectric permittivity constant of a vacuum (8.86×10^{-12} F/m)
ε'	Dielectric constant (real part of complex permittivity) (unitless)
ε''	Loss factor (imaginary part of complex permittivity) (unitless)
f	Frequency of electromagnetic wave (Hz)
θ	Angle of disc cutter edge (°)
λ_o	Wavelength (cm)
μ	Complex permeability (unitless)
μ_0	Magnetic permeability of a vacuum ($4\pi \times 10^{-7}$ H/m)
μ'	Real part of complex permeability (unitless)
μ''	Imaginary part of complex magnetic permeability (unitless)
ρ	Density (kg/m^3)
σ	Applied stress (MPa)
σ_{BTS}	Brazilian tensile strength (MPa)
σ_{PLT}	Point load strength (MPa)
σ_{UCS}	Unconfined compressive strength (MPa)
ω	Angular frequency ($2\pi f$)

Ψ	Is the Auxiliary angle parameter(unitless)
a	Notch length (mm)
a	Half-length of a crack (m)
A	Unit area (mm^2)
B	Magnetic field (Tesla)
B	Disc thickness (mm)
BTS	Brazilian tensile strength (MPa)
c	Critical (peak) value at failure (unitless)
C	Constant (unitless)
CAI	CERCHAR Abrasivity Index (unitless)
$C_{p,w}$	Specific heat capacity of water (J/kg/°C)
$C_{p,r}$	Specific heat capacity of rock sample (J/Kg/°C)
d	Disc cutter diameter (m)
D	Sample diameter (mm)
D_p	Penetration depth (m)
e	Euler's number = 2.72
E	Electric field (V/m)
E	Young's modulus of the material (N/m^2)
$Erms$	Root mean square of the electric field (v/m)
F	Maximum load (kN)
F	Normal load applied to the disc cutter (N)
G	Energy release rate (J/m^2)
G_C	Critical value (J/m^2)
HOME	Heat over microwave efficiency (%)
J	Is the electric current density (A/m^2)

K	Stress intensity factor (MPa m$^{-0.5}$)
K_{IC}	Stress intensity factor of Mode I fracture toughness (MPa m$^{-0.5}$)
K_{IIC}	Stress intensity factor of Mode II fracture toughness (MPa m$^{-0.5}$)
K_{IIIC}	Stress intensity factor of Mode III fracture toughness (MPa m$^{-0.5}$)
t	Sample thickness (mm)
L	Distance that a disc cutter can roll on hard rock in (m)
m_r	Rock sample mass (kg)
m_w	Water mass in the calorimeter (kg)
P_d	Power density of a unit volume (W/m^3)
P	Applied load (N)
P_{max}	Maximum load observed at failure (kN)
P_{in}	Microwave power input (W)
P_{Rev}	Penetration per revolution (m/$_{Rev}$)
Q_r	Heat absorbed by the rock sample (kJ)
Q_w	Heat absorbed by the water (kJ)
R	Radius (mm)
s	Span between the supports (mm)
T_{eq}	Temperature read by the calorimeter (°C)
$T_{i.r}$	Initial temperature of rock sample before microwave treatment (°C)
T_r	Final temperature of rock sample after microwave exposure (°C)
T_w	Initial temperature of water prior to calorimetry (°C)
tanδ	Loss tangent (unitless)
UCS	Unconfined compressive strength
w	Thickness of disc cutter edge (m)
WOME	Weakening over microwave energy (%/kWh/t)

x	Is the disc cutter penetration depth (m)
Y'	Dimensionless stress intensity factor
β	Is the dimensionless geometry factor

Chapter 1   Introduction

1.1 Future mining trends

The general trend in future mining is a surge in automation, requiring fewer manual laborers and more experts (e.g., engineers) to optimize maintenance planning and environmental control. These future experts will need to cover the entire value chain, which means they will need to be able to constantly interact with each other, forming a virtual control room. Furthermore, as automation becomes more deeply entrenched in the mining industry, the mining processes themselves will become more uniform across different mines. This will enable the experts to deal with more than one mine simultaneously (Bäckblom et al.,2010).

Many mining companies are looking to achieve continuous mining, where subterranean environments require a process that is continuous mining instead of the current strategy, which is a batch process that uses blasting and drilling. Lean production is based on continuous mining and simplified automation using reliable equipment and is therefore unrealizable in the current mining environment. Even so, continuous mechanical excavation would improve the production output of companies like Boliden, which currently employs the "cut and fill" mining method. Similarly, LKAB, which employs "sub-level caving" mining, will like to rely on the drill-and-blast ore production approach for the short-term future, though future development work could use mechanical excavation to avoid human exposure in production areas. Furthermore, production could be automated or remote-controlled, with ground support in entry zones and other areas of the infrastructure remaining strong and ductile in order to deal with dynamic loads and deformations. For non-entry zones, ground support would be used mainly for equipment protection. The support could be both reusable and self-propelled, like in long-wall mining strategies employed for coal mining. The Future Mine's main features are presented below (Bäckblom et al.,2010).

1. **Central Control Room (CCR).** The CCR gathers information online from various sources, such as machinery and workers. The constant flow of information from all areas of the work site enables the entire operation to be controlled and appropriately fine-tuned from a single location, whether onsite or remotely. This includes controlling and fine-tuning every aspect of production, from characterizing the resources to finalizing the end product. Cameras (e.g., wearable ones) and sensors enable a constant stream of images to be received virtually as the action occurs, allowing for further control, monitoring, and fine-tuning of production.

2. **No human presence in the production areas.** The work processes are automated and remotely controlled. Robots provide the necessary preventive maintenance for equipment as well as for special circumstances such as safe retrieval operations. Robot maintenance and equipment repair can be done in underground vaults. Diesel is mass-banned underground, so the equipment is powered by electricity.

3. **Continuous mechanical excavation.** Lean mining and automation require a continuous work flow. Hence, Future Mine is characterized as a continuous non-stop process, including operations that handle hard rocks. Continuous excavation requires continuous onsite preventative maintenance.

4. **Pre-concentration.** In order to reduce the amount of energy needed during the haulage and transport stages, the barren rock should be separated when still underground. This will also mitigate any possible environmental impact on the site's surface.

5. **Resource characterization: Mineralogy.** The Future Mine uses systems for product control (geometallurgy) that will maximize the mined rock's value.

6. **Resource characterization: Structural control.** The Future Mine uses systems that boost process control by describing the structure and other features of the rock.

7. Final product. The Future Mine is sustainable, so the waste rock is converted into a product. Also, the metal is manufactured at the mine site to reduce transportation requirements (Bäckblom et al.,2010). Figure 1 highlights the important features for the future mine
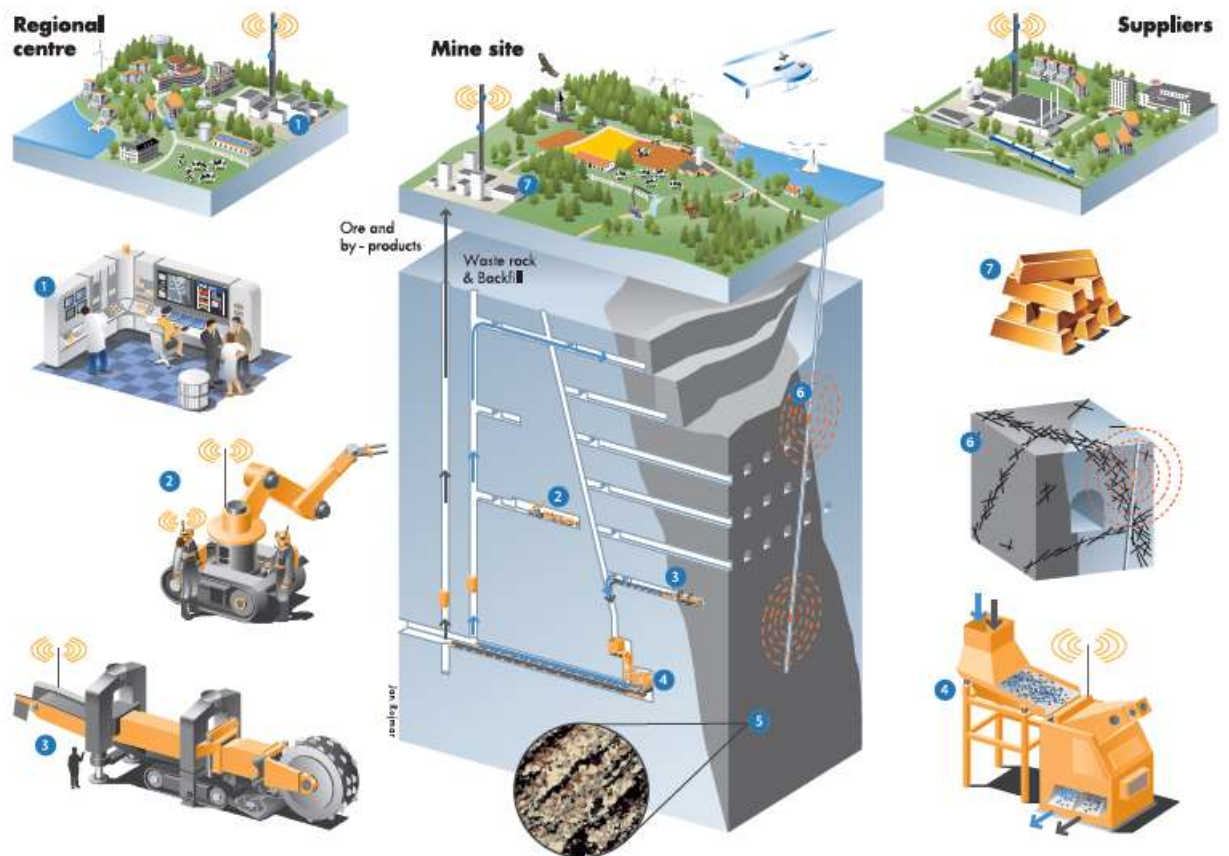
Figure 1. Important features of the underground Mine of the Future (Bäckblom et al.,2010).

1.2 Continuous mining excavation

The future of the mining industry needs to be lean, green and safe. To remain a crucial supplier of modern society's need for minerals and metals, the mining process needs to adopt green technology and implement innovative organizational processes.

Because of the steady depletion of high-grade ore deposits that are found either on or near the surface, the latest advances in exploration and mining strategies are focusing on techniques for deeper mining excavations that are not only sustainable but also continuous and automated. Research indicates that the best way to improve mine productivity is to implement processes that are continuous mining (Womack and Jones, 1997).

One of the main challenges confronting continuous mechanical operation in hard rocks is rock fragmentation, which faces numerous challenges including the problems of the mechanical cutting tools (Rostami, 2011).

Rock fragmentation is a two-step process: first, the rock must be fractured, which weakens it, then it must be physically broken into pieces. In an underground excavation, rock fragmentation can be achieved by blasting with explosives or using continuous excavation machinery. In hard rock applications, the latter method is associated with high equipment wear rates and low penetration rates, as well as high operating costs. To address this limitation, various thermal and non-thermal methods have been proposed to weaken the rock prior to excavation, including laser, water jet, torching, expanding cement, electric pulse, ultrasonic, and microwave irradiation. These techniques have been addressed in an extensive literature review by the McGill Geomechanics Group headed by professor Hassani with collaboration from The South African Council for Scientific and Industrial Research, The Colorado School of Mines, Natural Resources Canada, and CANMET Mining and Mineral Sciences Laboratories explosive-free rock breakage (EFRB) report (Hassani, 2010a). For example,

lasers have mostly been limited to tightly controlled lab drilling tests in an attempt to find the best type and strength of the laser. Lasering essentially melts and vaporizes the rock material, which means that any application of lasering in a mining site would have to be done under strict safety rules. Fluid-based high-pressure jets can also be used in the breaking down of rock. However, this method has as yet only shown limited effectiveness with hard rock. Electrical technologies, such as pulse blasting, have been shown to be highly effective on broken material. These methods, however, remain in the very early developmental stage, with only small-scale applications performed thus far, and in very controlled settings. While pulse blasting in particular has been performed with enormous success, the technology is yet too costly (equipment and power consumption) to make it feasible for practical use on a large scale in the mining industry. Therefore, in the (EFRB) report (Hassani, 2010a), it was concluded that microwave irradiation appears to have the potential to reduce hard rock strength prior to impact by machine excavators.

This is mainly due to:

- Microwave irradiation heats materials based on their dielectric properties; thus, energy is not wasted heating the entire host rock.

- Transfers energy (not heat) rapidly and indirectly (without contact).

- Is conducive to a high level of automation;

- Can be quickly started and stopped; and

- Is safe when appropriate precautions are taken.

Microwaves are a type of electromagnetic (EM) wave. Whereas EM waves were discovered in the mid-1800s, it was not until 1945 that the application of microwaves for heating was developed. Beginning in the 1990s, applications of microwave technology to mining excavation and mineral processing were studied. Microwave irradiation heats brittle material based on the principle of orientation-polarization. Rock is a heterogeneous material comprising

several mineral components with differing physical and electrical properties. The mineral components receive inductive heat and therefore expand at different rates. Under microwave irradiation, cyclical expansions and contractions of minerals create cracks between grain boundaries. The degree to which a rock sample is weakened by microwave treatment depends on the crack density as well as the electrical properties of the constituent minerals.

Continuous mining is the goal of future underground hard rock mining. To achieve this, various technologies are being investigated. Microwave irradiation is a promising technique to precondition hard rocks to enhance the performance and lower the energy requirements of continuous mining machinery (tunnel boring machines or new hard rock excavators).

DeBeers Group is an international corporation (Part of Anglo American group) that specializes in diamond mining and is looking for a way to replace the explosives method that is commonly used to break the rocks, especially kimberlite rocks which host diamonds. In addition, the Group is looking to achieve continuous mining in their mines in the future and to ensure the integrity of the enclosed diamonds during the process. A major testing program was conducted for DeBeers Canada Inc as part of a research program on the effect of microwave irradiation on rocks being conducted in the Department of Mining and Materials Engineering at McGill University, and as a result of the limited amount of works reported on kimberlite rocks, will be the main focus of this research in addition to granite, limestone as well as basalt samples. In this research and in collaboration with the DeBeers group, kimberlite, granite and limestone samples were obtained from Victor mine in northern Ontario and Gahcho Kue mine in the Northwest Territories of Canada to investigate how microwave irradiation affects mechanical strength, physical properties (i.e., mineral composition, rock quality designation (RQD), specific gravity, porosity, and specific heat capacity), abrasivity, and microcrack formation in kimberlite and associated rocks such as granite, limestone, as well as basalt rock samples as a

comparison. More than 2000 tests were carried out on untreated and treated samples, which included mechanical and physical tests.

The goal is to contribute to increasing production efficiency and improving the performance of continuous mining operations by evaluating and lowering the bit/disc wear of the excavators and increasing the penetration rate. Additionally, microwave irradiation of hard rock could improve the efficiency of comminution (crushing and grinding processes) during mineral processing and heat the ore body to differentiate waste from ore for sorting purposes. The parameters investigated in this research work will also contribute to numerical modeling and simulation which are being investigated and developed in parallel as well as equipment design.

1.3 Mechanical rock breakage

Mechanical rock breakage equipment such as tunnel boring and raise boring machines, road headers, continuous miners, and longwall drum shearers have been developed to break rocks with the aim of boosting productivity while reducing costs (Hassani, 2010a; Wijk, 1992). The application of this equipment faces significant challenges when operating in abrasive and hard rocks, including high wear rates for cutting tools, high costs of tool replacement, and low productivity rates (Rostami, 2011). Tunnel boring machines are used for a wide variety of soil and rock types, and in mine drift construction, they have the advantages of high safety and minimal need for support (Rostami, 2011; Zheng et al., 2016). Raise boring machines can be used to excavate vertical, horizontal, and inclined shafts, but they are limited by the length and the size of the excavation, similar to the shaft drilling machine. Road headers are used to excavate tunnels and mine entries and can be one of two types: transverse (ripping) and axial in-line (milling). Their production rates range from 10 to 20 t/h. Continuous miners are commonly used in coal mines. Their cutter heads are typically 3–4 m long, their diameter is between 0.8 and 1.4 m, and their production rates are typically 1,000 t/h. Longwall drum

shearers are used in more than 50% of coal mines in the United States. They have a diameter of 0.8 to more than 3 m and operate from 1.5 to 6 m high. The typical productivity rates of longwall drum shearers are 5,000 t/h.

1.4 Microwave-assisted rock breakage

The application of microwaves to rock excavation grew out of earlier experiments using high-definition radar for the same purpose. Researchers have explored microwaves at frequencies ranging from 500 MHz to 100 GHz and have shown that microwave treatment is a promising explosive-free technology to preweaken and induce microcracks within rocks/ores. In recent years, researchers have studied the application of microwave-assisted rock breakage in drilling (patented by McGill University) and tunnel boring into hard rocks such as basalt, quartz, and granite to reduce bit and cutter wear. Furthermore, numerous studies have investigated how microwave irradiation can be applied to mineral comminution because it induces microcrack formation, which renders the rock more susceptible to crushing and grinding to reduce particle size and liberate minerals during separation. A schematic illustration of the main idea of a microwave-assisted rock pre-conditioning system prior to breakage by mechanical techniques, (e. g. road headers, continuous miner, and TBMs) is drawn in Figure 2
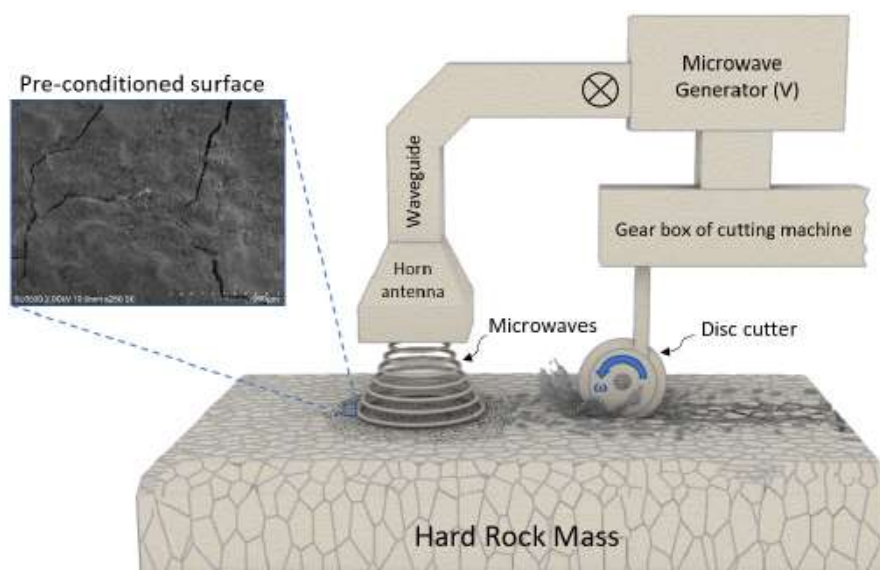
Figure 2. A schematic illustration of the main idea of a microwave-assisted rock pre-conditioning system prior to breakage by a disc cutter (Teimoori, 2021)

Therefore, This research is investigating the most important mechanical properties of the kimberlite, and associated rocks by conducting **UCS**, **BTS**, and **CAI** tests. These tests are popular methods to quantify the rock's mechanical strength and they are an important predictor of TBM performance.

More details about these tests are explained in sections (3.6.1, 3.6.2 and 3.6.3)

1.5 Environmental impact and the cost

Rock fragmentation can be achieved by blasting with explosive materials or using continuous excavation machinery. The significant challenges with the explosives include noise, vibration, pollution, and potential issues such as damage to nearby structures, which considerably affect the environment (Natanzi and Laefer 2014). Thus, there has been significant industrial interest in replacing conventional methods of rock breakage with novel systems to achieve explosive-free rock breakage operations for continuous mining (Hassani 2010a; Murray et al., 1994; Singh and Singh, 2005). These new systems are expected to be environmentally friendly because of their less violent nature and to enhance levels of safety and productivity (Singh, 1998). (EFRB) techniques have been discussed in detail in (section 2.1.2). Consequently, in the (EFRB) report (Hassani, 2010a), it was concluded that electromagnetic induction (microwaves) have been introduced for rock pre-conditioning in recent decades to reduce the rock strength prior to impact by machine excavators. This facilitates the simultaneous and continuous performance of all rock excavation operations and improves the production rate while reducing costs. One of the main issues with the microwave technique is the amount of energy used which is not practical at present and is more costly than explosives which are still the cheapest, especially in an open cut on the surface. In this research, microwave energy

efficiency analysis has been studied and investigated which can be improved in the future, especially since microwave technology is evolving, therefore in near future, these results can be achieved with much less energy consumption.

1.6 Research Objectives

The objectives of this thesis project are as follows:

- Evaluate the effect of microwave irradiation on the mechanical properties of kimberlite, granite, limestone and basalt.

- Analyze the influence of microwave irradiation on mechanical excavator performance.

- Analyze microwave energy absorption by rock samples; and

- A propose appropriate microwave system design with regards to power, exposure time, and distance from the antenna.

1.7 Methodology

The following tests were conducted on rock samples using multi- and single-mode cavities:

- Material characterization.

- Thermal analysis.

- Unconfined compressive strength (UCS).

- Brazilian tensile strength (BTS).

- CERCHAR (Centre d'E´tudes et des Recherches des Charbonnages de France) Abrasivity Index (CAI).

- Pulse sound velocity; and

- Mode I fracture toughness.

The following tests were conducted on single-mode cavity microwave systems:

- Efficiency analysis;

- Energy absorption analysis;

- Ramp-up time calculations;

- Analysis of the effect of distance from the horn antenna

- WOME analysis; and

- Analysis of quenching effect on rock strength reduction.

1.8 Thesis overview

This thesis is divided into five chapters.

Chapter 1 briefly describes mechanical and microwave-assisted rock breakage, the research objectives, and the methodology that will be applied in this research.

Chapter 2 is a comprehensive literature review of rock breakage techniques and the historical context of microwave application. It covers the principles of EM waves for heating and preconditioning rocks, the mechanism of heating polarization, factors affecting thermal absorption, and the effect of microwave on magnetic properties. It reviews applications of microwaves to rock breakage and mineral processing and presents experimental studies on microwave-assisted drilling and rock excavation systems and microwave heating modeling. The chapter concludes with a brief discussion on P- and S-wave measurements and explains fracture mechanics, including the mode of fracturing, Griffith's criterion, and Irwin's modification.

Chapter 3 provides information regarding the physio-mechanical and mineral composition of kimberlite. The dielectric properties of untreated kimberlite, granite and limestone are measured using the coaxial probe technique. This chapter describes how samples were prepared, their mechanical properties were measured, how they were irradiated using a multi-mode microwave and single-mode microwave, and how their surface temperature was measured using a thermal camera and infrared gun. Basalt samples were heated in a single-

mode microwave and calorimetry was applied to determine their energy absorption, conduct a "heat over microwave efficiency" or HOME analysis, calculate microwave ramp-up, and determine the optimal position of the sample relative to the microwave horn antenna. WOME was defined and analyzed for basalt samples. Finally, the quenching effect of rock strength reduction after microwave treatment was studied.

Chapter 4 presents the results and discussion of the work of the research related to thermal analysis, mechanical properties analysis, the optimal distance from the microwave horn antenna in the single-mode microwave, ramp-up time, HOME and WOME analysis, and quenching effect on rock strength reduction after microwave treatment.

Chapter 5 presents the main conclusions of this work and the future work.

Chapter 2 Literature Review

2.1 Rock breakage techniques

2.1.1 Methods using explosives (drilling and blasting)

Although traditional cost-effective approaches to underground and surface rock excavation still mainly revolve around blasting and drilling, the explosive energy unleashed by these methods is poorly applied: only ~20% of the energy is applied to rock fragmentation. Approximately 80% is lost as noise, air blast, and ground vibration. Ground vibration is known to damage surrounding areas. When those areas include man-made structures (e.g., railroads, bridges, dams, or buildings), costs can be incurred. Drilling and blasting can also have negative effects on the surrounding natural environment (Singh and Singh, 2005). Thus, the use of explosives has fallen out of favor due mainly to safety and environmental issues.

2.1.2 Explosive-free rock breakage techniques

Several explosive-free rock breakage methods are either in development or are currently used in the field. In conjunction with McGill University, CANMET Mining and Mineral Sciences Laboratories with Natural Resources Canada conducted a comprehensive review of a wide range of explosive-free rock breakage technologies. The Colorado School of Mines and the South African Council for Scientific and Industrial Research also contributed to the study (Hassani, 2010a). The review highlighted two mechanical systems. The impact ripper uses a hydraulically driven pointed hammer to generate fractures in the rock on impact. It is constructed as a longwall machine and operates continuously using a conveyor to transport the broken material. The radial-axial splitter uses tensile force via conventional boom drills to cause surface breakouts inside a borehole. Several field tests were conducted, but the superiority of traditional drill-and-blast productivity remained uncontested. The main issues

with the new technology centered on the extensive remobilizing time required on-site, which slowed production and raised costs (Bilgin et al., 2002; Willis and Ashworth, 2002).

2.1.2.1 Mechanical cutting systems

Numerous mechanical excavation technologies have been used in the past, are currently in use, or are in development through field testing or machine design improvements before being released to the market (Hassani, 2010a). Examples include the mobile miner, continuous miner, full-face excavator, disc boom miner, oscillating disc cutter, activated disc cutter, narrow reef miner, various types of "moles", mini-disc drum cutter head, and roadheader. For underground mining, the primary system currently in use is the tunnel boring machine, and for surface mining, the main excavator is the mechanical surface miner. Using these technologies enables continuous mining at a site, with the goal of boosting productivity while reducing costs. However, many of these technologies have been discontinued by the manufacturers (e.g., mobile miner, mini full-facer, disc boom miner and mini-mole), due to high cutting tool wear and lower-than-expected production rates (Hassani, 2010a; Wijk, 1992).

Selective mining is possible using mechanical excavators, lowering the need for hoisting and other rock transportation requirements. However, mechanical cutting is not efficient with harder rocks. Borehole-based technologies have a low advancement rate and frequently require thermal and water jet preconditioning (Hassani, 2010a; Hassani et al., 2016).

2.1.2.2 Lasers

Lasers have only been used in limited laboratory drilling tests, initially in the Soviet Union several decades ago, and subsequently in the United States, Japan, and Australia. Current research on lasers for rock cutting is being conducted in the United States at the Argonne National Laboratory (Hassani, 2010a). The disadvantage preventing their widespread use alone

or in combination with other explosive-free rock breakage technologies is that they can melt or even vaporize rock (Hassani, 2010a; Gahan, 2002).

A laser's efficiency is defined by its properties, including whether it is emitted in pulsed wave or continuous wave mode, maximum power, wavelength, and pulse width. These properties determine the interaction with the rock and the transferred energy level. Because most rocks have minimal reflectivity, they are easily penetrated by laser beams, which created focused, intense power zones. However, existing tests use beams on the scale of centimeters, which are impractical for mining and tunneling projects. Their potential application at a commercial scale is on a time horizon of several years (Hassani, 2010a; Jansen et al., 1991).

2.1.2.3 Fluid

High-velocity fluids (jets) have been used in many industries to cut and polish a variety of materials. Jet boring has been used since the 1970s to excavate coal, which is then hydro-hoisted to the surface (Edwards, 2004; Farmer and Attewell, 1965; Goodfellow, 1992; Hassani, 2010a). This approach is less effective for hard rock—especially when it is heterogeneous and features irregular formations and variable hardness—and specific energy requirements are high. Nonetheless, improvements in the configurations and materials of nozzles have boosted the efficacy of this method in rock breaking, especially when used as a preconditioning method in conjunction with mechanical rock cutters and drill bits (Crow, 1973, 1974; Hassani, 2010a).

Expansion fluids (e.g., cement or foam) can be injected into boreholes during large-scale hydrofracturing of rock masses. Despite being readily adaptable to traditional equipment and highly useful in boulder-breaking, this method is quite slow (Barker and Timmerman, 1981; Hassani, 2010a; Xiaohong et al., 2000). Large-scale hydro-mining large excavations are still quite rare worldwide.

In most underground mining operations, fluids are used to fragment large boulders that might otherwise obstruct ore passes and transport broken material via pipelines. In addition, jets are commonly used to remove loose and broken material from the mechanical cutting edge to decrease the likelihood that the bit/rock interface will become clogged. The fluid also cools the mechanical drill bit, lengthening its lifespan. High-velocity fluids are also used to widen existing haulages so that explosives are unnecessary. If the liquid is employed for pressurization, the air must be removed from pilot holes, in some cases limiting the method's application. Moreover, should rock breakage be incomplete, the pressure drop will lead to the loss of the hole (Babu and Krishnaiah, 2003; Hassani, 2010a; Hagan, 1992).

2.1.2.4 Thermal treatment

Thermal fragmentation via heating and cooling was used for thousands of years to fragment rock—long before the more energy-intensive explosive techniques became universally applied. Thermal heating of rock is based on bulk heating, whereby heat is transferred from the surface to the interior through conductivity. By comparison, microwave heating transfers heat from the interior to the surface, and surface temperatures increase with increasing microwave power and exposure time (Kahraman et al., 2020b).

Heat causes thermal stress that fractures the rock, while the rock particle expansion creates microcracks that result in fragmentation (Hassani, 2010a; Jansen et al., 1991). Techniques that use heat for rock breaking apply the heat indirectly or directly on (e.g., fire) or below the rock surface (e.g., electron beams). Surface heating causes chipping in spallable rocks and fracturing in non-spallable rocks. In subsurface heating using electron beams, first developed by Hassani (2010a), X-rays generate thermal stress and induce fracturing.

In recent decades, torches have been used to drill production holes at open-pit mining sites. Numerous field and mine production tests have shown that, while it is still not as effective as

drill-and-blast applications, thermal fragmentation can produce substantial rock spalling, making it especially useful when applied in combination with mechanical approaches to break down hard rocks and more competent rock masses (Council, 1994; Hassani, 2010a).

2.1.2.5 Electrical methods

Electrical technologies remain limited in terms of practical application to large-scale rock breaking. Pulse blasting has been successful in breaking extremely hard rock, but high energy consumption and specialized equipment make the technique very expensive (Hassani, 2010a). More recently, chemical explosives have been replaced by electrical blasting materials such as metal wiring to create a blasting method that is safer and more environmentally friendly. However, this approach is not yet widely applied and is being further studied (Hassani, 2010a). Plasma blasting technology has had some success, but it is expensive, the equipment has a short lifespan, and it is generally impractical compared to other rock-breaking methods. For instance, capacitors are quite costly, but they substantially boost the speed of mining processes. Hence, if improvements were made in capacitor technology, plasma blasting could be further developed and applied. Other techniques for breaking rocks using electricity are electrical pulse blasting and electrothermal rock breaking. Overall, however, these methods are still in the developmental phase (i.e., theoretical studies and small-scale equipment applications) and have had only limited application in commercial excavations (Hassani, 2010a; Bluhm et al., 2000).

2.1.2.6 Microwave irradiation

The response of a given rock to microwave irradiation depends on its mineral composition. Microwave energy heats rock from the inside out, which decreases rock strength because stress and microcracks are generated by varying rates of volumetric expansion of the minerals within the rock. The overall reduction in rock strength lowers the energy requirements for

17

fragmentation by mechanical machines such as tunnel boring machines (Hassani, 2010a; Scott, 2006; Lu et al., 2020) and mineral separation (crushing and grinding) in processing plants.

Microwave treatment has been used successfully in the laboratory to fragment rock (e.g., Hassani et al., 2016; Hassani, 2010a; Lu et al., 2020; Nekoovaght et al., 2014) and can be expanded to full-scale field application to weaken rocks prior to mechanical rock breakage in a continuous fashion. But the technique requires more development and testing to make it operationally practical in the challenging rock cutting environment (Gwarek and Celuch-Marcysiak, 2004; Hassani et al., 2008; Hassani, 2010a).

2.2 Historical context of microwave treatment

James C. Maxwell discovered EM waves approximately 150 years ago. He determined that electrical and magnetic fields can join to create EM waves, which propagate through space perpendicular to each other and at the speed of light (Figure 3). In the late 1880s, his theory was applied by Heinrich Hertz to prove the existence of radio waves. German scientist Ernst Eduard Wilhelm Kassner patented the apparatus to generate short EM waves (Wilhelm, 1937).
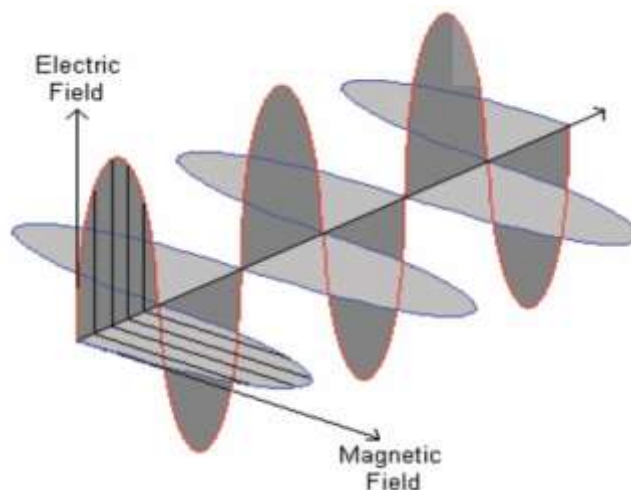
Figure 3. Propagation of electromagnetic waves (Scott, 2006).

During WWII, microwaves were used for telecommunication, such as radar detection. In 1946, American engineer Percy Spencer discovered the heating application of microwaves and designed the first microwave oven. This invention was subsequently developed for residential and commercial use worldwide (Osepchuk, 1984; Grundas, 2011). The first microwave heating applications in the food industry were roasting coffee beans and drying foods. Subsequent advancements in the manufacturing of magnetrons led to increased production of microwave ovens for cooking. Currently, microwave technology is applied to other fields such as navigation, medical science, power transmission, weather control, and heating and drying. Heating remains the most common domestic and industrial application of microwaves (Gupta and Leong, 2008).

2.3 EM waves

Microwaves are forms of EM radiation with wavelengths of 1 mm to 1 m and frequencies of 300 MHz to 300 GHz (Figure 4). Microwaves are divided into three bands:

1. Ultra-high frequency: 300 MHz to 3 GHz

2. Super high frequency: 3–30 GHz

3. Extremely high frequency: 30–300 GHz

The most common frequency used for microwave ovens, mineral processing, and telecommunications is 2.45 GHz (ultra-high frequency).
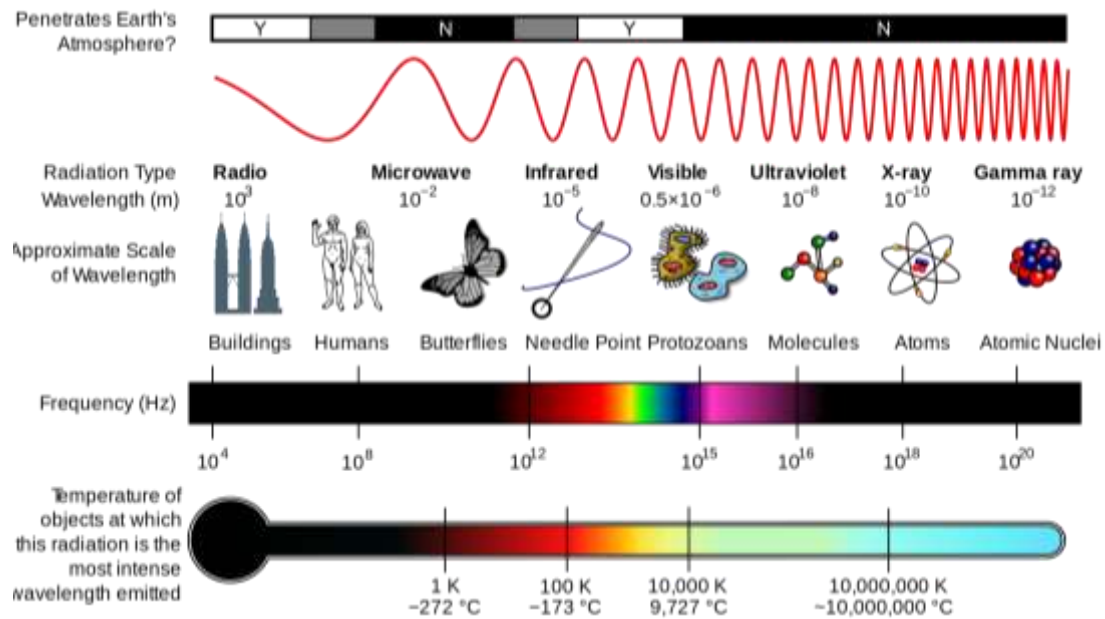
Figure 4.The electromagnetic spectrum(Zheng, 2017).

2.4 Mechanism of heating polarization

The heating of materials originates from the polarization of charges under an electric field (Metaxas and Meridith, 1983). Polarization can be:

- ionic in materials with ionic structures such as electrolyte solvents;

- dipolar in materials with a molecular structure such as water; or

- electronic and atomic.

The heating and drying of rocks originate mostly from electronic polarization (Von Hippel, 1954), whereby the center of the electron cloud (negative charge) is displaced relative to the nucleus (positive charge) of an atom in contact with an external electric field (Figure 5). A dipole moment is created (Von Hippel, 1954). In atomic polarization, electrons and the nucleus of each atom are shifted in opposite directions under the influence of an external electric field. Therefore, the electron cloud does not sit centrally around the nucleus.

Figure 5. Schematic diagram of electronic polarization(Von Hippel, 1954).

When a material with a molecular structure is exposed to microwave energy, dipole molecules begin to rotate due to attraction and repulsion forces from the positive and negative electrical poles (Figure 6 right), which generates heat. By comparison, in materials with an ionic or atomic structure, ions exhibit "back and forth displacement" under microwave irradiation, which generates heat (Figure 6 left). Microwaves heat "materials of low electrical conductivity by an applied high-frequency electric field (Meredith, 1998; Pickles 2008)."
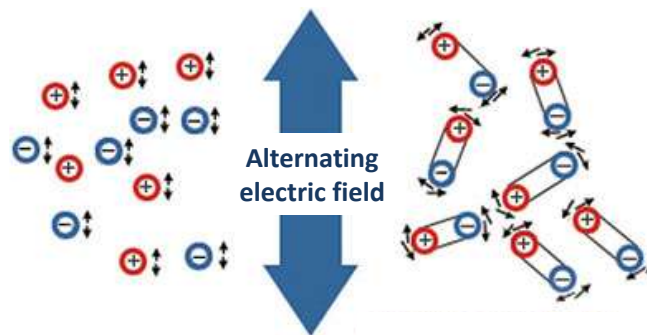
Figure 6. Ionic (left) and dipolar (right) polarization (Hassani, 2010a)

2.5 Microwave power density

The electric and magnetic field distribution in microwave oven cavities can be multi- or single-mode (Kingman et al., 2004a). As an EM wave propagates, nodes of energy (each known as a mode in which more energy is concentrated) are created by the constantly alternating wave. The distance between nodes is directly related to the wavelength of the standing wave. Waveguides always have two dimensions that are smaller than the wavelength, which causes the wave to travel in the third direction. Therefore, only one mode is generated. If the end of

the waveguide is closed, and a specimen is located at the energy node, a single-mode cavity is created. When two or three dimensions of a closed cavity are longer than one wavelength, more than one node of energy is created: this is called a multi-mode cavity. Multi-mode cavities are "mechanically simple, closed metal boxes (cavities), consisting of two dimensions of several wavelengths long which support many modes" (Kingman, 2009).

The factors that influence the heat generated in dielectric materials (the "load" in the microwave cavity) relate to the size, shape, and location of the load, as well as the microwave oven configuration (Kingman et al., 2004a). The power absorption by a dielectric material is expressed as a power density P_d in W/m^3 and is given by (equation 1; Metaxas and Meredith, 1983):

$$P_d = 2\pi f \varepsilon_0 \varepsilon'' \, Erms^2 + 2\pi f \mu_0 \mu'' \, Erms^2 \tag{1}$$

Where f is the frequency (Hz) of the EM wave; ε_0 is the dielectric permittivity constant of a vacuum (8.86×10^{-12} farads per meter or F/m); ε'' is the dielectric loss factor (imaginary part of complex permittivity) and represents the energy loss in materials through dissipative phenomena; $Erms$ (v/m) is the root mean square value of the electrical field inside the material; μ_0 is the magnetic permeability of a vacuum ($4\pi \times 10^{-7}$ H/m), and μ'' is the imaginary part of the complex magnetic permeability and represents the energy loss from materials under the impact of a magnetic field.

Since μ'' is equal to zero in nonmagnetic materials, the second part of the equation is not considered in the power density calculation. According to this equation, as the electrical field grows stronger, the heating rate increases. Therefore, using a single-mode cavity is one way to increase the heating rate since the electrical field can be concentrated on a small volume. The heating rate can be optimized by placing dielectric materials in a position where the electrical field is maximal (Kingman et al., 2004a).

The power density of the microwave system can be modified in several ways, such that multiple configurations can achieve the desired density and hence, the desired outcome in terms of lowering the grinding energy. For example, Kingman et al. (2004b) found that grinding energy reductions of 30% can be obtained using microwave energy inputs < 1 kWh/t.

2.6 Factors affecting thermal absorption

2.6.1 Power level, exposure time, and particle size

Materials exposed to microwave irradiation at higher power levels and longer times absorb more heat. Jones et al. (2005) showed that as power level increased, more heat was absorbed by minerals, resulting in better mineral liberation due to more thermal stress (Figure 7). On the other hand, decreasing the particle size limited heat absorption and resulted in less thermal damage between grain boundaries.
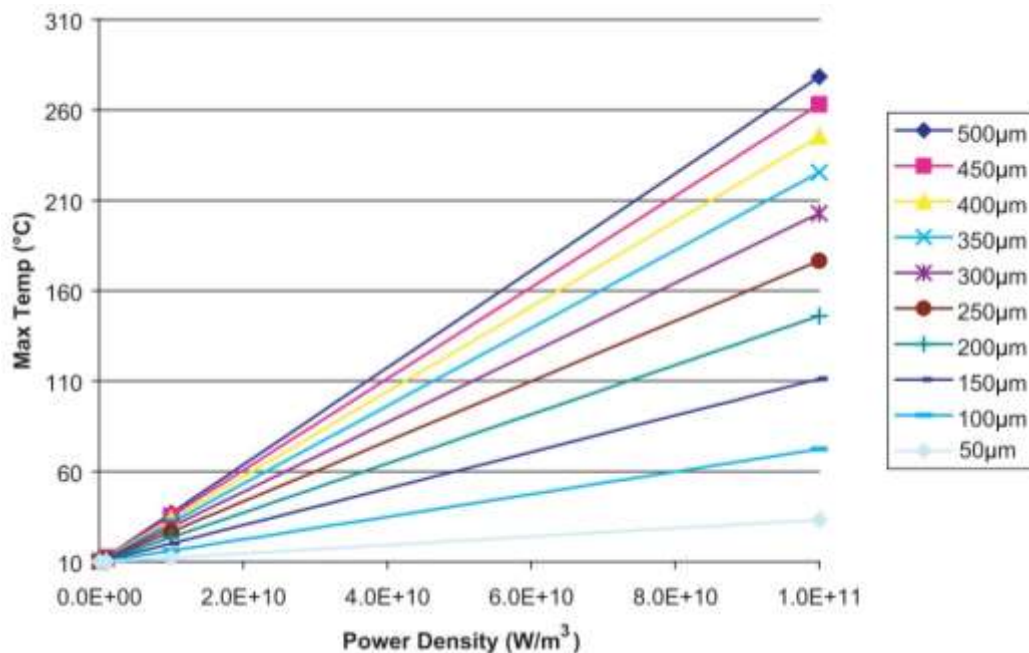
Figure 7. Maximum temperature versus power density for ten particle sizes (Jones et al., 2005).

Other studies have demonstrated that microwave treatment of rocks at high power for a short time can increase microcrack creation around particle boundaries, resulting in better breakage

and mineral liberation(Ali and Bradshaw, 2009; Ali and Bradshaw, 2011; Whittles et al., 2003). For example, microwave treatment in a multi-mode cavity at high power (15 kW) for 0.5 s significantly decreased rock strength (Kingman et al., 2004a).

2.6.2 Dielectric properties affecting microwave absorption

As noted above, materials absorb microwaves according to their dielectric and magnetic properties (Figure 8). Transparent materials (insulators) such as glass transmit microwaves without heating. Opaque materials (conductors) such as metals reflect microwaves and do not heat up. Dielectric materials (absorbers) such as rocks and minerals absorb microwaves and convert the absorbed energy into heat.
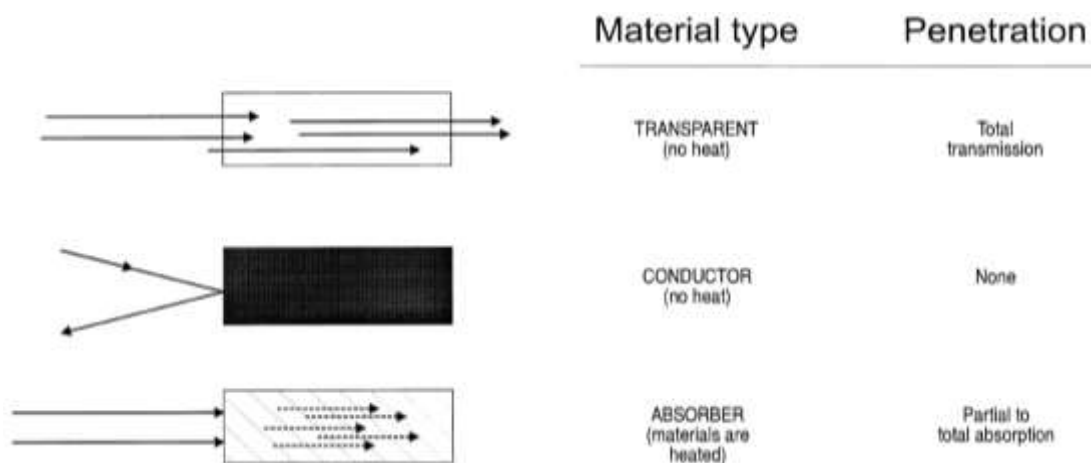
Figure 8. Material reactions to microwave irradiation (Haque, 1999).

Dielectric and magnetic properties are represented by the complex permittivity (ε; a measure of the capacitance or ability to store energy) and complex magnetic permeability (μ):

$$\varepsilon = \varepsilon' - i\varepsilon'' \tag{2}$$

$$\mu = \mu' - i\mu'' \tag{3}$$

Where ε' is the dielectric constant (real part of complex permittivity) and represents the polarization of materials in an electric field to store the energy; and μ' is the real part of complex

permeability and represents a material's reaction in a magnetic field. The complex relative permittivity (ε_r) is obtained from the relationship between ε and ε_0 (equation 4) and is expressed in F/m (Jones, 1964):

$$\varepsilon_r = \frac{\varepsilon}{\varepsilon_0} \tag{4}$$

The loss factor (ε'') and loss tangent (tanδ) are two important and related parameters to determine the ability of the material to absorb microwaves (equation 5). A material with a high ε'' relative to ε' (and therefore a high tanδ) is easily heated by microwaves. A material with a low ε'' relative to ε' (and therefore a low tanδ) is transparent to microwaves.

$$\tan\delta = \frac{\varepsilon''}{\varepsilon'} \tag{5}$$

2.6.3 Penetration depth

The penetration depth of EM waves is directly proportional to the EM wavelength and inversely proportional to the EM wave frequency (Jones, 1964). Maxwell's equations in the presence of linear media are (Griffiths, 1999):

$$\nabla \cdot E = \left(\frac{1}{\varepsilon}\right)\rho_f \qquad \text{(Gauss's law)} \tag{6}$$

$$\nabla \cdot B = 0 \qquad \text{(no name)} \tag{7}$$

$$\nabla \times E = -\frac{\partial B}{\partial t} \qquad \text{(Faraday's law)} \tag{8}$$

$$\nabla \times B = \mu_0 J + \mu_0 \epsilon_0 \frac{\partial E}{\partial t} \qquad \text{(Ampere's law)} \tag{9}$$

Where E is the electric field (V/m) and B (Tesla) is the magnetic field, J (A/m²) is the electric current density, ρ_f is the free charge, which nearly immediately flows to the surface for conducting materials. The free charge for insulators is strongly bound to molecules and atoms; therefore $\nabla \cdot E$ is 0 in equation 9 for insulators.

The wave amplitude decreases exponentially by a factor of 1/e (where e is Euler's number = 2.72) after a distance called the penetration depth (D_P), as given by:

$$D_P = \frac{1}{\alpha} = \frac{1}{2\omega} \sqrt{\frac{\frac{2}{\mu' \varepsilon'}}{1+\left(\frac{\varepsilon''}{\varepsilon'}\right)-1}} \qquad (10)$$

Where α is the attenuation coefficient determining the rate at which the EM wave amplitude diminishes inside the material, and ω is the angular frequency, calculated as $2\pi f$.

In most materials $\varepsilon'' << \varepsilon'$ therefore, equation 10 can be Taylor expanded and reduced to equation 11:

$$D_P = \frac{\lambda_o \sqrt{\varepsilon'}}{2\pi \varepsilon''} \qquad (11)$$

Where λ_o is the wavelength in a vacuum.

The penetration depth directly depends on the dielectric properties of each material. For example, conductors such as metals have a low complex permittivity (ε) and reflect EM waves; therefore, the penetration depth is very low. Dielectric materials with high complex permittivity absorb EM waves and penetration depth is high (Chandrasekaran et al., 2012; Hassani et al., 2016; Griffiths, 1999).

2.6.4 Other factors

Other factors that influence microwave absorption are the surface area and the location of the load in the microwave cavity. Barani et al. (2012) found that expanding the volume without increasing the surface area of the load had no effect on thermal absorption by iron ore samples, whereas maintaining a constant sample volume while increasing the surface area led to more heat absorption. These authors also demonstrated that the samples reached a maximum temperature at a specific distance from the microwave center.

2.7 Effect of microwaves on magnetic properties

Microwave treatment increased the magnetic properties of iron ore and enhanced magnetic separation by 98% (Barani et al., 2011; Omran et al., 2014). As the microwave power level and exposure time increased, the magnetic properties increased, plateaued, then declined. This phenomenon can be attributed to increasing temperature altering the paramagnetic part of iron ore (hematite) to a magnetic phase. After reaching the maximum point, any increase in temperature melted and deformed the hematite, which decreases the magnetic properties.

2.8 Health and safety protocols when using microwaves

Thermal damage to tissue and organs may occur from high power levels and long microwave exposure times. Therefore, appropriate personal protective equipment must be worn to prevent damage to organs from microwaves at the mine site. The U.S. Bureau of Microwave Radiation Safety Standard C95.1 (1966) set the maximum EM energy to be emitted to protect human health at 10 mW/cm^2 (Steneck et al., 1980).

2.9 Factors affecting rock weakening by microwaves

2.9.1 Rock characteristics

Factors that influence the effectiveness of microwave treatment include the mineralogy, porosity, density, and moisture content of the rock since they are the main factors that affect the degree of heating (Kahraman et al., 2020b). Differences in thermal expansion rates among minerals in the rock create fractures, facilitating breakage and reducing the energy associated with size reduction (Fitzgibbon and Veasey, 1990; Kumar et al., 2010). However, the energy needed for bulk heating is much higher than that needed for breakage (Ali and Bradshaw, 2010).

2.9.1.1 Dielectric properties

Under microwave irradiation, EM waves penetrate the rock. Dielectric minerals in the rock heat to high temperature because they possess high complex permittivity: EM waves are dissipated as heat. Transparent minerals do not readily heat because they possess a low complex permittivity: EM waves pass through them without generating heat (Sun et al., 2016). Kingman et al. (2000) determined that ores with consistent mineralogy and absorbent minerals in a transparent gangue were the most responsive ores to microwave treatment in terms of decreased requirements for grinding energy. On the other hand, ores featuring minute, lossy, finely disseminated particles across discrete elements exhibited the worst response. With the exception of zinc oxide, dark-colored compounds (e.g., Fe_2O_3) heat more quickly than light-colored compounds (e.g., Al_2O_3) (Table 1).

Table 1. Heating times and maximum temperatures for some metal oxides and sulfides exposed to 2.45 GHz microwaves (Ford and Pei, 1967)

Compound	Color	Heating time (min.)	Maximum temperature (°C)
MoS_2	Black	0.1	900
UO_2	Dark green	0.1	1100
Charcoal	Black	0.2	1000
Fe_3O_4	Black	0.5	500
CuO	Black	4	800
CuS	Dark blue	5	600
FeS	Black	6	800
Fe_2O_3	Red	6	1000
ZnO	White	4	1100
PbO	Yellow	13	900
Al_2O_3	White	24	1900
MgO	White	40	1300
CaO	White	40	200
MoO_3	Light green	46	750

Chen (1984) exposed more than 40 minerals to microwaves and demonstrated that most silicas, carbonates, sulfates, and some oxides and sulfides transmit microwave radiation. In contrast, most sulfides, arsenides, sulfosalts, sulfarsenides, and some metal oxides such as hematite and magnetite absorb microwave energy. These experiments also showed that mineral behavior under microwave radiation depends on the reactions of the individual components of the

mineral. For example, sphalerite containing iron—(Zn, Fe)S—absorbs more heat than pure sphalerite—ZnS—since iron is a good absorber of microwave radiation. Rocks consisting of metallic minerals absorb microwave irradiation (Kahraman et al., 2020b).

Ore minerals are strong EM absorbers, and gangue minerals are transparent to EM waves. Under microwave irradiation, differential or selective heating is created between the mineral grains and the surrounding transparent matrix (gangue). Thermal expansion of minerals causes tensile stress along mineral boundaries, resulting in microcracks that reduce rock strength. This in turn facilitates rock breakage and drilling, reduces bit wear, and decreases energy consumption during mineral processing (crushing and grinding) (Ali and Bradshaw, 2010; Jones et al., 2005; Walkiewicz et al., 1991). Microwave treatment of ores with consistent mineralogy and good absorbers in a transparent gangue resulted in the lowest grinding energy requirements, whereas treated ores featuring minute, finely disseminated lossy particles across discrete elements had the highest grinding energy requirements (Kingman et al., 2000). Zheng et al. (2020) proposed classifying minerals as low, medium, or high loss based on the magnitude of their loss factors after microwave treatment as a means to predict their response to microwave treatment.

2.9.1.2 Rock type

The rock mineral composition affects thermal properties such as heat capacity and conductivity, thermal diffusivity, and expansion. These factors influence the susceptibility of the rock to microwave-assisted breakage. For example, the susceptibility of limestone to microwave treatment appears to be related to the Fe_2O_3, MgO, and CaO content (Bilen, 2021). Limestone fragments easily when treated with microwave: when exposed to 900 W of microwave radiation for 5 min. in a multi-mode cavity, limestone samples disintegrated (Murová et al., 2000). Andesite rock samples respond differently to microwave irradiation:

samples melted completely (i.e., became amorphous), but did not change weight or chemical composition when subjected to 1350 W microwave irradiation for 10 min., followed by 2700 W for 30 min. (Znamenáčková et al., 2003). The BTS of the norite samples did not change during the first 10 s of microwave exposure, but was significantly reduced at exposure times of 65 and 120 s.

2.9.2.2.1 Basalt

Basalt appears to be very susceptible to microwave treatment. Nekoovaght (2009) found a 30% reduction in CAI and UCS and an 80% reduction in BTS of basalt treated in a multi-mode cavity at 0.8–3 kW power for 15, 60, and 240 s. When basalt samples were exposed for 6 min. to 750 W microwave power, spallation, chipping, and visible cracks formed, the UCS decreased from 118.2 to 78.5 MPa, and the point load index decreased from 5.62 to 3.73 MN/m^2 (Satish, 2005; Satish et al., 2006). The pulse sound velocity—a measure of the uniformity, number, and distribution of internal voids and cracks in rock samples—of basalt samples increased from 3500 to 5500 m/s after treatment in a multimode cavity with 3.2 kW microwave power for 2 min.; further, crack generation was initiated in the centers of samples where the internal temperature rose relative to the surface temperature (Hartlieb et al., 2012). Both transgranular and intergranular fractures result from microwave irradiation and are the main reasons basalt samples break (Yang et al., 2020). Yuan et al. (2020) established a novel theoretical model of the initial microcracks, which could be applied to hard rocks like basalt.

The power level and exposure time interact to affect the response of basalt samples to microwaves in a multimode cavity at a 2.45 GHz frequency. The fracture toughness decreased and fracture density increased with increasing power from 1 to 5 kW and exposure time from 5 to 30 s, and these changes were related to temperature differences (Didenko and Prokopenko, 2009; Nejati et al., 2012). The rate of strength reduction was higher at higher power levels, and

less energy was needed to burst basalt specimens (Lu et al., 2019). Lu et al. (2020) also saw a linear decrease in triaxial compressive strength, resistance to deformation, Poisson's ratio, and elastic modulus of cylindrical basalt specimens (100 mm high by 50 mm diameter) with exposure time. Increasing the power level and exposure time reduced the UCS and BTS of basalt treated in a multi-mode microwave cavity (Hassani et al. 2016).

Hassani et al. (2011) showed that basalt sample geometry plays a role in the effectiveness of microwave treatment: disc-shaped Californian and Chinese basalt samples were heated more than cylindrical samples and showed a greater decrease in BTS.

2.9.2.2.2 Granite

Similar to basalt, increasing the power level and exposure time reduced the UCS and BTS (Hassani et al. 2016) and dynamic mode-I fracture toughness (Li et al., 2020) of granite treated in a multi-mode microwave cavity. Three-dimensional numerical models of granite—validated by experimental data—revealed a positive relationship between irradiation duration and temperature and stress, particularly for exposure times exceeding 15 s (Toifl et al., 2016; 2017). However, granite is less susceptible to microwave irradiation than basalt because it heats up more slowly and contains quartz (Hartlieb et al. 2016). The quartz content of granite affects microcrack generation. At temperatures > 500°C, the quartz phase changes from A to B, which imparts plastic features to granite and prevents microcrack generation (Hartlieb et al. 2016).

Crack patterns have implications for granite strength. Cubic granite samples formed cracks and zones of globular melting in biotite-rich areas at 600°C, and samples fragmented at 800°C (Zeng et al., 2019). Scanning electron microscopy showed that intergranular cracks were common in the biotite grains and caused several smaller cracks to initiate in minerals close to the biotite. The UCS of granite specimens decreased from 88.17 MPa at 25°C to 18.61 MPa at 800°C. Between 300 and 600°C, the UCS reduction was due to moisture release, breaks, and

quartz transition, whereas from 600 to 800°C, it was due to melting, influx, and mineral solidification (Zeng et al., 2019).

Research on granite has also directly linked crack patterns caused by microwave treatment to cutting forces. Samples of Neuhauser granite ($50 \times 50 \times 30$ cm) comprising 27% quartz, 53% feldspar, and 20% micas with an initial UCS of 210 MPa and CAI of 4.2 were subjected to 2.45 GHz microwave spot treatment on 18 spots at 24 kW power for 45 s. Treated samples required 22.5% less average cutting force, which translated into 4.7 kWh/t cutting energy savings (Hartlieb et al., 2017). The penetration rates of tunnel boring machines increased with microwave exposure time and power level (Hassani and Nekoovaght, 2011).

2.9.2.2.3 Kimberlite

A review of the Russian literature by Prokopenko (2011) reported that in porous rocks like kimberlite, fracturing due to the vapor pressure rise in pores would predominate during microwave treatment. Thus, kimberlite can be broken or crushed easily under low-temperature conditions if the rock is first soaked in water for approximately 2 h prior to microwave irradiation (Didenko et al., 2005). Kimberlite samples treated at 600 W power at 2.45 GHz frequency were destroyed when heated to 150°C at a rate of 40°C/s, with the maximum pressure in the rock pores reaching 105 Pa (Kobusheshe, 2010). The porous nature of kimberlite gives it an anisotropic nature, which leads to inconsistencies in electric field properties within the microwave cavity (Kobusheshe, 2010).

It is crucial to note that there is a very limited amount of works reported on the mechanical and physical properties of kimberlite rocks, which will be the main focus of this research in addition to granite, limestone as well as basalt samples for comparison. The research involves investigating kimberlite rocks to determine how and what extent microwave irradiation impacts their mechanical properties as well as their abrasivity.

2.9.2 Microwave system parameters

The microwave frequency, power, and exposure time interact with rock characteristics. For example, a study of nearly 100 rock types found that increasing the microwave frequency reduced the loss factor, particularly at frequencies below 5 GHz, but had no effect on the loss tangent at 5 GHz or higher frequencies (Ulaby et al., 1990). Kahraman et al. (2020a) exposed nine types of magmatic rocks to 2.45 GHz microwaves for various times. The BTS and UCS decreased with increasing microwave power (1–6 kW) and exposure time (60–420 s), and these changes were linked to increases in the surface temperature of the rock samples. An examination of 11 rock-forming minerals to 2 kW microwaves in a multimode oven concluded that most respond differently in their absorption to microwave irradiation (Lu et al., 2017). Hassani and Nekoovaght (2011) determined that using a single-mode microwave, high power, and long exposure times significantly reduced the UCS of basalt samples and the BTS of norite samples.

2.10 The effect of moisture content on the heat distribution and mechanical properties of the rocks after microwave treatment

Water is an excellent absorber of microwave energy (Gabriel et al., 1998); the electrical permittivity of the water is higher than any other material. Moisture trapped inside the rock subjected to microwave irradiation will raise the temperature significantly since water is a good absorption of microwave energy. The previous literature review showed the experimental work with some of the materials that have moisture gave the opposite results.

Work with granite has highlighted the importance of water content during microwave treatment, but study results are conflicting. Microwave radiation affected dry granite samples more than wet samples, yielding a 70% reduction in compressive strength at 850 W power, and a 38% rise in cutting rate (Sikong and Bunsin, 2009). However, microwave-treated, water-

saturated granite samples heated up twice as quickly as dry samples, but no difference was detected between wet and dry basalt in a study by Peinsitt et al. (2010). Also, Jin (2015) noticed that water did not affect heat distributions and mechanical properties of basalt rocks after microwave treatment. The low porosity of basalt might be the primary cause for these results as well as the evaporation of water after microwave treatment.

2.11 Microwave-assisted drilling, rock excavation, and grinding

The performance of mechanical excavation technologies depends on rock strength and abrasiveness. Roadheaders are limited in their application to rocks with UCS < 150 MPa (Hassani,2010a). Tunnel boring machines have high productivity than the other mechanical excavation technologies such as Mobile Miner, Mini- Disc Drum Cutterhead, but they are costly to operate where rocks are very hard and abrasive because of disc cutter wear.

The concept of using microwave irradiation to reduce rock strength before excavation was first proposed by Maurer (1968), who designed a microwave with a maximum power of 4.8 kW to treat blocks of rocks. Depending on the microwave exposure time and block size, spallation began on the rock surface, and fractures began to develop. However, microwave treatment did not completely fracture some types of rock. Mechanical forces were still needed. Thus, Maurer proposed microwave-assisted drilling to drill hard rocks—combining mechanical and microwave methods (Figure 9).
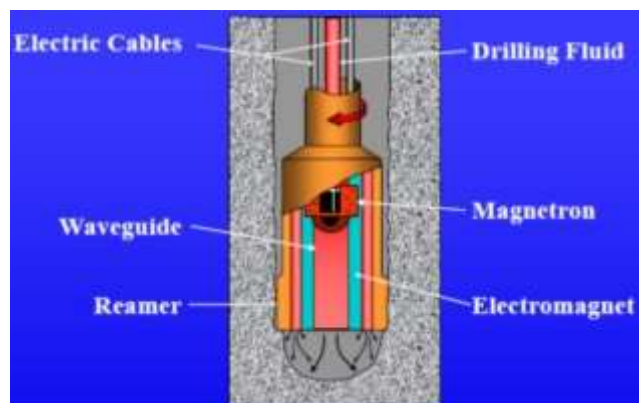
Figure 9. Schematic design of microwave-assisted drilling (Maurer, 1968).

In 1991, microwave-assisted hard rock cutting was first patented by a group of researchers in the United States (Figure 10). With this invention, rock was preweakened with microwaves, and then a cutting member was advanced to cut the strata.

20: microwave generator; 21: microwave energy source; 22: waveguide transmission line; 23: beam shaping optics; 24: exit aperture; 25: microwave beam; 30: mount for generator unit; 50: conventional mining machinery; 51: cutting member; 52: cutting edge; 100: mining environment; 101: rock strata; 102: hard rock; 103: fractures
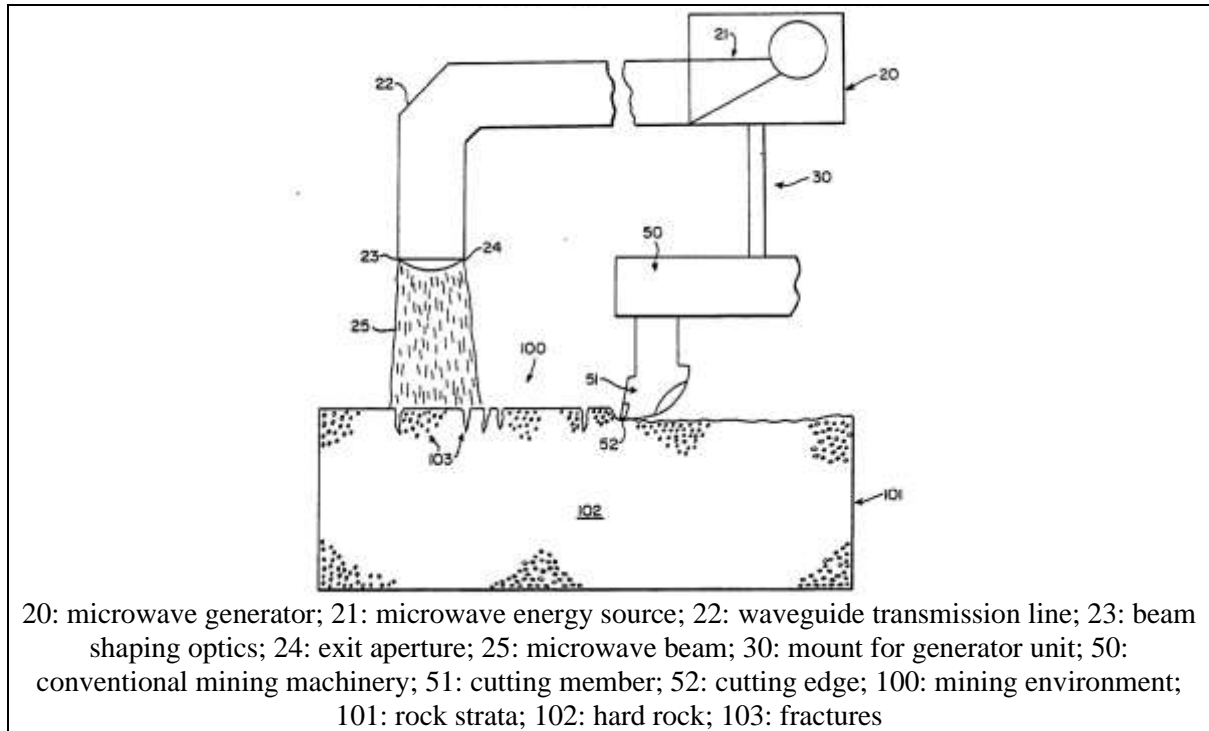
Figure 10. Cutting apparatus equipped with microwave (Lindroth et al., 1991).

In a conceptual design of a microwave-assisted drilling machine patented by McGill University (Figure 11), the microwave antenna is placed at the bit face to emit microwaves at the rock surface when the bit is rotating.

18: excavation bit; 50: base body; 52: cutting surface; 54: sections; 56: two wings; 58: cutting tool; 60: housing; 62: cover plate; 64: opening; 66: cutting tool holders
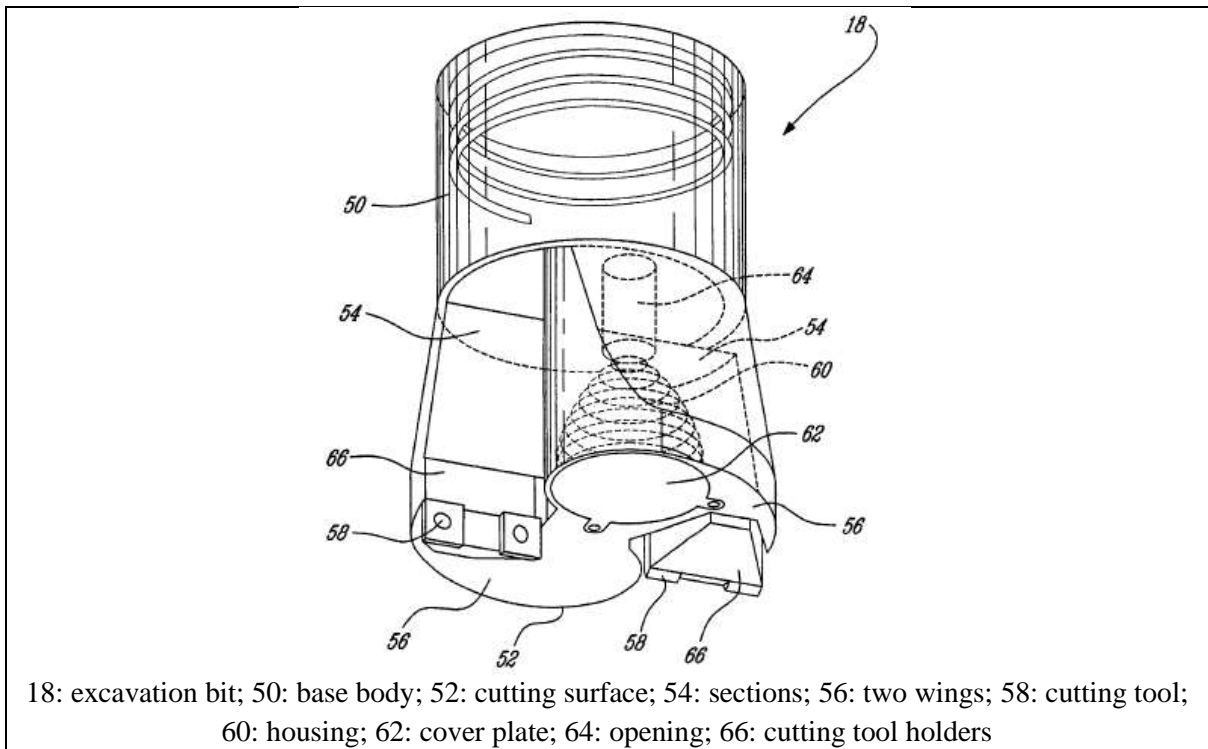
Figure 11.Conceptual design of a drag bit equipped with microwave (Ouellet et al., 2013).

Jerby et al. (2002) designed a microwave drill system based on generating a hot spot on the surface of an object; microwave irradiation from a rectangular waveguide was transmitted to a coaxial waveguide (Figure 12). The central electrode (central antenna), which also functioned as a drill bit, concentrated the microwaves to a point to weaken the surface prior to drilling. Later work expanded the basic design to create a system capable of drilling a 26 cm deep × 12 mm diameter hole in concrete silently and without vibration (Figure 13; Jerby et al., 2018).
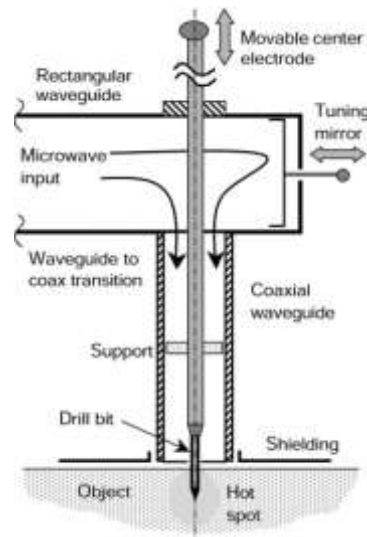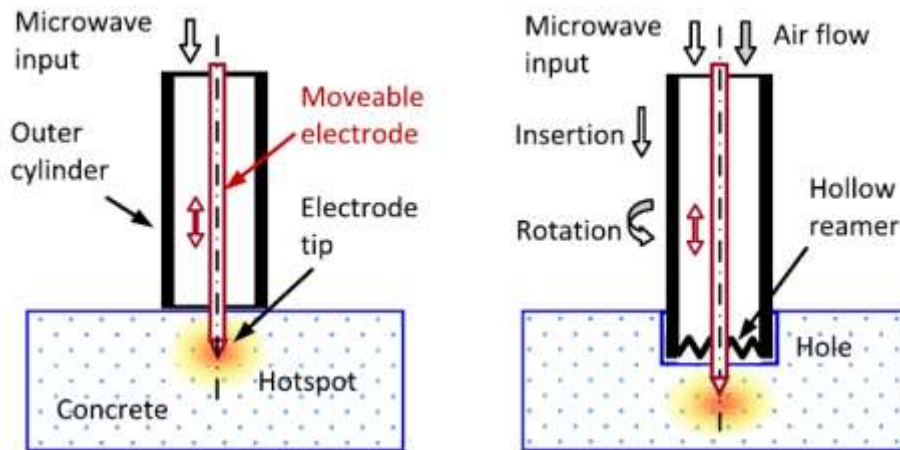
Figure 13. Basic (left) and expanded (right) schematic of a microwave drill (Jerby et al., 2018).

Hassani and Nekoovaght (2011) proposed single-mode microwave-assisted drilling or cutting for rock breakage or tunneling (Figure 14). Hartlieb and Grafe (2017) found that microwave irradiation (24 kW at 2.45 GHz frequency) decreased the cutting force of a conical pick by 10% when cutting granite samples using an open-ended waveguide. Table 2 summarizes some of the literature investigating microwave-assisted rock breakage and drilling.
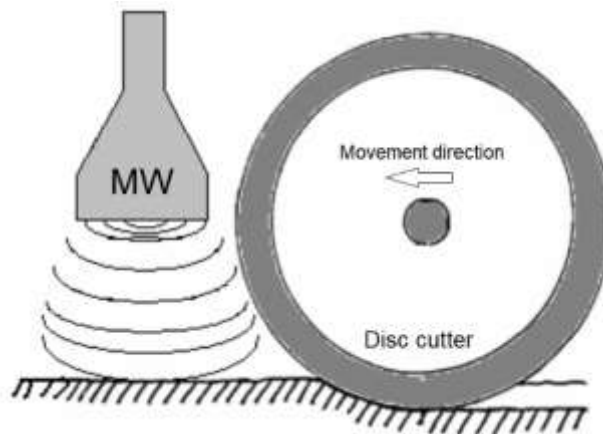
Figure 14. Schematic of a microwave-assisted disc cutter on a tunnel boring machine (Hassani and Nekoovaght, 2011).

Table 2. Summary of investigations on microwave-assisted rock breakage and drilling

Title	Reference
Driving of workings by a cutter-loader with electrothermal rock breaking	Gushchin et al., 1973
An appraisal of rock excavation by mechanical, hydraulic, thermal and EM means	Cook and Harvey, 1974
Rock breaking by microwave radiation-effects of local heating and thermal fracture	Koiwa, 1975
Rock, frozen soil and ice breakage by high-frequency EM radiation: A review	Hoekstra, 1976
Driving horizontal workings by means of an entry drifting machine with electrothermomechanical cutting	Gushchin et al., 1979
Rock excavation by microwave – Capability of high-power microwave rock breaker (100 kW, 200 kW) for rock excavation	Takahashi, 1979
A study of electrothermomechanical destruction of hard rocks with a rotary heading machine	Protasov et al., 1984
Rock excavation with microwaves	Santamarina, 1989
Microwave-assisted drilling in hard rock	Lindroth et al., 1993

2.12 Modeling microwave heating

As discussed above, rocks do not heat uniformly under microwave irradiation due to differential energy absorption by mineral components, which results in the appearance of "hot spots." Two approaches can mathematically model this physical phenomenon: 1) solving Maxwell's equation coupled with the forced heat equation and 2) applying Lambert's Law. Maxwell's equation describes "the propagation of the electric and magnetic fields, and the forced heat equation, which describes the absorption and diffusion of heat" (Hill and Marchant, 1996). Lambert's Law states that, in a medium, layers of equal thickness absorb an equal fraction of the energy traversing the medium. Lovás et al.(2010) modeled microwave heating and found that the temperature distribution model based on solving Maxwell's equation was closer to experimental results than the model created by applying Lambert's Law. Therefore, solving Maxwell's equation approach appears to be the more accurate modeling approach.

Many commercial software packages can simulate microwave heating by solving Maxwell's equation, mostly based on the finite element method. For example, COMSOL Multiphysics® can model heat distribution in chalcopyrite and pyrite during microwave irradiation by simultaneously solving Maxwell's equation and the forced heat equation (Figure 15).
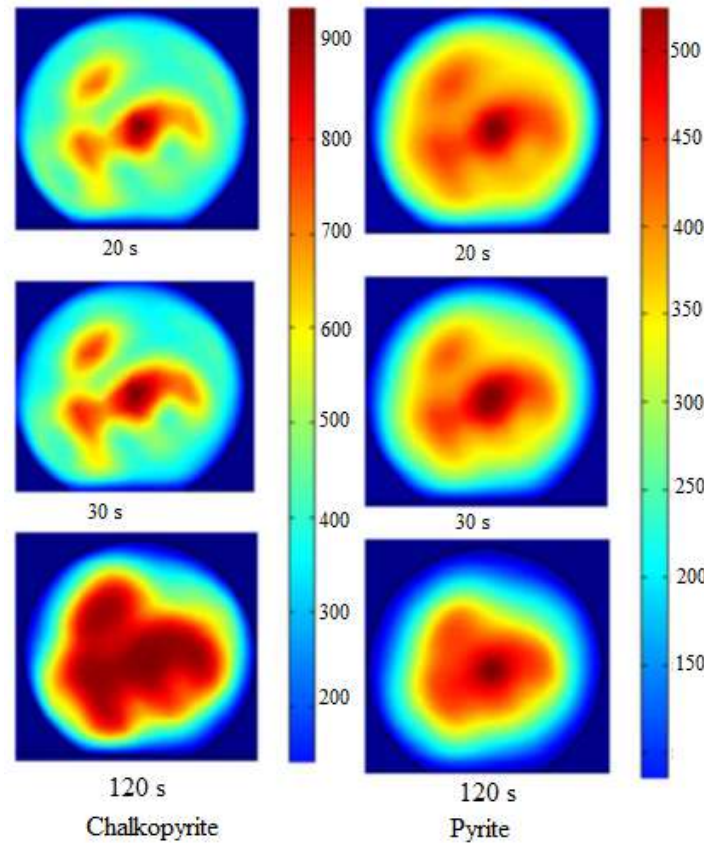
Figure 15. Heat distribution in chalcopyrite and pyrite after three microwave exposure times(Lovás et al., 2010).

2.13 P- and S-wave measurement

The P-wave velocity test involves attaching an ultrasonic transmitter and receiver at the ends of a rock sample and recording how fast P-waves travel through the rock sample. P-wave velocity devices are portable; hence, they are applicable in both fields and laboratories for rock characterization. During more large-scale seismic refraction and reflection surveys to measure the material stiffness and identify significant material interfaces at depth (Takahashi, 2004), P-waves partially convert to S-waves at interfaces between soil and/or rock layers with a

relatively low seismic velocity underlain by a high seismic velocity layer. Though the velocity in the lower crust differs by region, this appears to be temperature-dependent, suggesting that mafic lithologies in most regions are likely a main constituent of the lower crust. In addition, seismic reflections were commonly observed, provided by lithological layering in both crustal cross-sections and lower-crustal xenolith suites (Mooney, 1992). As the seismic waves enter the mantle, the change in P- and S-wave velocities indicate the boundary between the upper and lower mantle and proves the existence of the lithosphere and asthenosphere.

Godio and Dall'Ara (2012) used seismic wave velocity measurements to evaluate the rock mass at the tunnel face. Broad frequency (1–30 kHz) acoustic logging was applied to estimate P- and S-wave velocities. Weak zones in quartzite were indicated by a sudden decrease in both velocities; discontinuities and fractures were shown by reflection and/or diffraction effects.

2.14 Fracture mechanics

A fracture separates a body into two or more pieces due to applied stress, which can be constant or change slowly with time, at temperatures lower than the material's melting temperature. Fractures may also occur due to creep (time-dependent deformation, usually at high temperatures) and fatigue (when cyclic stresses are applied) (Callister and Rethwisch, 2020). Fracture is a failure mechanism of brittle materials, which has important implications on the performance of structures. Rock mass faulting and geotechnical, mining, or civil engineering facility failures pose substantial safety hazards and can cause damage to and/or stoppage of operations (Brace and Bombolakis, 1963; Backers, 2005).

Monitoring rock mass behavior is essential to predicting and preventing failure (Szwedzicki, 2003). Rock fracture mechanics assesses the safety and stability of structures that interact with rock. It has been applied to underground storage of oil, gas, or air; radioactive waste disposal; carbon sequestration; and mineral resource exploration technologies such as blasting, hydraulic

fracturing, and mechanical mining (Ayatollahi and Aliha, 2007; Backers, 2005; Wei et al., 2018). Rock fracture mechanics can also be used to measure the weakening effect of microwave radiation on rocks. It can describe various phenomena such as the conditions under which fractures form in a particular type of rock, whether the fracture expands in a linear or anisotropic manner, and fracture toughness—the ability of a material to resist fracturing.

2.14.1 Griffith's criterion

In 1921, Griffith published the concept of crack propagation in brittle materials, which led to the development of modern linear fracture mechanics. Griffith states that when the surface energy of crack faces is less than the potential energy forming the crack, the crack will propagate. (a) is the Crack length (m), σ_f is the stress at fracture (MN/m^2) and C is the constant (equation 12):

$$\sigma_f \sqrt{a} \approx C \tag{12}$$

Furthermore, Griffith found an expression for C in terms of the surface energy of the crack by solving the elasticity problem of a finite crack in an elastic plate in terms of the material Young's modulus E (N/m^2) and γ is the fracture surface energy (J/m^2):

$$C = \sqrt{\frac{2E\gamma}{\pi}} \tag{13}$$

For the key factors of Griffith's theory, the energy release rate, G (J/m^2), can be expressed as follows, where σ is the applied stress (Mpa) and a is one-half the crack length (m):

$$G = \frac{\pi\sigma^2 a}{E} \tag{14}$$

When the critical value G_c (J/m^2) (equation 15) is less than G, the crack will propagate. However, this criterion does not apply to highly deformed materials before crack propagation or to soft materials (Griffith, 1921).

$$G_c = \frac{\pi \sigma_f^2 a}{E} \qquad (15)$$

2.14.2 Irwin's modification

Irwin (1957) modified Griffith's theory for ductile materials such as steel. He claimed that, though the relationship in equation 15 persists, γ is usually much higher than the values assumed by Griffith due to microscopic yield stress in the plastic zone at the tip of the crack (Figure 16).
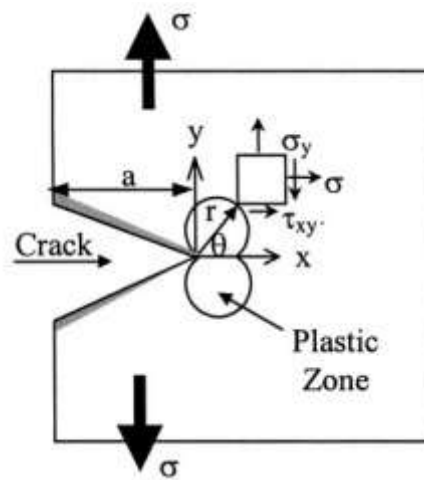
Figure 16. Crack in plastic zone and stress at the crack tip of ductile material (Perez, 2004)

The size of the plastic zone increases with the loading, causing the energy to dissipate as heat and providing thermodynamic resistance to fracture. Hence, Griffith calculates G as:

$$G = 2\gamma + G_p \qquad (16)$$

Where G_p is the plastic dissipation per unit area of crack growth. Therefore, the modified version of Griffith's energy criterion can be expressed as follows:

$$\sigma_f \sqrt{a} = \sqrt{\frac{2EG}{\pi}} \qquad (17)$$

2.14.3 Mode I fracture toughness testing

Failure can occur in three modes, based on the relationship of the stress to the crack; therefore, there are also three modes of fracture toughness based on a crack surface displacement or crack tip loading (Figure 17; Callister and Rethwisch, 2020; Wei et al., 2018). Mode I refers to the opening of the crack due to tensile stress acting normal to the plane of the crack. Mode II refers to the sliding of the crack planes due to shear stress parallel to the crack plane and perpendicular to the front plane of the crack. Mode III refers to the sliding of the crack planes due to shear stress parallel to both the plane of the crack and the front plane of the crack (Irwin, 1957).

Mode I: Opening   Mode II: In-plane shear   Mode III: Out- of plane shear
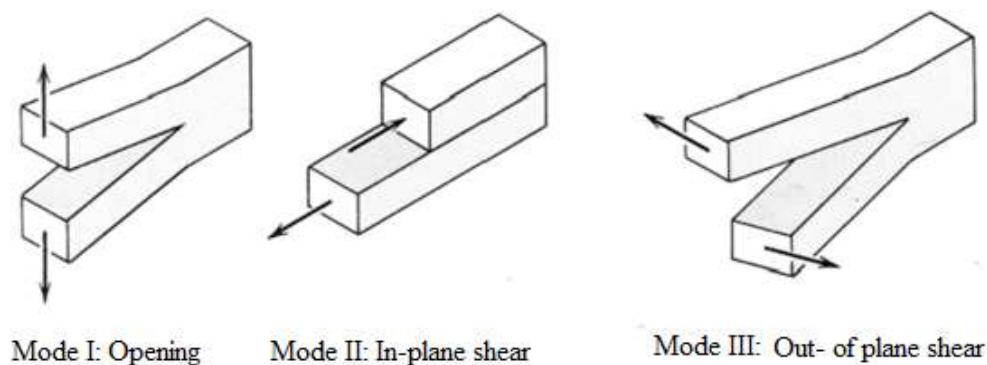
Figure 17. Three modes of fracturing (Callister and Rethwisch, 2020)

Irwin developed the stress intensity factor (K in MPa·m$^{-0.5}$) to express the stress state at the tip of the crack at the point of failure. The terms K_{IC}, K_{IIC}, and K_{IIIC} represent the value of K under Mode I, II, and III loadings, respectively, and at critical (i.e., peak) stress (c) immediately before failure (Callister and Rethwisch, 2020). Mode I testing methods are the most advanced and popular in use. The critical stress intensity factor defines the linear-elastic fracture toughness of material at the point when crack propagation suddenly becomes rapid and unlimited. When K_I is larger or equal to K_{Ic}, the crack will propagate (Suresh, 1998). If the load operates on a crack in the manner represented in Figure 18, there will be no strain component to the front and back faces.
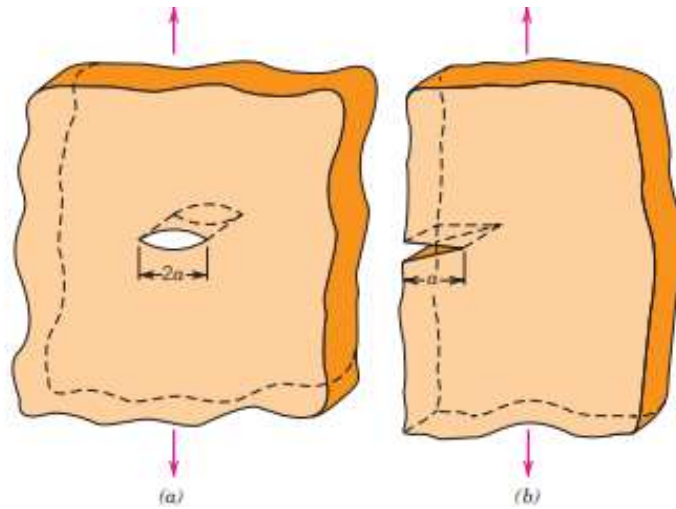
Figure 18. (a) Interior crack in a plate of infinite width and (b) the edge crack in a plate of semi-infinite width(Callister and Rethwisch, 2020).

Numerous standard methods have been proposed to measure the Mode I fracture toughness of rocks, K_{IC}. Within the following non-exhaustive list, the International Society of Rock Mechanics recommends methods 6, 14, 15, 18, and 19.

1. Brazilian disc (Guo et al., 1993),

2. flattened Brazilian disc (Wang and Xing, 1999),

3. hole-cracked flattened Brazilian disc (Wang et al., 2010),

4. double-edge-cracked Brazilian disc (Chen et al., 2001)

5. cracked straight through Brazilian disc (Atkinson et al., 1982),

6. cracked chevron notched Brazilian disc (Fowell et al., 1995)

7. center-cracked horseshoe disc (Haeri et al., 2018),

8. hollow center-cracked disc (Bush, 1976; Ouchterlony, 1981),

9. radial cracked ring (Shiryaev and Kotkis, 1983; Chen et al., 2008),

10. modified ring (Thiercelin and Roegiers, 1988; Tutluoglu and Keles, 2012),

11. double torsion (Shyam and Lara-Curzio, 2006),

12. diametric compression (Szendi-Horvath, 1980),

13. edge crack triangular (Aliha et al., 2013),

44

14. chevron bending (Ouchterlony, 1988; Iqbal and Mohanty, 2007),

15. short rod tests (Ouchterlony, 1989),

16. straight notched disc bending (Tutluoglu and Keles, 2011),

17. straight (or single) edge cracked round bar bend (Bush, 1976; Ouchterlony, 1981),

18. notched semi-circular bend (NSCB) (Kuruppu, 1997; Tutluoglu and Keles, 2011; Kuruppu et al., 2014; Chong and Kuruppu, 1984), and

19. Cracked chevron–notched semi-circular bend CCNSCB (Wei et al., 2015).

2.15 Research gaps and outlook

Taking all the discussed literature into account, Several experimental studies on the effect of microwave irradiation on different types of rocks and minerals have been conducted during the last 20 years. Recent studies are committed to exploring the viability of hard rocks weakening before mechanical excavation. In this context, researchers are investigating the application of microwave irradiation to rocks prior to the use of mechanical rock-breaking techniques. These studies showed that the application of microwave irradiation is a promising technique for the pre-conditioning of hard rocks in the mining and civil industries. microwave irradiation heats rocks from the inside out. The heat then causes stresses due to differences in the volumetric expansion rate between the rocks' mineral components. These stresses result in micro-cracks, which have the potential to weaken the rocks. The overall strength of the rocks is thus reduced, making it easier for mechanical machines to break them down. Although several studies have been done in recent years to investigate the effects of multi-mode and single-mode microwave irradiation on rocks, (1) due to its containing the diamonds, no comprehensive work reported on the mechanical and physical properties of kimberlite rocks as well as the mineral composition and the dielectric properties, (2) there was no investigation of the overall energy efficiency of microwave-assisted rock breakage. Therefore, given the above picture of the gaps

in the literature, the present thesis takes into account all the previous efforts and aims to study the effects of microwave irradiation on Canadian kimberlite, granite, limestone and basalt rocks with major experimental tests using both single-mode and multi-mode cavity. In addition, the current thesis for the first time investigates the energy balance analysis to determine if this technique is feasible in the future mine for microwave-assisted rock breakage as a realistic possibility way for reducing the global mining energy consumption.

2. 16 Summary

In this chapter, the literature review of rock breakage techniques including drilling and blasting and the EFRB techniques have been introduced. Most parameters that are involved in a microwave-assisted rock heating process are introduced and discussed. Health and safety protocols when using microwaves and the factors affecting rock weakening by microwave are discussed. In addition, this chapter introduces The effect of moisture content on the heat distribution and mechanical properties of the rocks after microwave treatment as well as P-and S- wave measurements are discussed. Fracture mechanics are explained in detail including the three modes of fracture toughness. Mode I fracture toughness is illustrated in detail. Finally, the research gap and the outlook are shown. In conclusion and based on the literature review and the research gaps, This research work for the first time will investigate the effect of microwave irradiation on the physical and mechanical properties of kimberlite rocks and study the most important topic for the microwave application which is the overall microwave efficiency by introducing the calorimetric idea to enable us to determine the exact amount of energy absorbed by the samples. Parameters HOMW and WOME will be studied, defined and analyzed.

Chapter 3 Methods and Experimental Setup

Preface

This chapter aims to investigate the effects of microwave irradiation on kimberlite and associated rocks (granite and limestone) and basalt rocks for comparison. In addition, this chapter aims to investigate the total energy efficiency of microwave irradiation of hard rocks. The organization of this chapter is as follows. First, (section 3.1) provides comprehensive details on Kimberlite rocks as well as the Geological setting of Canadian kimberlite. Then, section (3.2) provides information regarding the physical properties of untreated rock samples and the mineral composition of kimberlite. The dielectric properties of untreated kimberlite, granite and limestone are measured using the coaxial probe technique. Section (3.3) describes how samples were prepared for the mechanical tests (USC, BTS, CAI and PSV) and how their mechanical properties were measured. Sections (3.4 and 3.5) show how the samples were irradiated using a multi-mode microwave and single-mode microwave, and how their surface temperature was measured using a thermal camera and infrared gun. Section (3.6) provides details on the mechanical property testing after microwave treatment and the equipment used. Moreover, this section provides an in-depth discussion on the effects of microwave irradiation on the K_{IC} using the NSCB method, the way of the sample preparation as well as the experimental procedures and the equipment used. To better understand the strength weakening of microwave, in this section, Weakening over Microwave Energy (WOME) was defined and calculated. This chapter ends by discussing a very important topic which is the overall energy efficiency where basalt samples were heated in a single-mode microwave and calorimetry was applied to determine their energy absorption, conduct a "heat over microwave efficiency" or HOME analysis, calculate microwave ramp-up, and determine the optimal position of the sample relative to the microwave horn antenna (sections 3.7, 3.8 and 3.9). Finally, the

quenching effect of rock strength reduction after microwave treatment was studied (section 3.10).

3.1 Kimberlite

Kimberlite is an igneous rock that mainly occurs as eroded volcanic pipes and dyke systems. Volcaniclastic kimberlite (VK) often occurs as carrot-shaped diatremes that can reach a depth of > 2 km from the eruptive land surface. The crater on top of a diatreme can have a diameter up to 1 km and is filled by primary pyroclastic deposits or resedimented material from the tephra-ring surrounding the crater. In more profound levels of the diatreme, the volcaniclastic rocks may adopt specific textural and structural features, which led to the term "Tuffisitic kimberlite" (TK). However, not all diatremes show this particular kind of infill (Hetman et al., 2004; Smith, 2008). Hypabyssal kimberlite (HK) intrusions occur in dyke systems or as local fragments.

The typical phenocrystic mineralogy of kimberlite comprises olivine in a groundmass of calcite, perovskite, apatite, spinel, and other phases. In addition, mantle-derived xenoliths and xenocrysts of garnet, olivine, and diamond occur (Sparks, 2013). Kimberlite deposits that host diamonds in economic quantities are of particular interest to the mining industry.

3.1.1 Geological setting of Canadian kimberlite

Several kinds of kimberlite occur throughout the northern expanses of Canada's vast wilderness areas. These are characterized by external pipe shapes and pipe infills. The differences in kimberlite rock types derive mainly from variations in geological settings (Figure 19; Hetman et al., 2004). In general, every kimberlite field features at least one type of kimberlite pipe, primarily resedimented VK, pyroclastic kimberlite, pyroclastic TK, TK breccia, and HK (Smith, 2008).
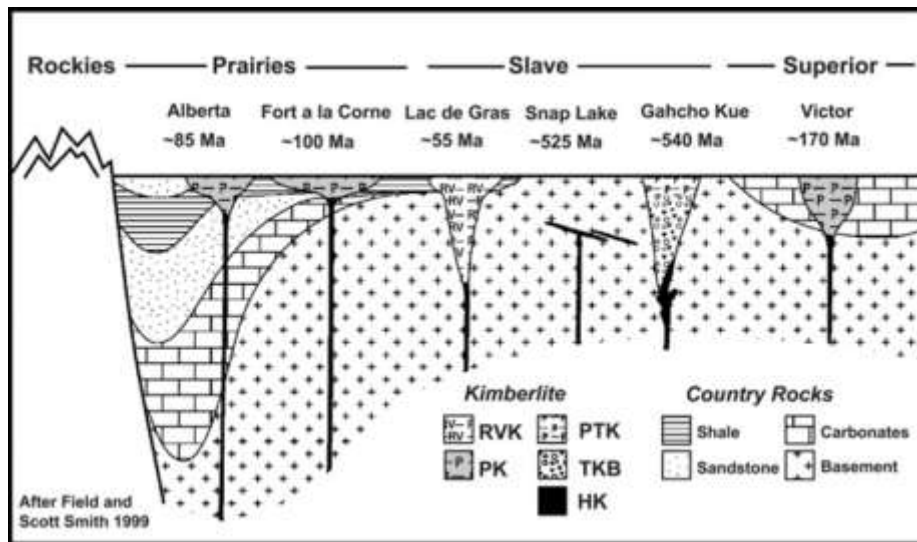
Figure 19. Schematic west-to-east cross-section of Canada showing pipe shapes, pipe infills, and geological setting reconstructed to time of emplacement; RVK: resedimented volcaniclastic kimberlite; PK: pyroclastic kimberlite; PTK (Hetman et al., 2004).

Most kimberlite fields are situated in the remote areas of Fort à la Corne, Lac de Gras, the Gahcho Kue pipes, and Attawapiskat (Hetman et al., 2004). The mid-sized Fort à la Corn field, situated 60 km east of Prince Albert, Saskatchewan, comprises prairie kimberlites (Figure 20a). Pyroclastic kimberlite makes up the primary infill. Of the more than 70 formations present, nearly two-thirds contain diamonds (Berryman et al., 2004). These formations feature xenolith-poor VK comprising mainly a mixture of single-crystal and juvenile lapilli (Field & Smith, 1999). The 140/141 kimberlite formation is designated as Saskatchewan's most significant known kimberlite formation. This large, irregular formation features a complex infill comprising various phases of pyroclastic kimberlite (Berryman et al., 2004).
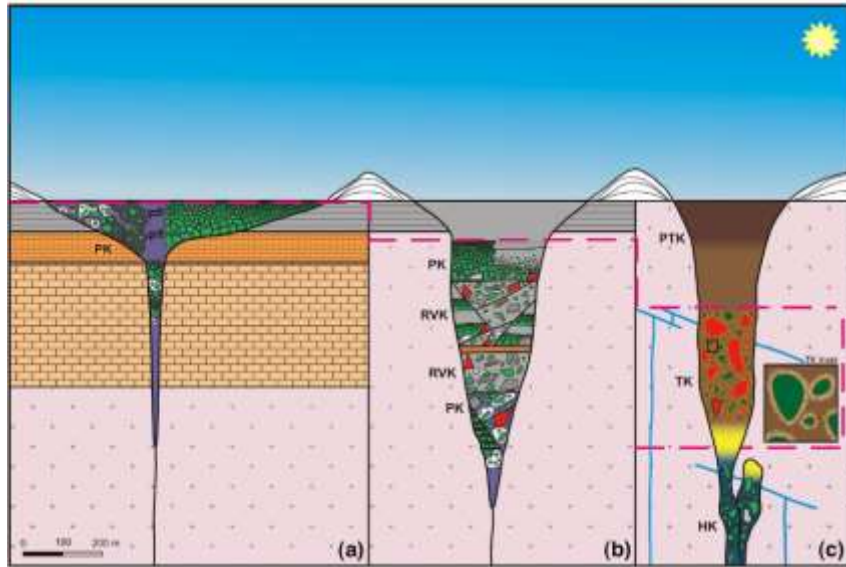
Figure 20. Simplified schematic geology of kimberlite pipes in Saskatchewan, reconstructed to the time of emplacement(Smith and Barbara, 2008).

(a) Fort à la Corne; (b), Lac de Gras; and (c) Gahcho Kue; RVK: resedimented volcaniclastic kimberlite; PK: pyroclastic kimberlite; PTK: pyroclastic tuffisitic kimberlite; TK: tuffisitic kimberlite; HK: hypabyssal kimberlite; dashed pink line indicates present surface. In panel (a), orange denotes siltstone, cream denotes carbonates, grey denotes shale in the country-rock, and purple denotes a matrix comprising carbonate and serpentine. In panel (b), stippled white denotes juvenile lapilli, green denotes discrete olivine grains, red denotes fresh granitoid, dark grey with horizontal lines denotes xenoliths of shale, brown denotes wood, dark grey with olivines denotes autoliths, pale grey denotes disaggregated shale, orange denotes siltstone, and ornamented grey to the right denotes mudstone. In panel (c), lighter green denotes olivine grains, blue denotes a fine-grained groundmass zone, darker green denotes serpentinized olivine, orange denotes very fine-grained kimberlite magma selvages, brown denotes serpentine, white in the enlarged inset denotes the matrix, and yellow indicates a textural transition between TK and HK.

Another major formation of kimberlites in Canada can be found in the Archean Slave craton region in Nunavut and the Northwest Territories, which covers approximately 300,000 km^2 of northern tundra. It features 2.73 to 2.58 Ga basement gneiss complexes that have been intruded

50

by granitic plutons and then overlain with supracrustal rocks (Sarkar et al., 2015). Near the central section of the craton is the Lac de Gras kimberlite field, which is a section of the Cretaceous/Tertiary kimberlite magmatism corridor. This corridor runs more or less north-south and spans a 2000-km stretch from Montana to the Northwest Territories, crossing through the province of Alberta (Sarkar et al., 2015). At approximately 9000 km^2 in area, the Lac de Gras kimberlite field is expansive compared to other fields.

The kimberlites at Lac de Gras feature mostly VK and HK-type formations (Field and Scott Smith, 1999), and resedimented VK is the main pipe infill for the kimberlites (Figure 20b). The resedimented VK is a combination of juvenile lapilli, discrete olivine grains, fresh granitoid, xenoliths of shale, wood, and autoliths. All of these are set within a mixed disaggregated shale matrix. The siltstone and mudstone indicate the presence of kimberlite-poor sediments. Additionally, as shown on the right side of Figure 20b, the discrete olivines and stippled grey disaggregated sedimentary material has been mixed, while on the left side of Figure 20a, we see the discrete olivines presented in a purple serpentine matrix.

TK makes up the main pipe infill in the Gahcho Kue kimberlites (Figure 20c). However, HK olivine grains set in a fine-grained groundmass make up the root zone. Note that the TK presents wholly serpentinized olivine. The majority of the substances are very fine-grained kimberlite magma selvages, called juvenile pelletal lapilli, which differ from the pyroclastic juvenile lapilli depicted in panel (b). Moreover, the matrix is primarily made up of serpentine that environmental forces can easily affect. The matrix usually includes microlites. Overall, the TK distribution of olivines resembles the HK distribution. Several pipes across all the fields reveal a textural transition between TK and HK.

The Gahcho Kue kimberlite cluster features five pipes (Tesla, Tuzo, Hearne North and South, and 5034), which have infills—mainly composed of TK breccia and HK—and contrasting

external shapes that usually correlate to kimberlite infill texture. For example, TK breccia is generally found in smooth-sided circular pipes (e.g., Hearne South and Tuzo), whereas HK tends to manifest as complex irregular pipes (e.g., 5034). In the Tesla and Hearne North formations, the pipes feature HK and TK breccia. Further, in the Gahcho Kue transition zones, igneous textures from magmatic HK overlay magmaclastic TK (Hetman et al., 2004), with the HK and TK textures appearing fairly uniformly. However, there is a clear oscillation of magmatic and magmaclastic textures in the transition zone, leading to small-scale intermixing. These zones indicate that the Gahcho Kue kimberlites were likely formed through intrusive magmatic processes (Hetman et al., 2004), with the TK being formed during magma disruption. Interestingly, the infills and pipe shapes at Gahcho Kue are more similar to those in the South African Kimberley fields than Canadian kimberlite formations at, for instance, Lac de Gras Attawapiskat, or Fort à la Corne (Hetman et al., 2004).

With an area of approximately 15 ha, the Victor kimberlite mine is the largest of the 19 kimberlite mines in the James Bay lowlands (approximately100 km west of Attawapiskat, Ontario). There are two fully separate but adjacent pipes: Victor South and Victor North. While Victor South comprises mostly pyroclastic kimberlite, Victor North features pyroclastic kimberlites and hypabyssal-like rock. Overall, the Victor pipes, including the kimberlite infills, are quite dissimilar to kimberlites found in South Africa and the Lac de Gras and Gahcho Kue kimberlites described above. The Victor kimberlite rocks emerged from several eruptive events, which caused both cross-cutting and adjacent craters infilled either from hypabyssal-like or pyroclastic kimberlites, likely of extrusive origin (Field and Scott Smith, 1999). Additionally, the Victor North pyroclastic kimberlites contain two nested vents, considered a relatively rare feature (Webb et al., 2004).

Work done at the Victor pipe site prior to 1989 showed it to be a single pipe of mostly HK along with other—at the time—unidentified textures. Following several drillcore examinations

in 1989, researchers found that the Victor pipe potentially included VK and the earlier determined HK. However, the VK differed significantly from that in pipes in southern Africa, whose main infills were TK.

Overall, upon closer examination, the three kinds of kimberlites reveal notable differences regarding shape, pipe size, and infill. They also differ with regard to the type of country rocks in which they occur and their geological characteristics (Figure 19 Figure 20) (Smith, 2008).

3.2 Material assessment

In this section, the rock properties were measured in the McGill Geomechanics Laboratory by the author. While dielectric properties were measured at Université de Montréal, the Department of Electrical Engineering by the author too. The mineral composition of the kimberlite rocks was measured at the Université du Québec à Montréal (UQAM).

3.2.1 RQD

The RQD has become a fundamental parameter in geotechnical and mining engineering. It is defined as the percentage of intact core pieces longer than 100 mm over the total drilling length (Table 3). The RQD value depends on location and drilling orientation where the core was obtained and core size (Figure 21).

Table 3. Rock quality designation (RQD) and associated rock mass quality

RQD (%)	Rock Mass Quality
<25	Very poor
25–50	Poor
50–75	Fair
75–90	Good
90–100	Excellent

Figure 21. Core samples.

The RQD of each core box was determined according to ASTM D6032/D6032m-17 (ASTM, 2017). The highest RQD was observed for VK (90%), followed by granite (87%), limestone (75%), TK (71%), and HK (63%) (Figure 22). RQD values for each box and means (± standard deviation) for each rock type are presented in **Appendix B**.
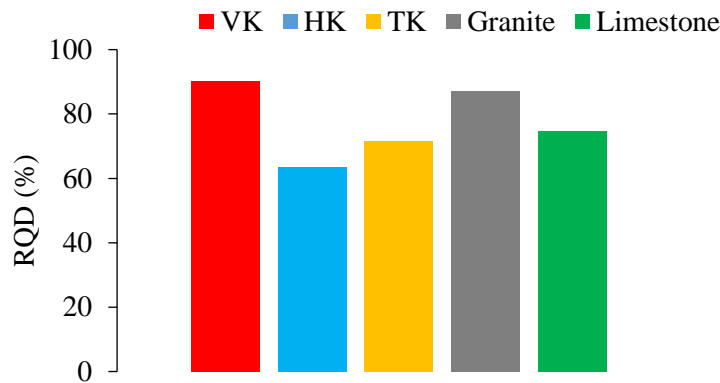
Figure 22. Mean rock quality designation (RQD) for five rock types; VK: volcaniclastic kimberlite; HK: hypabyssal kimberlite; TK: tuffisitic kimberlite.

3.2.2 Physical properties of untreated rock samples

3.2.2.1. Specific gravity

Specific gravity (unitless) is the ratio of the density of a material to the density of the reference material (distilled water). The specific gravity measured according to ASTM D6473-15 (ASTM, 2015) was similar among the five rock types (Figure 23). Detailed specific gravity data are presented in **Appendix C**.
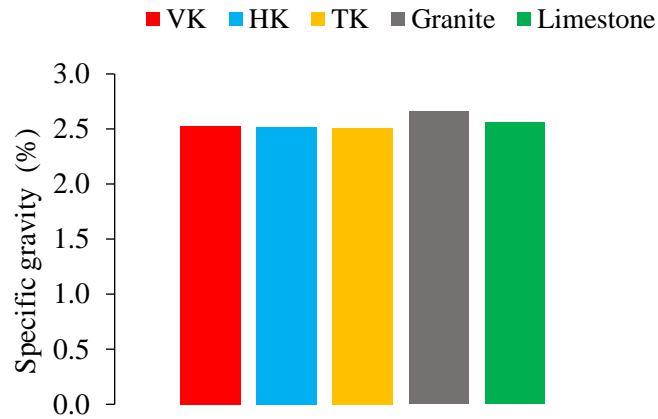
Figure 23.Mean specific gravity for five rock types: VK: volcaniclastic kimberlite; HK: hypabyssal kimberlite; TK: tuffisitic kimberlite.

3.2.2.2 Porosity

Porosity is the proportion (0–100%) of the volume of voids over the total volume in a given material. The porosity of the samples was measured according to ASTM C20-00 (ASTM, 2015). Mean porosity was low and varied among the rock types; it was highest for limestone and lowest for granite (Figure 24). Detailed porosity data are presented in **Appendix D**.
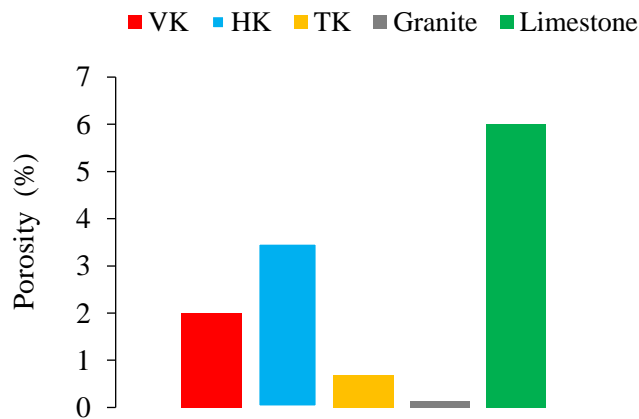
Figure 24. Mean porosity for five rock types; VK: volcaniclastic kimberlite; HK: hypabyssal kimberlite; TK: tuffisitic kimberlite.

3.2.2.3 Specific heat capacity

Specific heat capacity is the quantity of heat required to change the temperature of a unit mass of a substance by one-degree centigrade. The specific heat capacity of rock samples was measured according to ASTM D4611-16 (ASTM, 2016). HK had the highest specific heat capacity, thus requiring more heat to increase the temperature, whereas granite had the lowest (Figure 25). Detailed specific heat capacity data are presented in **Appendix E**.
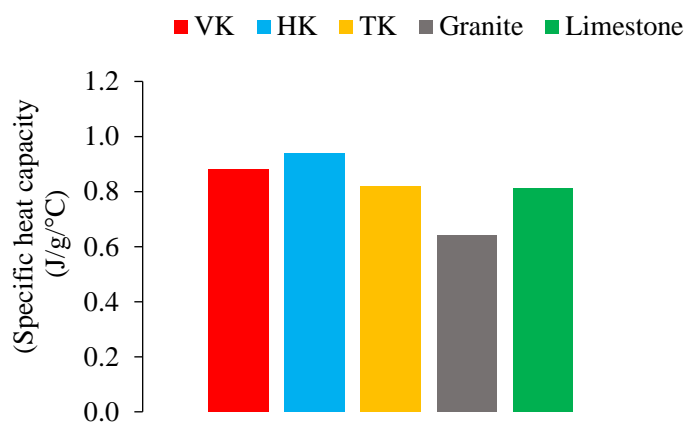
Figure 25. Mean specific heat capacity for five rock types; VK: volcaniclastic kimberlite; HK: hypabyssal kimberlite; TK: tuffisitic kimberlite

3.2.2.4 Moisture content

The moisture content of the VK, HK, TK, Granite and limestone samples were measured by determining the reduction in mass of the sample. The initial mass was recorded using the electronic balance. These samples were then placed in a lab oven at a temperature of around 110 ± 5 °C. The weight of the samples was measured again after 24 hours when they dried entirely in the oven. The average moisture content was found to be around 0.22%,0.89%,0.17%,0.01% and 0.08% for VK, HK, TK, Granite and limestone samples consequently.

3.2.3 Dielectric properties of untreated rock samples

3.2.3.1 Measurement

Dielectric properties provide insights into the ability of a material to absorb microwave radiation. Five methods can be used to measure dielectric properties over a range of frequencies and temperatures and depending on the loss factor of the material (Figure 26; Table 4). The coaxial probe is most appropriate for kimberlite, which has a high loss factor.
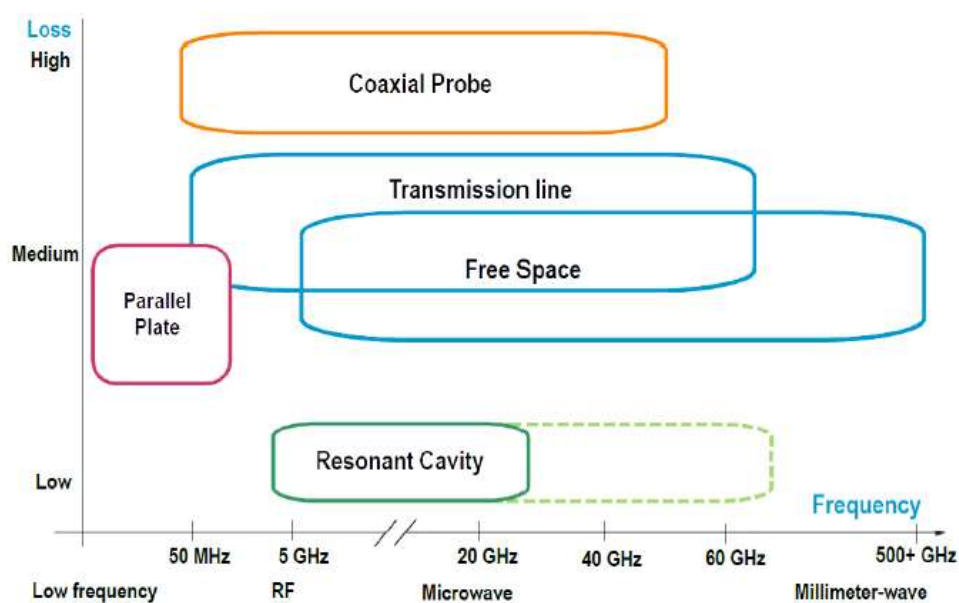
Figure 26. Techniques to measure dielectric properties over a range of frequencies and material loss factors (Begley, 2010).

Table 4. Advantages and disadvantages of dielectric property measurement techniques (Khan and Ali, 2012; Ouellet et al., 2013; Jha et al., 2011; Clerjon and Damez, 2009; Wee et al., 2009; Venkatesh and Raghavan, 2005); VK: volcaniclastic kimberlite; HK: hypabyssal kimberlite; TK: tuffisitic kimberlite.

Method	Advantages	Disadvantages	Rock type
Coaxial probe	Wide range of frequencies Easy sample preparation High accuracy for high-loss materials High equipment availability	Air gaps between probe & sample create errors Difficult to calibrate	VK, HK, TK, granite, limestone
Transmission line	Useful for anisotropic materials Suitable at high frequencies	Difficult sample preparation Not applicable at low frequencies Frequencies >10 GHz are usually immeasurable	

Method	Advantages	Disadvantages	Rock type
Free space	Wide range of frequencies Easy sample preparation No contact Suitable for high temperature Not useful for high- & low-loss materials	Diffraction error	Granite
Resonant cavity	Useful for low-loss materials High accuracy Useful in high temperature Easy to calibrate	Applicable at a single or resonant frequency Limited to a small sample size	Basalt
Parallel plate	Suitable for high-loss materials High accuracy at low frequencies Easy application	Not useful at high frequencies	Granite, limestone

The coaxial probe technique is commonly used for loss-prone in liquid, powder, or solid and semi-solid states; it is not accurate for materials with loss factors below the lower detection limit. The system consists of an external computer for data acquisition and a coaxial probe attached to a network analyzer by a coaxial cable (Figure 27). The frequency range on the network analyzer can be set to measure the loss factor and dielectric constant of the material at frequencies from 2 to 12 GHz.
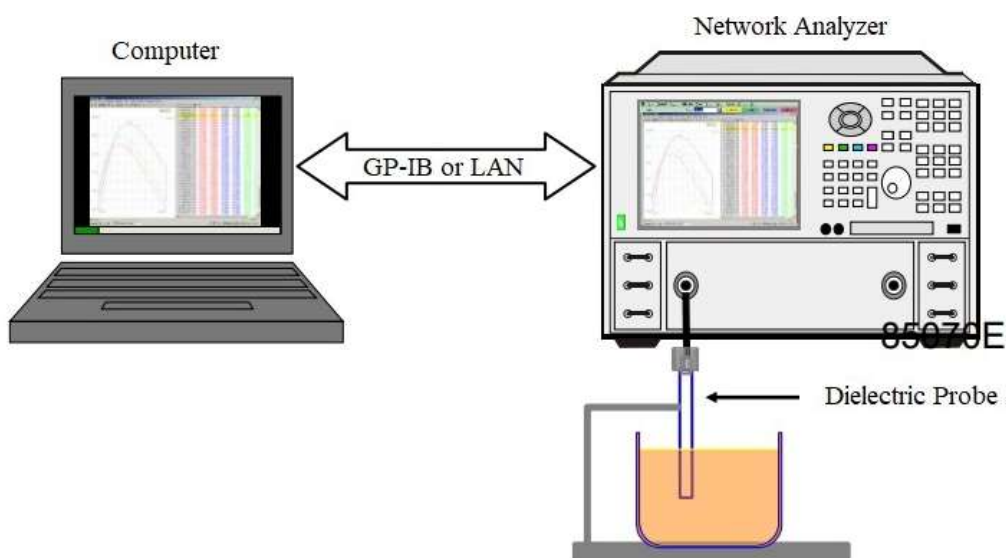
Figure 27. Calibration process using a coaxial probe measurement device(Begley, 2010); GP-IB: general purpose interface bus; LAN: local area network.

Samples of VK, HK, TK, granite, and limestone were cut into 63 mm diameter by 30 mm high discs (Figure 28). Experience with this method has shown that the rock sample must be at least 1.5 times thicker than the diameter of the probe. Because EM energy is transmitted and arced within the sample during microwave treatment, the surface of the sample must be flat and smooth because surface irregularities strongly affect the accuracy of the measurement. In addition, the air gap between the coaxial probe and the specimen surface must be minimized. Thus, the two ends of the disc specimens were polished to an accuracy of 5–10 μm of surface roughness before testing.

Figure 28. Kimberlite rocks were prepared for dielectric property measurement.

The probe was calibrated in a liquid with known dielectric properties (water) and then firmly pressed to the smooth, flattened surface of the rock specimen. The dielectric properties of the rock samples were measured by sending a signal from the probe to the sample and analyzing the reflected signal phase and amplitude (Figure 29). Measurements were recorded from five locations on each sample surface at an ambient temperature of 20°C; means were calculated.
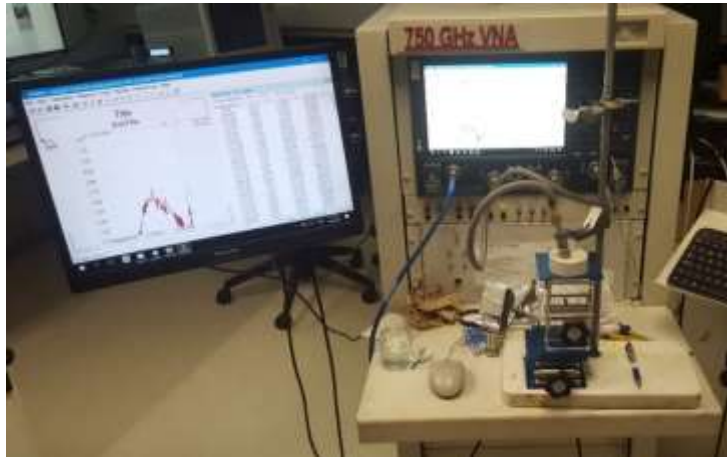
Figure 29. Laboratory coaxial probe apparatus used to measure dielectric properties located at Université de Montréal, Department of Electrical Engineering

3.2.3.2 Dielectric results

At 2.45 GHz, the frequency of the microwave systems used in this study, the complex permittivity (ε) was highest for the TK sample and HK and lowest for granite (Table 5). Recall that materials with a high complex permittivity absorb EM energy and heat to high temperature, whereas materials with a low complex permittivity are transparent to EM waves and do not readily heat. Thus, HK and TK appear to have a relatively high ability to store EM energy as heat, whereas the opposite is true for granite. The loss tangent ($\tan\delta = \varepsilon''/\varepsilon'$) was highest for VK and lowest for granite (Table 5). Since the loss tangent is a measure of dissipation of EM energy, VK readily dissipates EM energy and granite does not. The mean dielectric constant and loss tangent for VK (6.0 and 0.12, respectively) agree with those of Prokopenko (2011), who used the same method on kimberlite (6.5 and 0.15, respectively) at 2.45 GHz frequency.

Table 5. Mean dielectric constants (ε'), loss factors (ε'') and loss tangents ($\tan\delta$) for VK (volcaniclastic kimberlite), HK (hypabyssal kimberlite), TK (tuffisitic kimberlite), granite, and limestone at 2.45 GHz frequency.

Rock type	ε'	ε''	$\tan\delta$
VK	6.11	0.75	0.123
	5.84	0.63	0.108
HK	7.61	0.67	0.088
TK	7.84	0.65	0.083
	6.97	0.21	0.030
Granite	5.54	0.18	0.032

Rock type	ε'	ε''	tanδ
	5.98	0.20	0.033
Limestone	5.69	0.23	0.040
	5.92	0.28	0.047

The dielectric constants showed a declining trend as frequency increased from 2 to 10 GHz and then plateaued at > 10 GHz frequency (Figure 30). Across all frequencies, HK and TK had similar and relatively high dielectric constants relative to granite, limestone, and VK. Thus, HK and TK samples are expected to absorb more heat during microwave treatment.
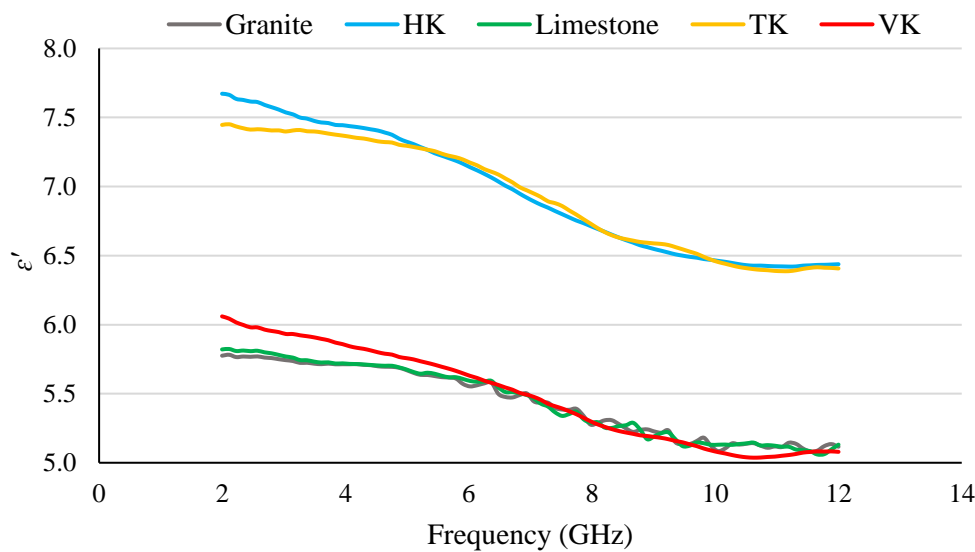
Figure 30. Dielectric constants (ε') for VK (volcaniclastic kimberlite), HK (hypabyssal kimberlite), TK (tuffisitic kimberlite), granite, and limestone from 2 to 12 GHz frequency.

For all rock types, the loss factor (Figure 31) and loss tangent (Figure 32) increased with frequency from 2 to 7 GHz, then declined from 7 to 12 GHz frequency. VK, HK, and TK had the highest loss factors and loss tangents across all frequencies, indicating that they should have a stronger ability to dissipate microwave energy.
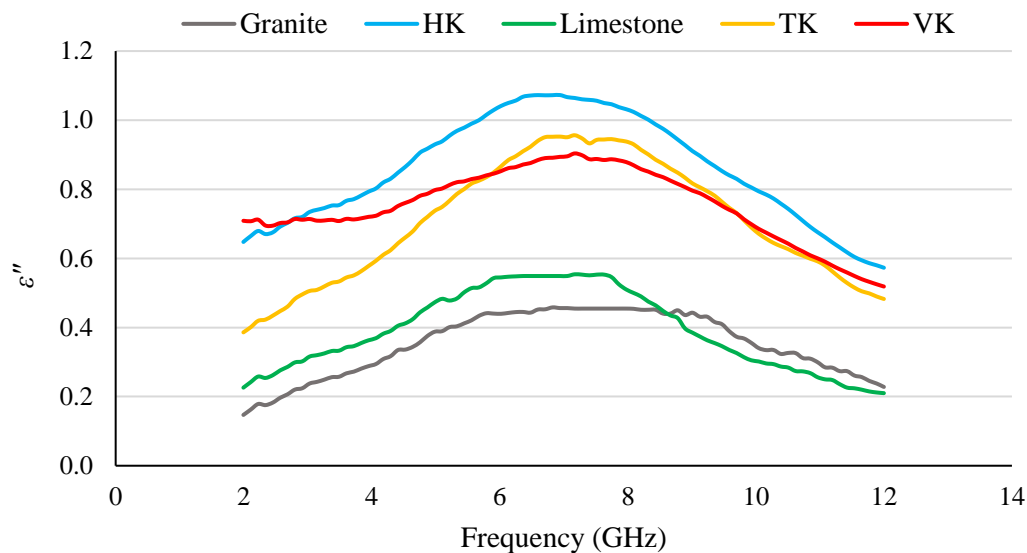
Figure 31. Loss factors (ε") for VK (volcaniclastic kimberlite), HK (hypabyssal kimberlite), TK (tuffisitic kimberlite), granite, and limestone from 2 to 12 GHz frequency.
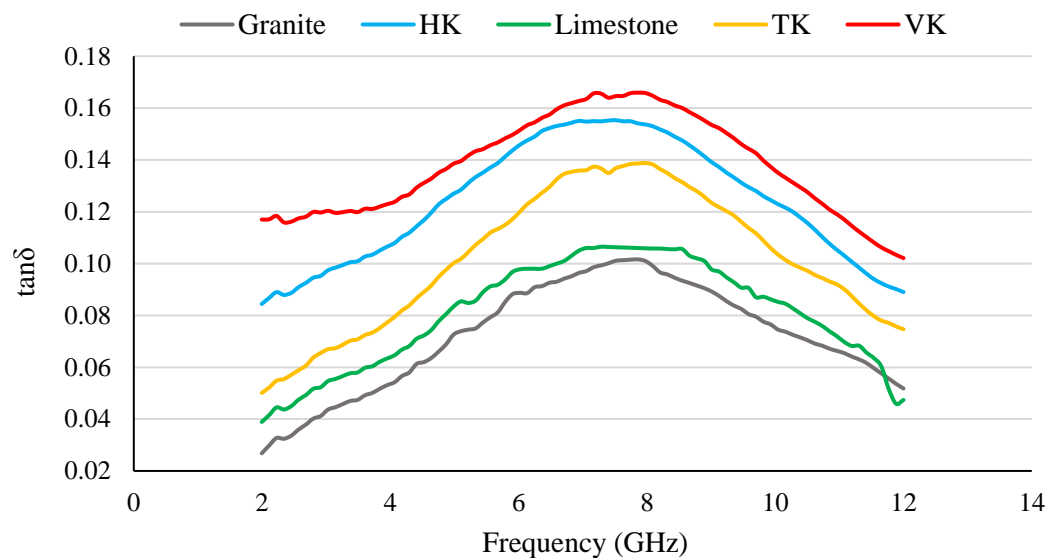
Figure 32. Loss tangents (tanδ) for VK (volcaniclastic kimberlite), HK (hypabyssal kimberlite), TK (tuffisitic kimberlite), granite, and limestone from 2 to 12 GHz frequency

3.2.4 Mineral composition

The kimberlite samples were taken randomly from the boxes and sent to the Université du Québec à Montréal (UQAM) for measuring the mineral composition.

The mineral composition of VK, HK, and TK was analyzed by X-ray diffraction. All three rock types contained illite, clinochlore, clinochrysotile, calcite, and magnetite (Table 6). Only VK contained dolomite, antigorite, and gypsum, and only TK contained microcline.

Table 6. Mineral composition of VK (volcaniclastic kimberlite), HK (hypabyssal kimberlite), and TK (tuffisitic kimberlite)

Mineral	VK	HK	TK
Illite (phlogopite)	Yes	Yes	Yes
Clinochlore	Yes	Yes	Yes
Clinochrysotile	Yes	Yes	Yes
Calcite	Yes	Yes	Yes
Magnetite	Yes	Yes	Yes
Albite	Yes	No	Yes
Quartz	Yes	No	Yes
Dolomite	Yes	No	No
Antigorite	Yes	No	No
Gypsum	Yes	No	No
Microcline	No	No	Yes

3.3 Rock sample preparation

A total of 51 core boxes containing boulders and cores extracted through blasting and drilling were obtained from Victor mine in northern Ontario and Gahcho Kue mine in the Northwest Territories (**Appendix A**). Using a 4-in (10.16-cm) wet diamond saw and applying standard cutting procedures, the 25.4 mm core samples were cut into cylinders (2:1 height: diameter) and discs (0.5:1 height: diameter) for microwave treatment and mechanical tests (Figure 33). The height and diameter of each sample were measured three times using a digital Vernier caliper, and the mean values were calculated.

Figure 33. Cylindrical (left) and disc-shaped (right) rock samples in the McGill Geomechanics Laboratory

The ends of each cylinder and disc were cut and polished according to ASTM D7012-04 (ASTM, 2004) and ASTM D3967-05 (ASTM, 2005) using a diamond wheel grinder and diamond saw, respectively (Figure 34). The specimen ends needed to be entirely flat to ensure an even distribution of the applied load in the UCS test.

Figure 34. Diamond wheel grinder (left) and diamond saw (right) in the McGill Geomechanics Laboratory.

3.4 Microwave systems

In this study, single- and multi-mode cavities were used for microwave treatments.

3.4.1 Multi-mode system

The multi-mode cavity, currently the most commonly used microwave system, is relatively simple from a mechanical perspective. The cavity is a metallic, cubed-shaped ($60 \times 60 \times 60$ cm), closed box with a frequency of 2.45 GHz (Figure 35, left). Since EM waves alternate constantly, the nodes inside the cavity constantly change location and cannot be controlled, nor can their location be calculated. To make this non-uniform energy distribution uniform, a stirrer (metallic blade) constantly scatters the EM waves in all directions inside the cavity. The power from the generator can be adjusted from 1 to 15 kW (Figure 35, right). The magnetron generates the microwaves, which are guided into the cavity through a waveguide—a hollow metallic

tube. An isolator on the waveguide ensures a one-way flow of energy: by absorbing reflected

EM waves, it protects the magnetron.
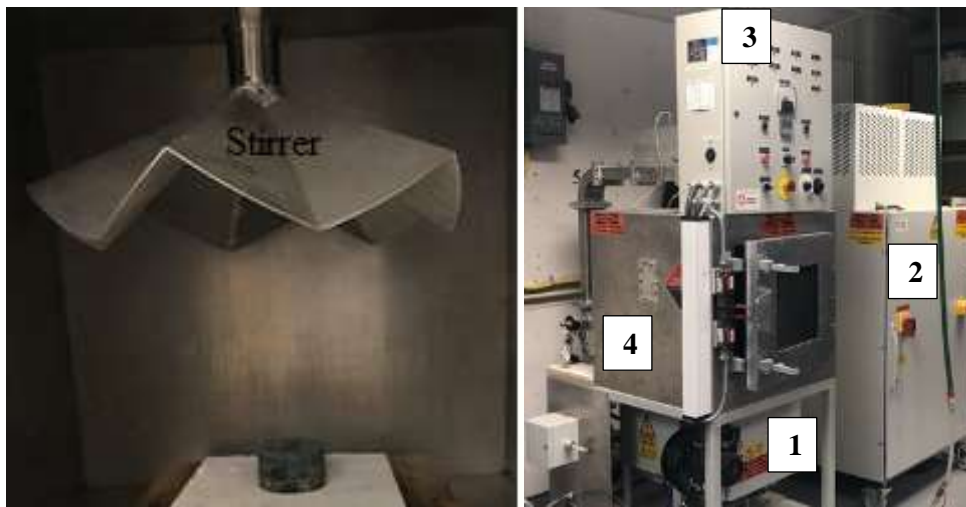
Figure 35. Multi-mode microwave cavity (left); Industrial microwave system in the McGill Geomechanics Laboratory (right) 1: magnetron; 2: power generator; 3: control system; 4: cavity; 5: waveguide.

3.4.2 Single-mode system

Single-mode cavities effectively focus microwaves in a small volume; therefore, they can create a high electric field. Because the electric field and power density are directly proportional (see Section 2.5), rapid heating is characteristic of single-mode cavities. There is no rotating stirrer fan in this system. Instead, a horn antenna on the executor at the end of the waveguide directs EM waves into the microwave cavity and focuses them (Figure 36)

Figure 36. Single-mode microwave cavity in the McGill Geomechanics Laboratory.

3.5 Heating rate and thermal profiles

Cylindrical specimens were treated for various times with ambient air in the multi-mode cavity at power levels of 2, 4, 6, 10, and 14 kW to determine the time required to reach 500°C, above which diamond crystals embedded in the rock could be damaged. At set time intervals, the surface temperature distributions on the top and center of the side of samples were measured using a Fluke TiS65 infrared thermal imaging camera (Figure 37, left). A Raynger MX4+ high-performance infrared gun was used to measure the specimen surface temperature directly (Figure 37, right). From a distance of 0.5–1 m from the specimen, the gun emits infrared light onto the surface within 20 points and calculates the mean temperature from these points. Fluke Smart View Software® 4.3 was used to analyze the infrared thermal images and obtain final temperature profiles. All results are reported as means of at least 3 to 5 experiments.

Figure 37. Fluke TiS65 infrared thermal imaging camera (left) and Raytec Raynger MX4+ high-performance infrared gun (right) is located at McGill Geomechanics Laboratory.

3.6 Mechanical properties

Microwave-treated specimens were cooled to room temperature before mechanical property testing. Untreated specimens served as controls. All results are reported as means of at least 3 to 5 experiments.

3.6.1 UCS

The UCS test is commonly used to quantify the rock's mechanical strength. It is also used to predict tunnel boring machine performance. A total of 412 treated and untreated (control) cylindrical rock samples (Table 7) were subjected to UCS tests according to ASTM D7012-04 (ASTM, 2004). The presence of fractures in some samples excluded them from UCS testing.

Table 7. Number of VK (volcaniclastic kimberlite), HK (hypabyssal kimberlite), TK (tuffisitic kimberlite), granite, and limestone samples subjected to strength tests

Rock type	Unconfined compressive strength (cylinders)	Brazilian tensile strength (discs)
VK	165	207
HK	60	101
TK	16	28
Granite	124	95
Limestone	47	115
Total	**412**	**546**

Treated specimens were subjected to 5, 10, and 15 kW of microwave power using a multi-mode cavity for up to 140 s. Treated and control specimens were placed in a loading frame on a metallic plate on a servo-controlled MTS 250 MN compression machine equipped with a 250 kN load cell (Figure 38). The top of the sample was restrained by the top plate attached to a calibrated load cell. As the top plate was raised, an axial load was applied to the sample. Loading continued until the sample developed an obvious shearing plane or the deformations became excessive. The UCS (σ_{UCS}, MPa) is defined as the maximum load, F (kN), per unit area, A (mm^2) (equation 18):

$$\sigma_{ucs} = \frac{F}{A} \tag{18}$$

Figure 38. Servo-controlled MTS 250 MN compression machine at the McGill Geomechanics Laboratory.

3.6.2 BTS

The BTS test is a geotechnical laboratory test that is commonly used for the indirect measurement of rock tensile strength due to its simplicity and efficiency. It is also used to predict tunnel boring machine performance. BTS tests were conducted on 546 disc-shaped treated and untreated samples (Table 7) according to ASTM D3967-05 (ASTM, 2005) using a Wykeham Farrance 100 kN mechanical gearbox press machine (Figure 39). Specimens were treated with 3 kW microwave power for up to 180 s using a multi-mode cavity, then subjected to two opposing normal loads at the disc periphery. The load was increased at a constant rate until failure. The σ_{BTS} depends on the material and ranges from 10 to 50 MPa. At failure, the BTS of the rock is calculated as follows:

$$\sigma_{BTS} = \frac{2P}{\pi Dt} \tag{19}$$

Where P is the applied load (N), D is the sample diameter (mm), and t is the sample thickness (mm). This equation uses the theory of elasticity for continuous isotropic media. It gives the tensile stress perpendicular to the loaded diameter at the center of the disc at the time of failure.

Figure 39.Wykeham Farrance 100 kN mechanical gearbox press machine at the McGill Geomechanics Laboratory.

3.6.3 CAI

The CAI test quantifies abrasivity, which can be used to predict the wear of equipment for tunneling, underground construction, mining, and quarrying. Abrasion is the wearing or tearing away of particles and material from a solid surface. The CAI test is based on a standard steel pin with a 90° conical tip, a diameter of at least 6 mm, a visible length of at least 15 mm, and known hardness. The pin is moved over the surface of the rock sample (CERCHAR, 1986) or is held stationary and the rock sample is moved under it (West, 1989). The CERCHAR device includes a dead weight, pin chuck steel pin, specimen, vice, and hand lever (Figure 40).

Figure 40. CERCHAR Abrasivity Index apparatus.

The CAI test was conducted according to ASTM D7625-10,2010 (ASTM, 2010) on the saw-cut cylindrical sample surfaces prepared for UCS tests (Figure 41 left) before and after 30-s exposure to 15 kW power microwaves using a multi-mode cavity. Each rock sample was firmly clamped in the rigid vice to prevent lateral movement. A static load of 70 N was then placed on the top of the pin, which was carefully lowered onto the rock surface and moved across the surface for 10 mm at 10 mm/s to scratch the rock. After the test, the flat wear on the tip was measured under a microscope to calculate the CAI. The CAI is equal to 10d, where d is the diameter of flat wear (mm) to an accuracy of 0.01 mm (Geotechdata, 2016). After each use, the tool tip was sharpened using a cutter grinder machine (Figure 41 right).

Figure 41. Rock cylindrical sample (left) and Cutter grinder machine(right)

Abrasivity is an essential parameter affecting the lifetime and disc cutter penetration depth per revolution (P$_{Rev}$; equations 20–22) of tunnel boring machines (Wijk, 1992; Hassani, 2010a):

$$L = \sum dw^3 \frac{\cot\theta}{Fn\sqrt{\sigma_{UCS}\sigma_{PLT}\,(CAI)^2}} \tag{20}$$

$$P_{Rev} = 3940 \frac{F}{\sigma UCS} \tag{21}$$

$$P_{Rev} = 624 \frac{F}{\sigma_{BTS}} \tag{22}$$

Where L is the distance that a disc cutter can roll on hard rock (m); P_{Rev} is the penetration per revolution (m/$_{Rev}$) ; d is the disc cutter diameter (m); w is the thickness of the disc cutter edge (m); θ is the angle of the disc cutter edge (°); F is the normal load applied to the disc cutter (N); P is the disc cutter rolling force (N); x is the disc cutter penetration depth (m); Ψ is the Auxiliary angle parameter (Figure 42); and σ_{UCS}, σ_{PLT}, and σ_{BTS} are the rock UCS, point load strength (PLT), and BTS (all in MPa), respectively.
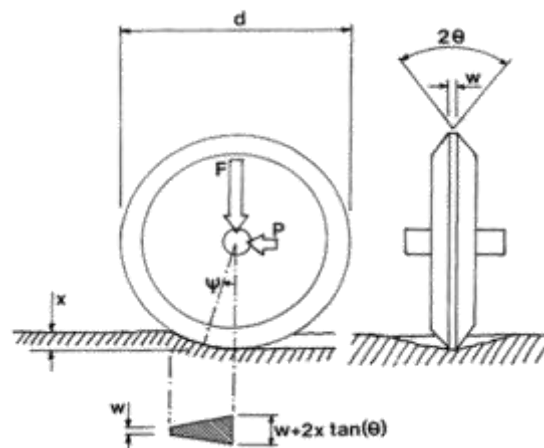
Figure 42. A disc cutter rolling on the rock surface (Wijk,1992).

3.6.4 Pulse sound velocity

A portable, ultrasonic, non-destructive digital indicating tester (PUNDIT) provided by Proceq Inc. (Figure 43) was used to measure the sound propagation speed through untreated and rock samples treated with microwave power levels of 5, 10, and 15 kW for up to 135 s using multi-mode cavity (Figure 35, left). Olympus Couplant B-glycerin was used to keep the rook and the transducers in good contact for efficient sound transmission. The pulse sound velocity for disintegrated samples was considered to be zero. Due to a shortage of intact specimens, tests were not conducted on limestone and TK.

Figure 43. PUNDIT device attached to a rock sample for pulse sound velocity measurement at the McGill Geomechanics Laboratory.

3.6.5 K_{IC} using the NSCB method

Sample preparation is easy for NSCB testing because the specimen has a simple geometry consisting of a semi-circular disc with a notch in the middle (Figure 44a). The disc is laid on two roller supports and another roller applies a load from the top (Figure 44b). The sample bends due to tension at the bottom and compression on top. In addition, since the crack is at the bottom, the tension is perpendicular to the crack (i.e., it will experience Mode I loading).

a)   b)
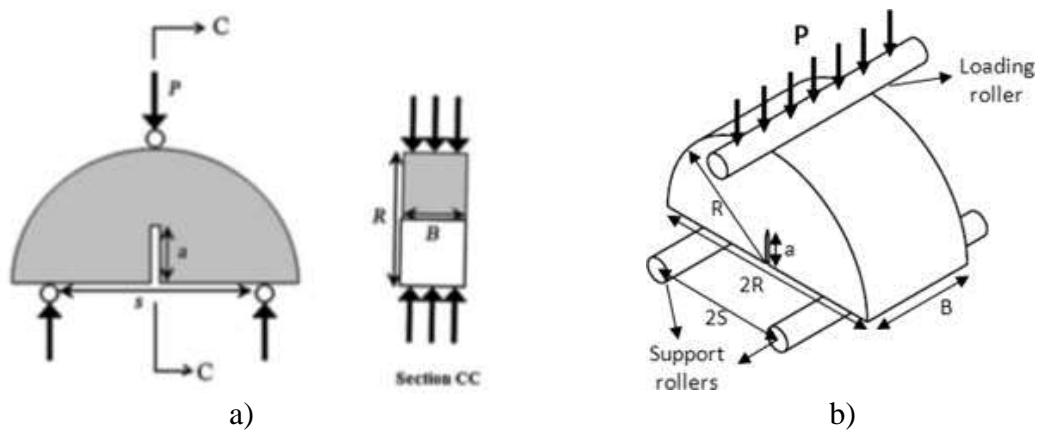
Figure 44. a) Notched semi-circular bend sample geometry and b) sample loading configuration (Tutluoglu and Keles, 2011; Kuruppu et al., 2014)

The load is steadily and slowly increased to avoid any dynamic effects, and the applied load and position of the rollers are continuously measured until the sample reaches the point of

failure (Figure 45). The test is invalid if the crack deviates more than 5% of the sample diameter from the notch plane, which would indicate that pure Mode I failure was not achieved.
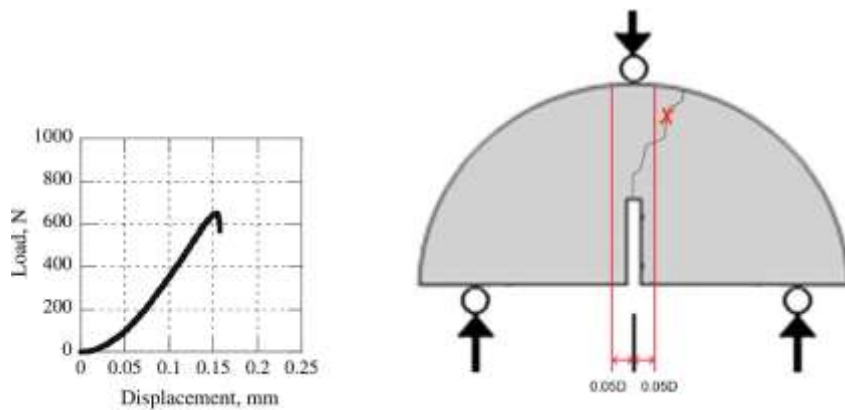
Figure 45. Notched semi-circular bend testing procedure

Since K is a function of the geometry of the sample and the applied stress, its derivation is unique to each situation, and formulas are often obtained through complex numerical analysis via computation software. Based on the geometry in Figure 45, the following formula was developed (ASTM, 2016; Chong and Kuruppu, 1984; Kuruppu et al., 2014):

$$K_{Ic} = Y' \frac{P_{max}\sqrt{\pi a}}{2RB} \tag{23}$$

$$Y' = -1.297 + 9.516\left(\frac{s}{2R}\right) - \left(0.47 + 16.457\left(\frac{s}{2R}\right)\right)\beta + \left(1.071 + 34.401\left(\frac{s}{2R}\right)\right)\beta^2 \tag{24}$$

$$\beta = \frac{a}{R} \tag{25}$$

Where P_{max} is the maximum load observed at failure; a is the notch length, B is disc thickness, R is disc radius (mm), Y' is dimensionless stress intensity factor, and s is the span between the supports, β is the dimensionless geometry factor. The specimen dimensions suggested by the International Society of Rock Mechanics are listed in Table 8; the thickness is adjusted based on the specimen diameter (Figure 46).

Table 8. Recommended dimensions of notched semi-circular bend specimens(Kuruppu et al., 2014)

Dimension	Value or range
Diameter (D)	Larger of $10 \times$ grain size or 76 mm
Thickness (B)	Larger of 0.4D or 30 mm
Crack length (a)	$0.4 \leq \frac{a}{R} (= \beta) \leq 0.6$
Span length (s)	$0.5 \leq \frac{s}{2R} \leq 0.8$
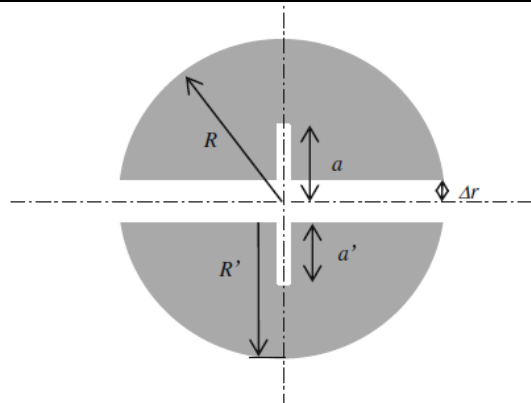
Figure 46. Proposed geometric guidelines for notched semi-circular bend specimens.

Other recommendations to ensure the accuracy of the results are:

- $t_{notch\ blade} = 1.5 \pm 0.2$ mm

- $D_{roller}{:}D = 1{:}20$, and $D_{roller} \geq 5$ mm

- If $2\Delta r > 0.05D$, $R = R' + \Delta r$, and $a = a' + \Delta r$ where $2\Delta r$ is the thickness of the saw used to cut the sample into two semi-circles.

- The plane surface along the thickness direction should be flat to 0.01 mm.

- The notch shall not depart from perpendicularity to the plane surface in the thickness direction by more than 0.5°.

- The plane of the resulting discs should not deviate from the perpendicularity to the core axis by more than 0.5°.

- When cutting a disc into two semi-circular discs, the cutting plane must not deviate by more than 0.2 mm from the diameter.

- The notch length should be averaged from both sides of the semi-circular disc. The

two readings should be within 2% of each other.

- The notch thickness should be uniform and shall not deviate by more than 0.2 mm

- A suitable recess on the top-loading plate may be required to hold the roller in position.

- Samples containing pre-existing cracks should not be analyzed because when the energy input is high, the crack will propagate through the existing cracks, rather than following the notch (e.g., along the blue line in Figure 47).

Figure 47. Unacceptable crack propagation within the sample.

3.6.5.1 Sample preparation and test set-up

Kimberlite (VK) rocks with 63 mm diameter cores and cut precisely into cylinders and the intact blocks of basalt cut from quarries in Chifeng, China was drilled at the McGill Geomechanics laboratory using a radial drilling machine to obtain cylindrical core samples with diameters of 50 mm and 70 mm. The cylindrical samples were sliced into disks with the dimensions shown in (Table 9) using a 4-inch wet diamond saw. Both ends of the samples were then grinded and flattened using a diamond wheel grinder machine.

Table 9. Dimensions of notched semi-circular bend basalt specimens

Descriptions	Value (mm)		
Diameter (D)	50	63	70
Thickness (B)	20	30	30
Crack length (a)	10	17.05	18.1
Span length (s)	39	44.2	45

A custom-made jig facilitated notched disc sample preparation (Figure 48a). The notch was machined using a diamond saw from the middle bottom of the disc (Figure 48b).

a)   b)   c)   d)
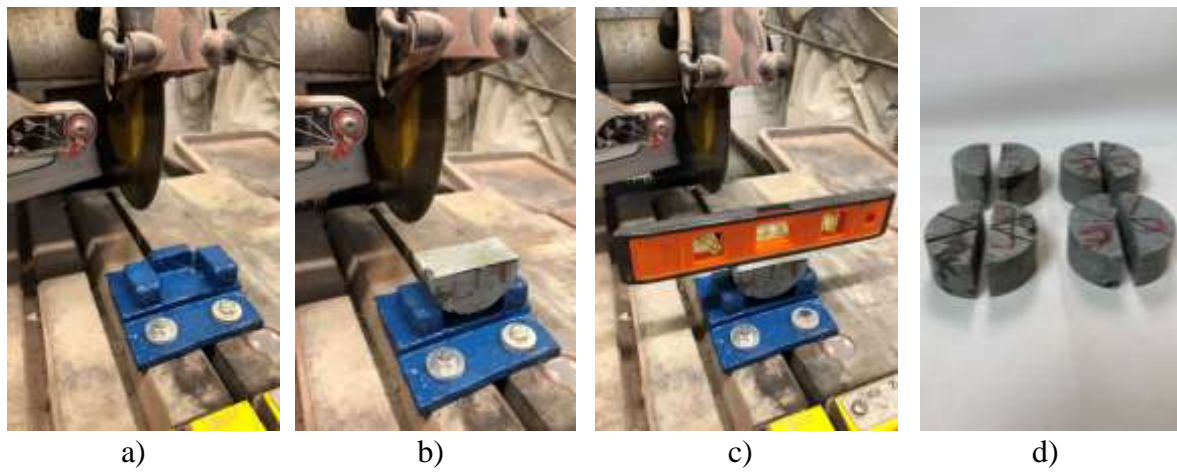
Figure 48. Sample preparation for fracture toughness testing: a) custom-made jig; b: creating notch length in disc; c) sample positioning, and d) notched semi-circular bend samples.

Sample diameter, cutting direction to produce semi-circular shapes, and position in the single-mode cavity were optimized. Samples with a small diameter are prone to higher error during cutting and notching, but samples with a larger diameter, though easier to cut and notch, require more materials and sample mass.

3.6.5.2 Experimental procedure

To investigate the direction of disc sample cutting, 50-mm diameter discs were cut on the heating line or perpendicular to the heating line, then irradiated with 3 kW microwaves for 4 s. To determine the optimum sample position within the cavity, samples were placed 15, 25, 35, 55, 75, and 95 mm from the horn antenna, treated with 3 kW power for 5 s, and placed directly inside the calorimeter to measure the absorbed heat and determine the most efficient position within the cavity. The HOME (Heat Over Microwave Efficiency) parameter is defined as shown in equation (31) (section 3.9) (Hassani et al., 2020). The K_{Ic} was determined after treatment with 3 kW power for 50 mm semi-circular discs (exposure times 4–7 s), 63 mm discs (10, 20, and 30 s) and 70 mm discs (10, 20, and 30 s).

The treated samples were placed on two roller supports for the fracture toughness test and were loaded by the vertical compressive load (P) using the Humboldt rig. (Figure 49a).

a)   b)
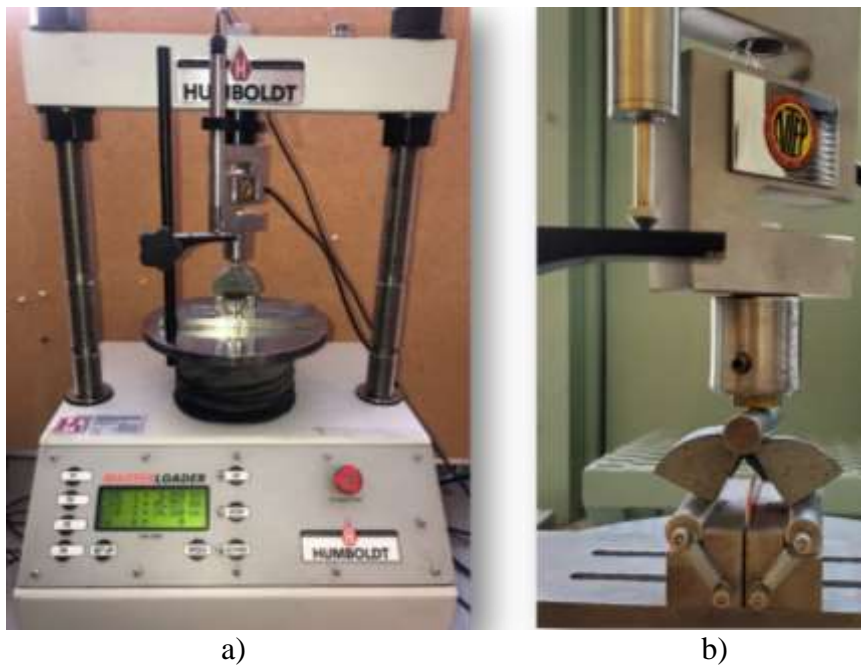
Figure 49. a) Fracture toughness test rig at the McGill Geomechanics Laboratory
and b) failed sample

The WOME (Weakening over Microwave Energy) expresses the weakening effects of the microwave treatment process by normalizing strength reduction (from MPa to % of K_{IC}) (Hassani et al., 2020) and then dividing that by the microwave energy input:

$$WOME = \frac{\text{strength reduction percentage achieved}}{\text{microwave energy input (kWh/t)}} \tag{26}$$

3.7 Ramp-up time

Calorimetry was used to measure the delay between the microwave energy generated and when it was transmitted from the magnetron to the microwave cavity by the waveguide. This ramp-up time is neglected in most studies. To quantify the ramp-up time, 1 L of water was exposed for 3–20 s to 5, 10, or 15 kW power. The heat energy (kJ) absorbed by water after microwave treatment was calculated using the equation: $Q = mCp \, \Delta T$.

3.8 Microwave energy efficiency analysis

To lower energy requirements for continuous mining, it is necessary to investigate the total energy efficiency of microwave irradiation of hard rocks. Calorimetry makes it possible to accurately determine the amount of heat/energy absorbed by samples after microwave treatment by considering all losses. It is important to know the weight of the sample to be used in the energy calculations. Therefore, each sample is weighed before the microwave treatment, then it is placed in the calorimeter. The temperature of the water inside the calorimeter will increase and the temperature of the rock will decrease until the rock and water reach the thermal equilibrium. Based on thermodynamic law, the heat lost by the rock (Qr, kJ) is equal to the heat gained by the water (Qw, kJ; equation 27). m_r is rock sample mass (Kg), $C_{p,r}$ is the specific heat capacity of the rock sample (J/Kg/°C), m_w is the Water mass in the calorimeter (Kg), $C_{p,w}$ is the specific heat capacity of the water (J/Kg/°C), T_w, the initial temperature of water prior to calorimetry (°C), The equilibrium temperature (T_{eq}, in (°C)) is integrated into the energy balance relation (equation 29) to calculate the rock sample temperature after microwave treatment (T_r in (°C); equation 30).

$$Qr = Qw \tag{27}$$

$$(mC_p\Delta T)r = (mC_p\Delta T)w \tag{28}$$

$$m_r\, C_{p,r}\,(T_r - T_{eq}) = m_w\, C_{p,w}\,(T_{eq} - T_w) \tag{29}$$

$$T_r = T_{eq} + \frac{m_w\, C_{p,w}\,(T_{eq} - T_w)}{m_r\, C_{p,r}} \tag{30}$$

3.9 Energy absorption analysis

The efficiency of converting microwave energy to heat within the rock sample was calculated using the Heat Over Microwave Efficiency (HOME) (Hassani et al., 2020), defined as the ratio of heat absorbed to the total microwave energy input (equation 31).

$$\text{HOME} = \frac{Heat\ Absorbed}{Total\ Microwave\ Energy} = \frac{m_r\ C_{p,r}\ (T_{i,r} - \boldsymbol{T_r})}{P_{in}\Delta t} \tag{31}$$

Where P_{in} is the microwave power input (kW), Δt is the microwave exposure time (s), and $T_{i,r}$ is the initial temperature of the rock sample before microwave treatment (°C).

3.9.1 Distance from the antenna in a single-mode cavity

EM waves are not disseminated in a single-mode cavity; thus, it is crucial to optimize the position and arrangement of samples relative to the horn antenna to maximize the HOME. The effects on HOME were tested on basalt for:

1. The vertical orientation of the long axis of one, two, or three 50×100 mm cylinders (Figure 50a–c);

2. The horizontal orientation of the long axis of one 50×100 mm cylinder (Figure 50 d);

3. 50 or 70 mm diameter and 20 or 30 mm thick discs (Figure 50 e); and

4. 20×15×10 cm (L×W×H) slabs to represent field conditions at a rock face more closely (Figure 50 f).

a)   b)   c)
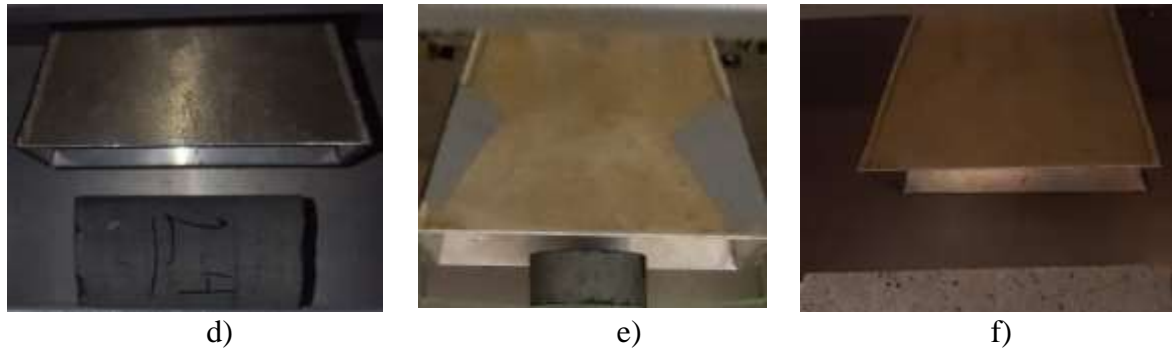
Figure 50. Basalt samples inside the single-mode microwave cavity: a) one vertical cylinder, b) two vertical cylinders, c) three vertical cylinders, d) horizontal cylinder, e) disc and f) slab.

Cylinders were exposed to 15 kW power for 15 s at distances ranging from 10 to 160 mm from the horn antenna. Discs were exposed to 3 kW power for 5 s at distances ranging from 15 to 95 mm from the antenna. Slabs were exposed to 15 kW power for 15 s at distances ranging from 15 to 95 mm from the antenna. After microwave treatment, cylinder, disc, and slab samples were immediately placed in the calorimeter for HOME analysis (section 3.9).

3.10 WOME analysis

As mentioned in section 3.6.5.2 and (equation 26), the WOME also expresses the weakening effects of the microwave treatment process by normalizing strength reduction (from MPa to % of UCS) (Hassani et al., 2020). Therefore, after studying the best position and the arrangement of the samples inside the single-mode cavity and calculating the HOME, it was essential to examine the efficiency of single-mode cavities in order to achieve better WOME. Thus, a series of experiments on basalt rocks were conducted to achieve higher microwave energy efficiency. Then, these experiments were compared with those achieved for the same (cylindrical and slab) samples of basalt tested under multi-mode cavity settings which were conducted by (Lu et al., 2019a; Lu et al., 2019b).

3.11 Quenching effect on BTS after microwave treatment in a single-mode cavity

Fifteen basalt samples were cut into 50 mm diameter ×25 mm height discs. Five replicates were subjected to each treatment: 1) control (no microwave treatment), 2) microwave treated and rapidly cooled, and 3) microwave treated and air-cooled. Treated samples were exposed to 15 kW of power for 5 s using the single-mode cavity. For rapid cooling, samples were placed directly inside the calorimeter at 22°C for 2 min., while for the air-cooling, the samples were cooled at 22°C for 20 min. Then, BTS testing was conducted (Section 3.6.2).

Chapter 4 Results and Discussion

The results are presented in this chapter as thermal analysis of the rock samples, mechanical properties, ramp-up time, Energy absorption behavior in a single-mode cavity, WOME analysis and Quenching effect on strength reduction after microwave treatment.

4.1 Thermal analysis: kimberlite, granite, and limestone

At a given power level, the surface temperature of all samples increased with exposure time (Figure 51–Figure *55*). As the power level increased, the rate of temperature increase became faster. Thus, a shorter exposure time was required to reach a given temperature at higher power levels. The heating rates at 14 kW exposure (slopes of regression lines in Figure 51–Figure *55*) are exactly as expected based on the complex permittivity ($\varepsilon = \varepsilon' + \varepsilon''$, a measure of a material's ability to absorb EM energy (Table 5). That is, TK had the highest complex permittivity and it heated the most quickly (7.91°C/s; Figure 53) followed by HK (7.78 °C/s; Figure 52) and VK (6.35 °C/s; Figure 51), whereas granite had the lowest complex permittivity and it heated the most slowly (4.82°C/s; Figure 54).
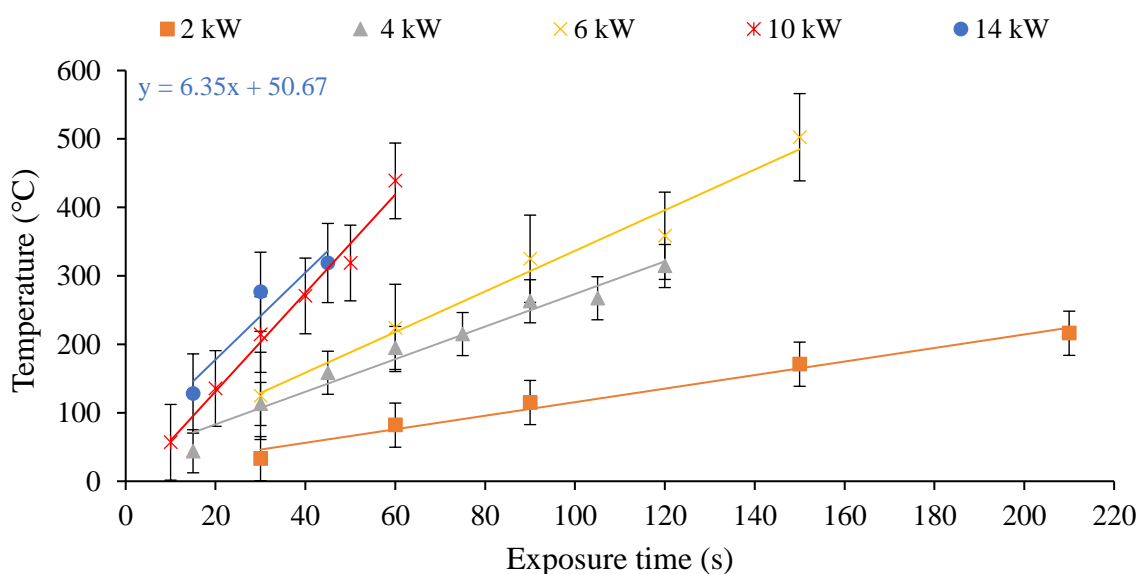
Figure 51. Mean (± SD) surface temperature of volcaniclastic kimberlite vs. microwave exposure time at five microwave power levels; regression equation is for the 14 kW line.
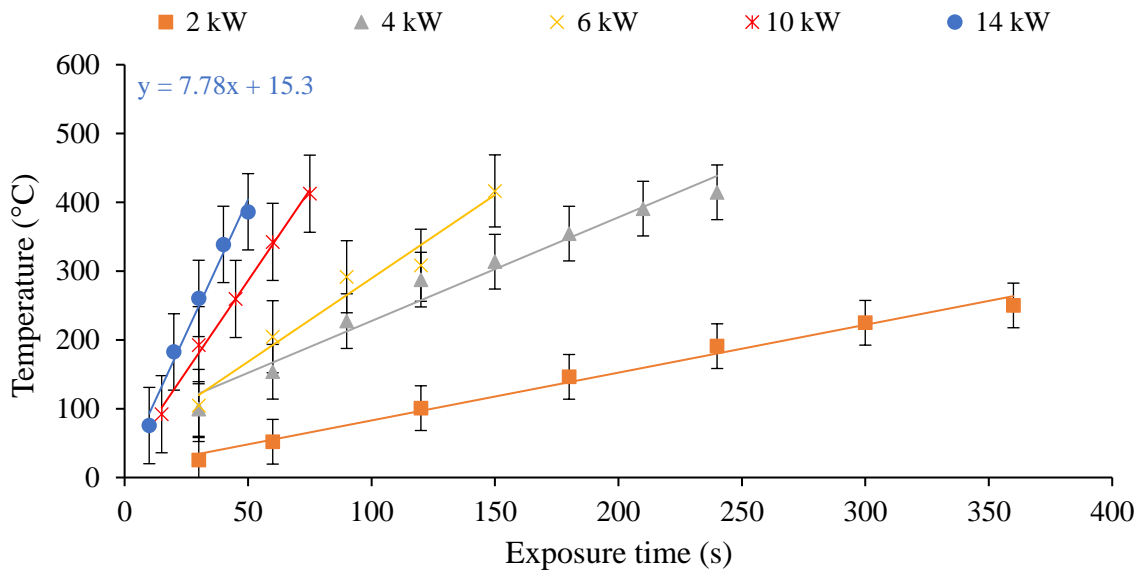
Figure 52. Mean (± SD) surface temperature of hypabyssal kimberlite vs. microwave exposure time at five microwave power levels; regression equation is for the 14 kW line.
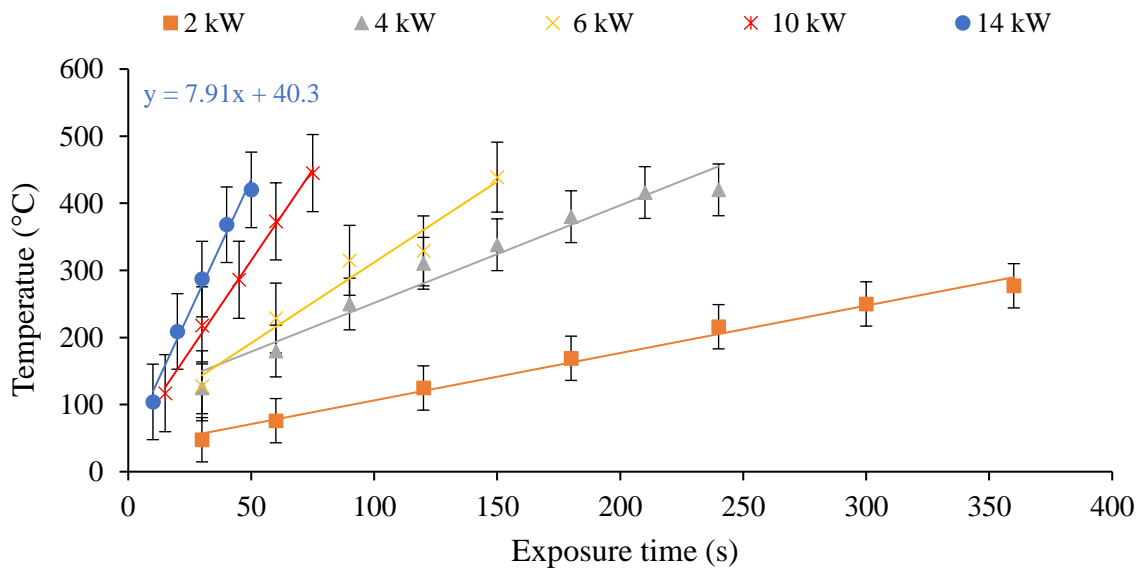
Figure 53. Mean (± SD) surface temperature of tuffisitic kimberlite vs. microwave exposure time at five microwave power levels; regression equation is for the 14 kW line.
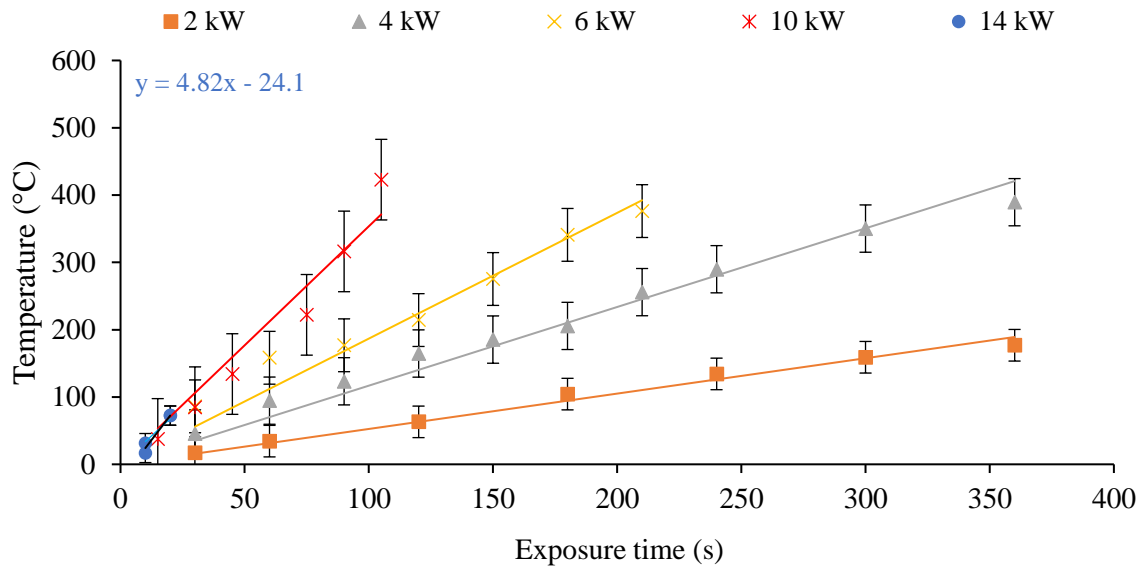
Figure 54. Mean (± SD) surface temperature of granite vs. microwave exposure time at five microwave power levels; regression equation is for the 14 kW line.
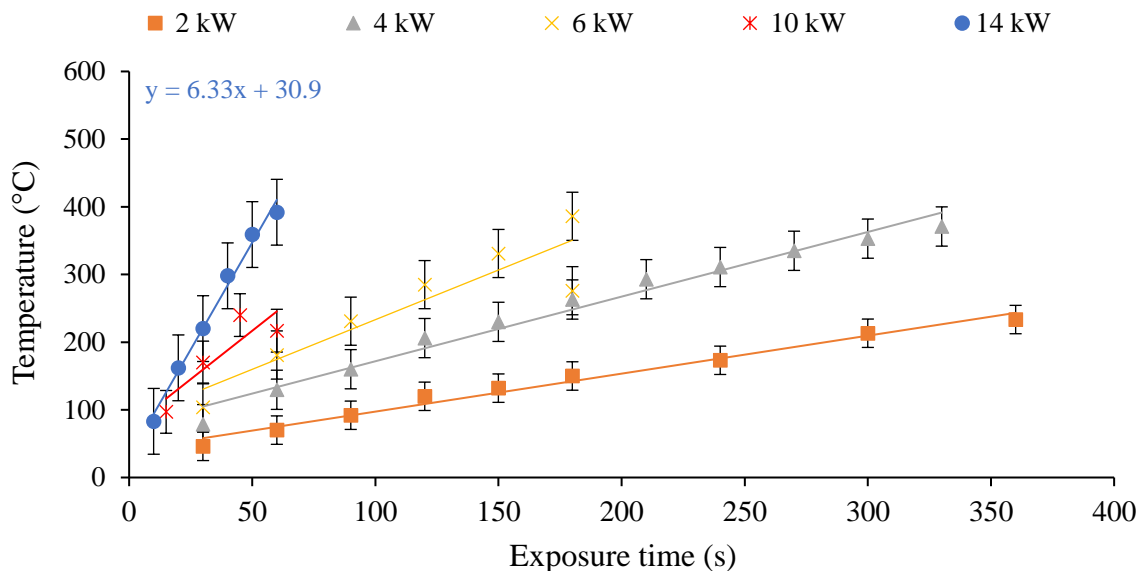
Figure 55. Mean (± SD) surface temperature of limestone vs. microwave exposure time at five microwave power levels; regression equation is for the 14 kW line.

Although the heating rate was as expected based on the complex permittivity, the final surface temperature was not as expected in the case of limestone. The complex permittivity of limestone was low, but it had the second highest surface temperature among the five rock types. At 14 kW power over a 50 s exposure time, limestone heated slowly (6.33°C/s; Figure 55), but the final surface temperature was 392°C, compared to 420, 386, 319, and 72°C for TK, HK,

VK, and granite, respectively. This might be due to the low loss tangent of limestone (Table 5): it did not readily dissipate heat energy and retained heat better than HK, VK, and granite.

4.2 Mechanical properties

4.2.1 UCS

The mean UCS for untreated samples was highest for granite (136 MPa; Figure 59) and lowest for TK (58 MPa; Figure 58). The UCS of all samples decreased with microwave exposure time at rates that increased with power level. For example, the UCS of VK decreased by 0.09, 1.06, and 2.97 MPa/s after treatment at 5, 10, and 15 kW power, respectively (Figure 56). Low power levels had a minimum effect on the UCS of VK (i.e., 17% reduction at 5 kW power after 115 s), whereas at 10 kW and 30 s exposure, the UCS decreased by 47%, and at 15 kW power, VK samples completely fragmented after 25 s of microwave treatment. HK lost strength most rapidly at the highest power level (Figure 57) and specimens disintegrated and extensively cracked after 40 s such that the UCS was zero. For TK, 59 and 66% reductions in UCS were measured after 45 s of microwave exposure at 5 and 10 kW power, respectively (Figure 58). Granite exhibited a similar pattern to VK: the UCS was zero by 30 and 50 s of treatment with 15 and 10 kW power (Figure 59). For limestone, the UCS declined similarly to TK, that is, by 56 and 59% at 5 and 10 kW power levels after 45 s (Figure 60). 10 kW was one of the power levels common to all rock types. The highest rate of UCS reduction at 10 kW power was observed for granite (2.65 MPa/s; Figure 59) and the lowest was for TK (0.864 MPa/s; Figure 58). For TK and limestone, 15 kW could not be applied as a result of limited samples as the majority of them were received as broken cores from the mine.
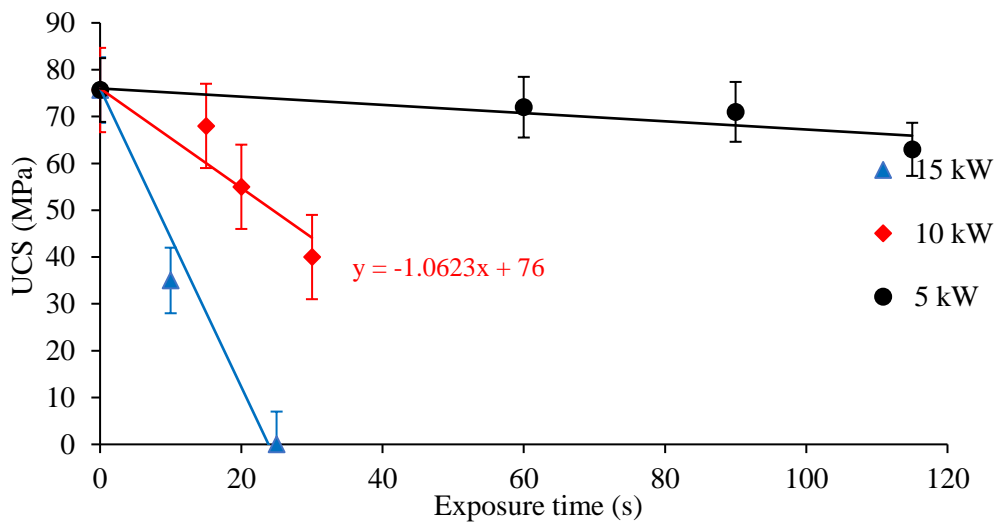
Figure 56. Mean (± SD) unconfined compressive strength (UCS) of volcaniclastic kimberlite vs. exposure time for three microwave power levels; regression equation is for the 10 kW line.
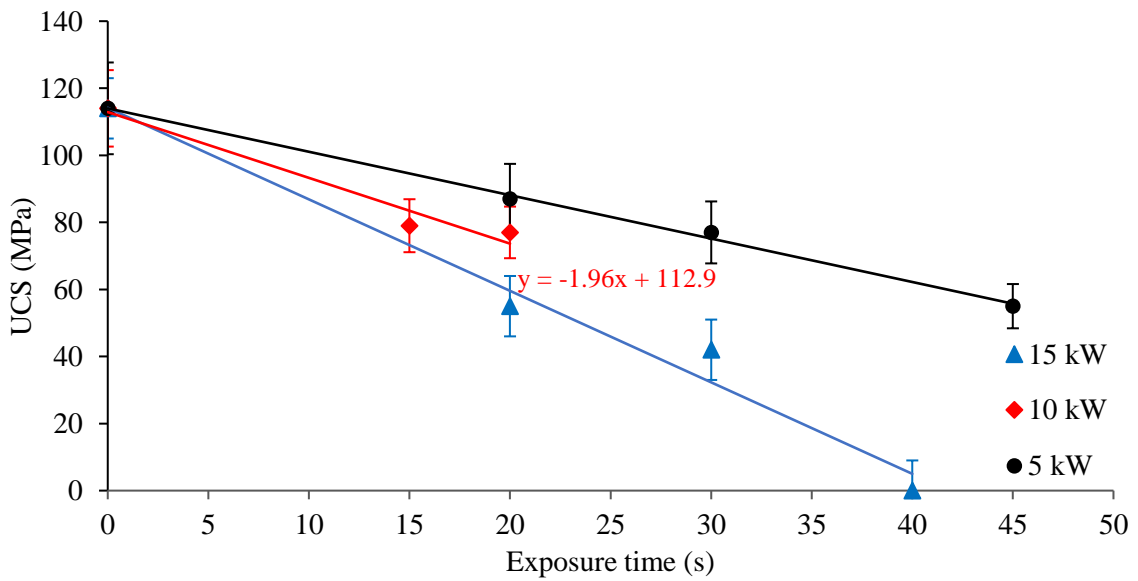
Figure 57. Mean (± SD) unconfined compressive strength (UCS) of hypabyssal kimberlite vs. exposure time for three microwave power levels; regression equation is for the 10 kW line.
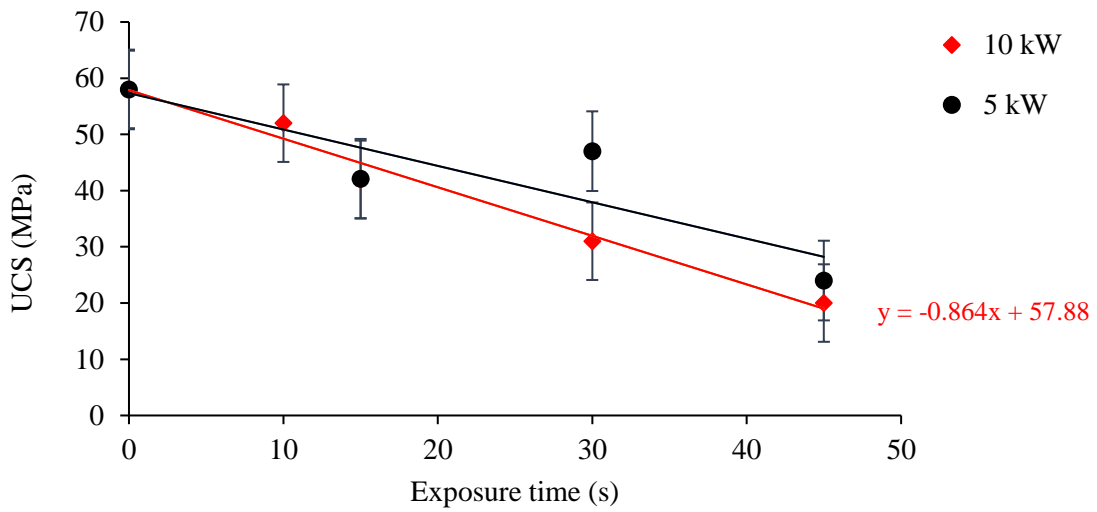
Figure 58. Mean (± SD) unconfined compressive strength (UCS) of tuffisitic kimberlite vs. exposure time for two microwave power levels; regression equation is for the 10 kW line.
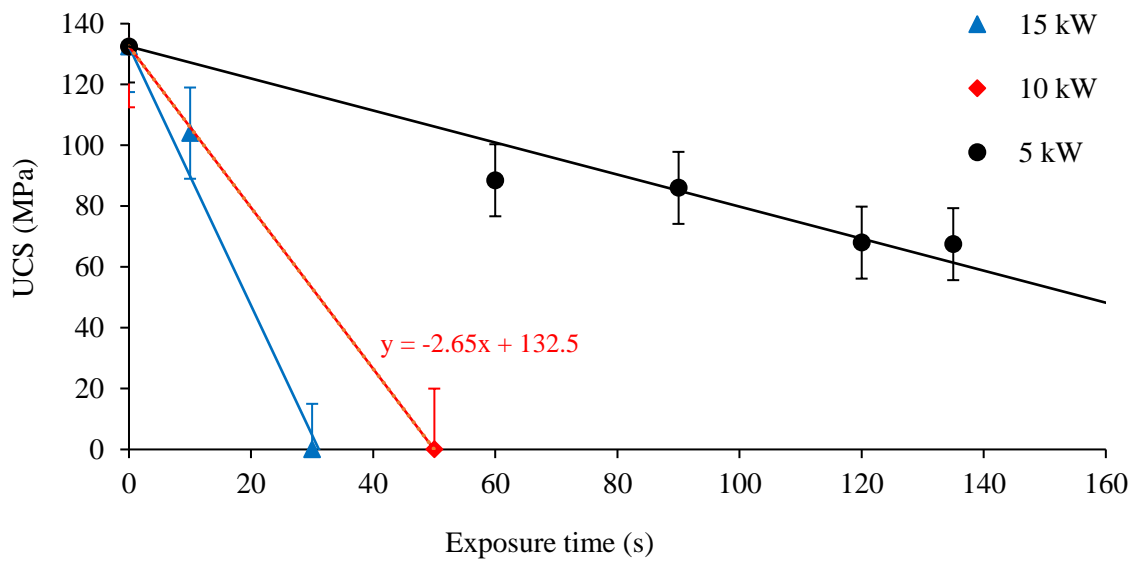
Figure 59. Mean (± SD) unconfined compressive strength (UCS) of granite vs. exposure time for three microwave power levels; regression equation is for the 10 kW line.
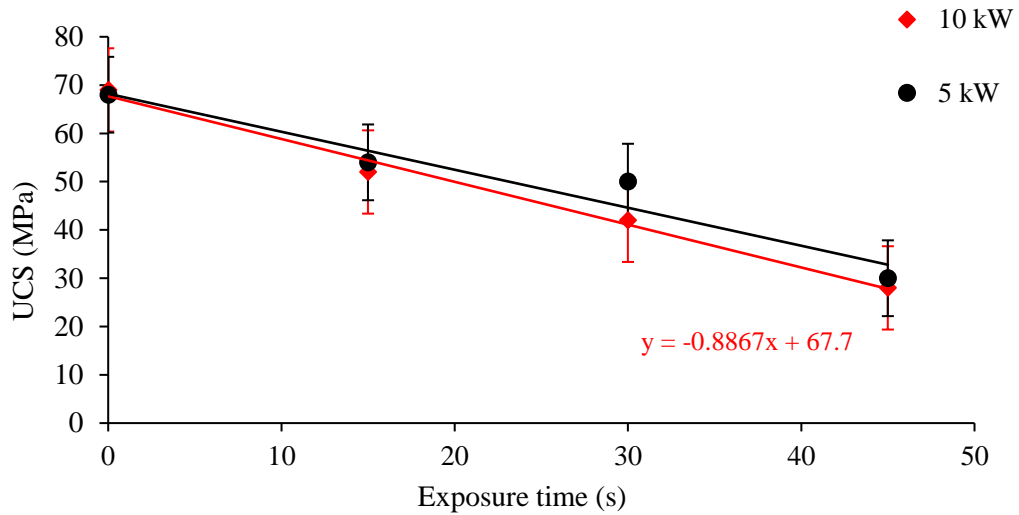
Figure 60. Mean (± SD) unconfined compressive strength (UCS) of limestone vs. exposure time for two microwave power levels; regression equation is for the 10 kW line.

4.2.2 BTS

The mean BTS of untreated VK, HK, TK, granite, and limestone were 8.75, 8.54, 7.00, 12.6, and 4.90 MPa, respectively (Figure 61–Figure 65). The BTS decreased the most rapidly for VK (Figure 61) upon exposure to 3 kW power microwaves (0.079 MPa/s) such that, after 60 s of exposure, the BTS decreased by 59% (8.75 to 3.59 MPa). In comparison to VK, BTS reduction at 60 sec for HK and TK was recorded as (34% and 24% at rates of 0.027 and 0.0382 MPa/s; Figure 62 and Figure 63). The lowest relative BTS reduction was observed for granite and limestone (14% and %19 reductions by 60 s at rates of 0.029 and 0.0115 MPa/s; Figure 64 and Figure 65).
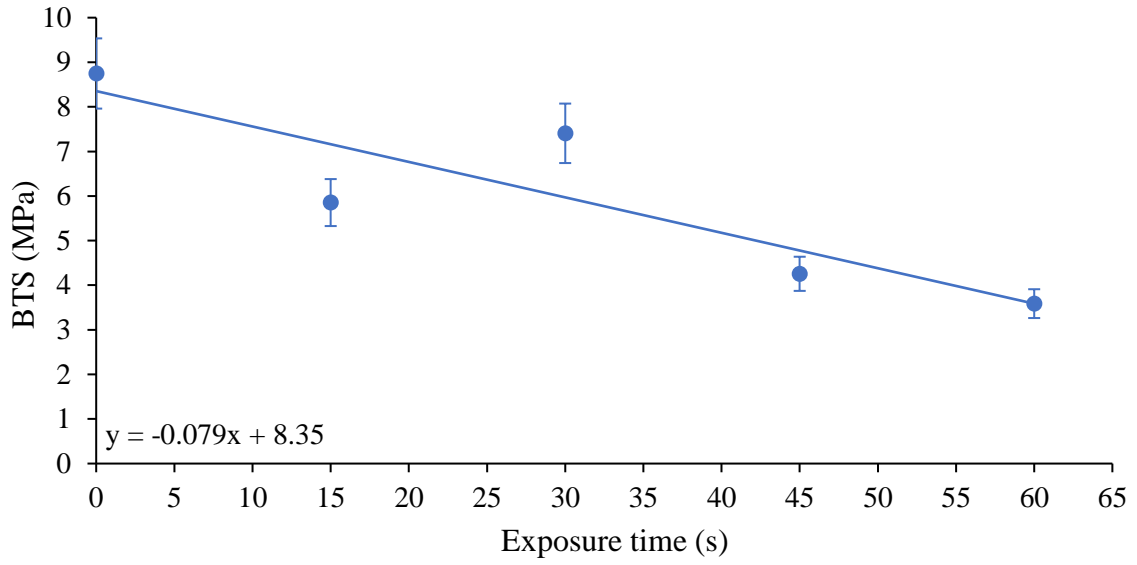
Figure 61. Mean (± SD) Brazilian tensile strength (BTS) of volcaniclastic kimberlite vs. exposure time at 3 kW microwave power level.
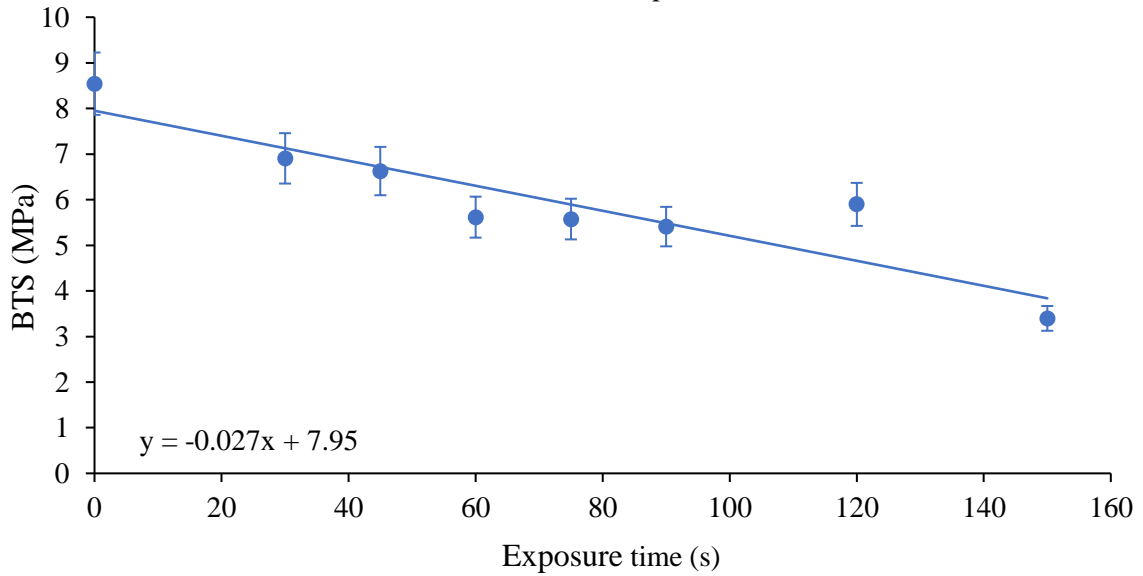
Figure 62. Mean (± SD) Brazilian tensile strength (BTS) of hypabyssal kimberlite vs. exposure time at 3 kW microwave power level.
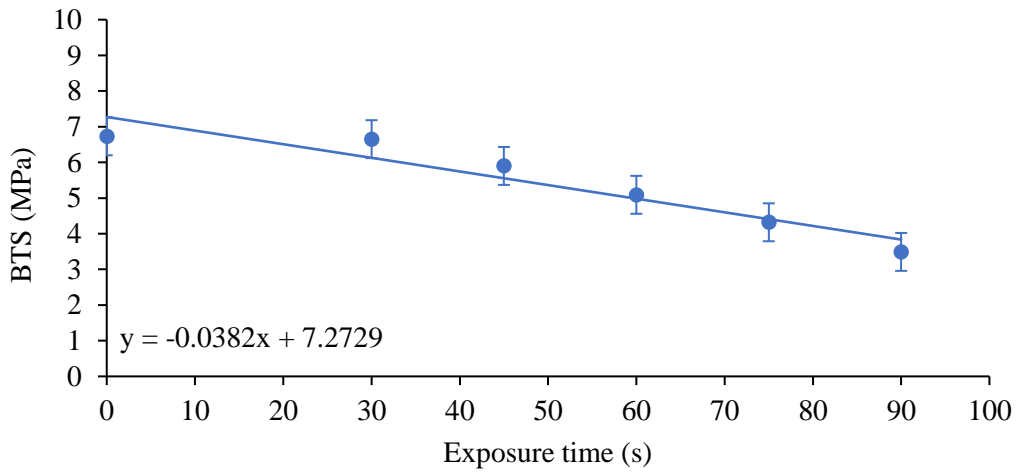
Figure 63. Mean (± SD) Brazilian tensile strength (BTS) of tuffisitic kimberlite vs. exposure time at 3 kW microwave power level.
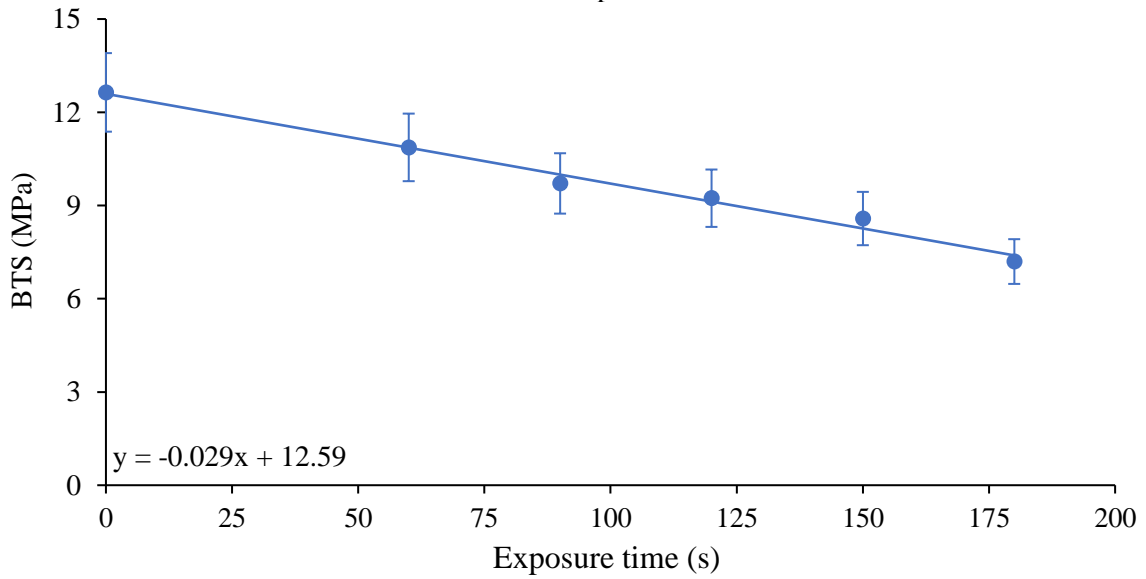
Figure 64. Mean (± SD) Brazilian tensile strength (BTS) of granite vs. exposure time at 3 kW microwave power level.
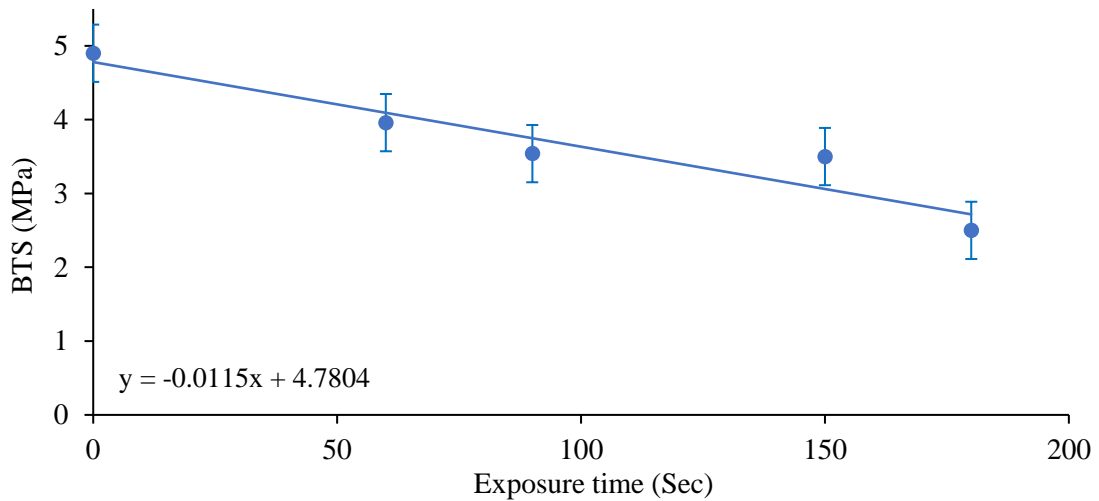
Figure 65. Mean (± SD) Brazilian tensile strength (BTS) of limestone vs. exposure time at 3 kW microwave power level.

4.2.3 CAI

The CAI was not affected by microwave treatment for 30 s at 15 kW power (Figure 66). The specimens could not be treated for longer due to the disintegration and melting of some samples.
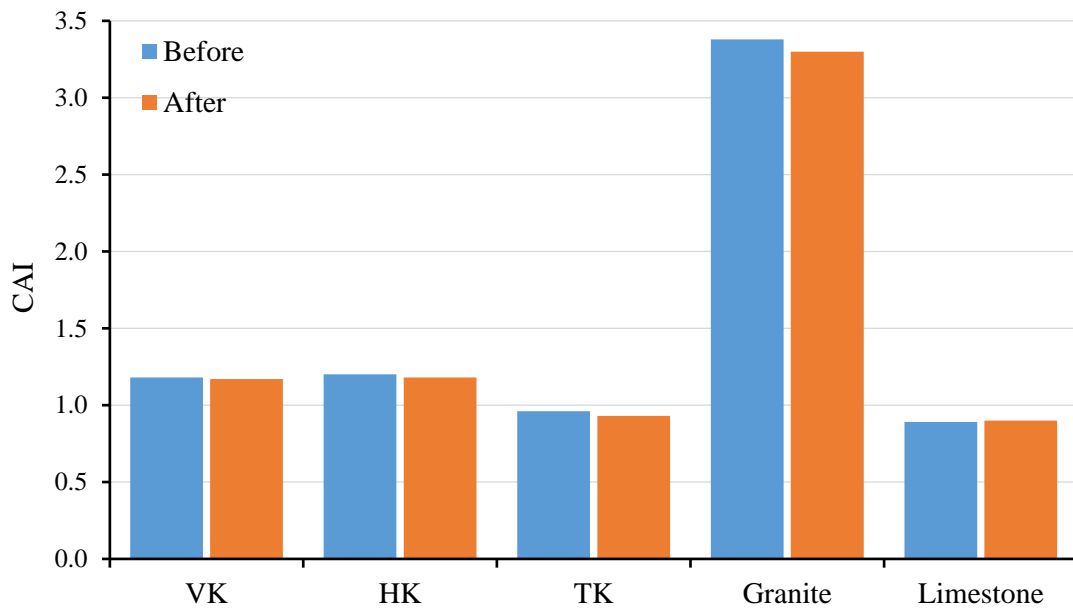
Figure 66. CERCHAR Abrasivity Index (CAI) for five rock types before and after 30-s exposure to 15 kW microwave power.

4.2.4 Pulse sound velocity

The pulse sound velocity for VK, HK, and granite decreased after microwave treatment (Figure 67–Figure 69). The percentage of the change increased with microwave power level and exposure time.
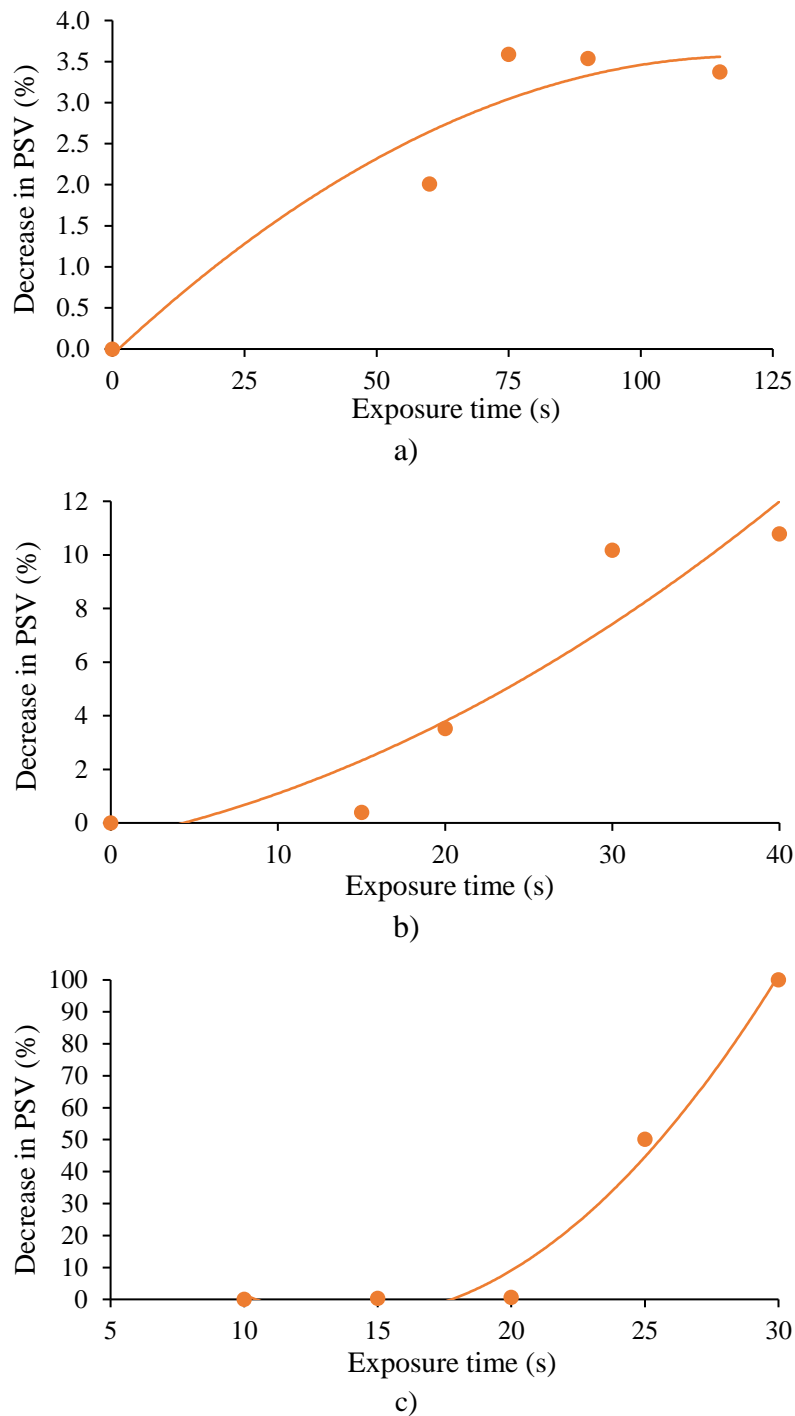
Figure 67. Magnitude of mean pulse sound velocity (PSV) decrease vs. exposure time to a) 5 kW, b) 10 kW, and c) 15 kW microwave power for volcaniclastic kimberlite.
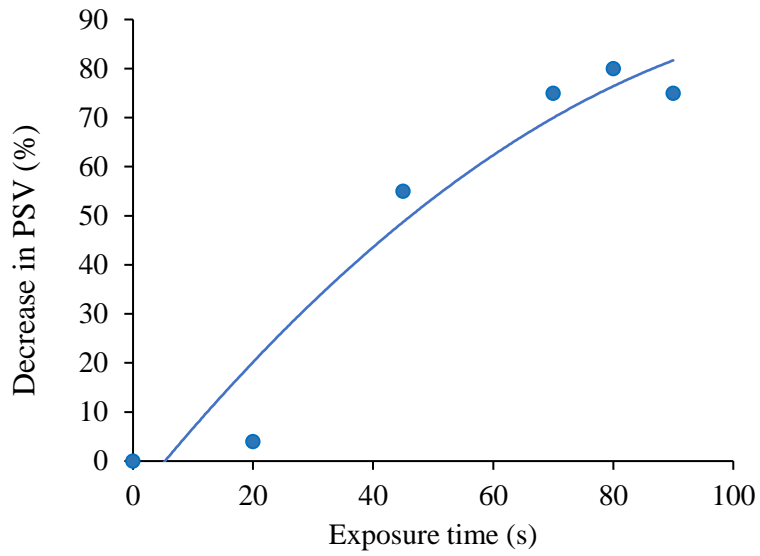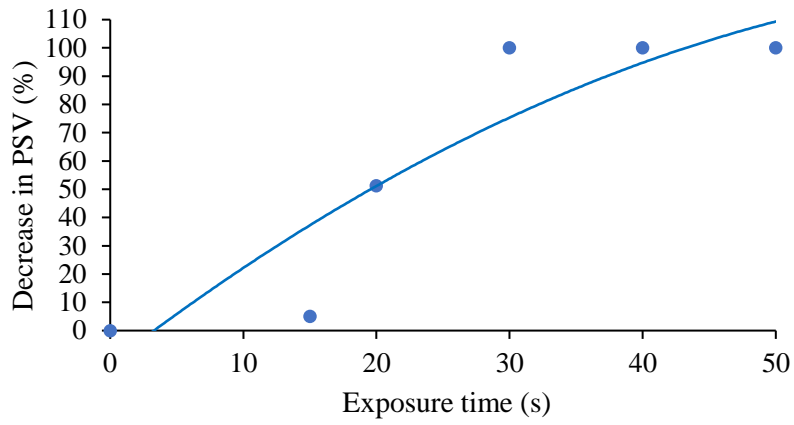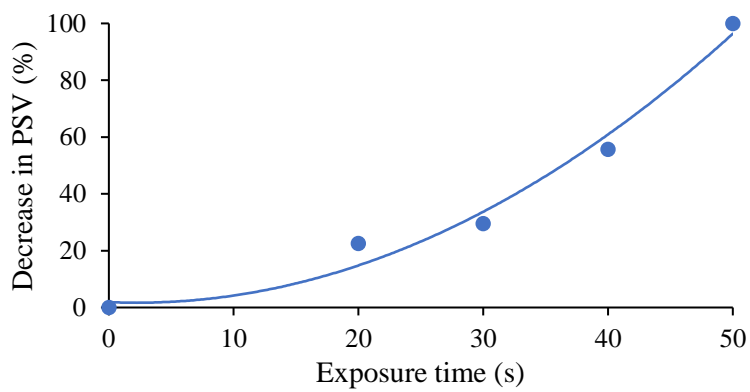
Figure 68. Magnitude of mean pulse sound velocity (PSV) decrease vs. exposure time to a) 5 kW, b) 10 kW, and c) 15 kW microwave power for hypabyssal kimberlite.
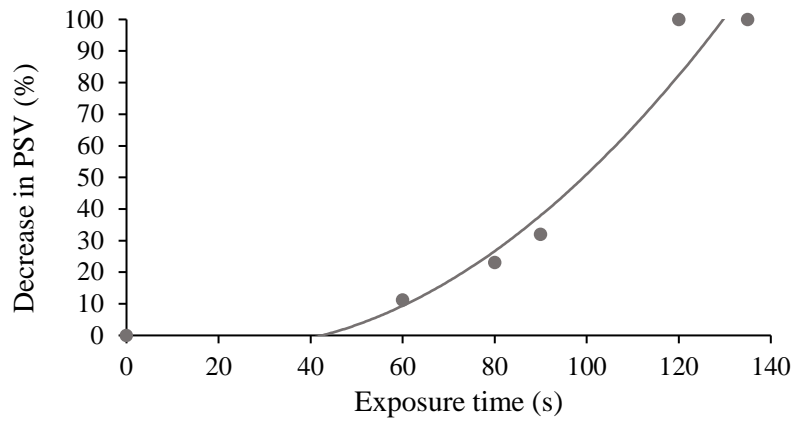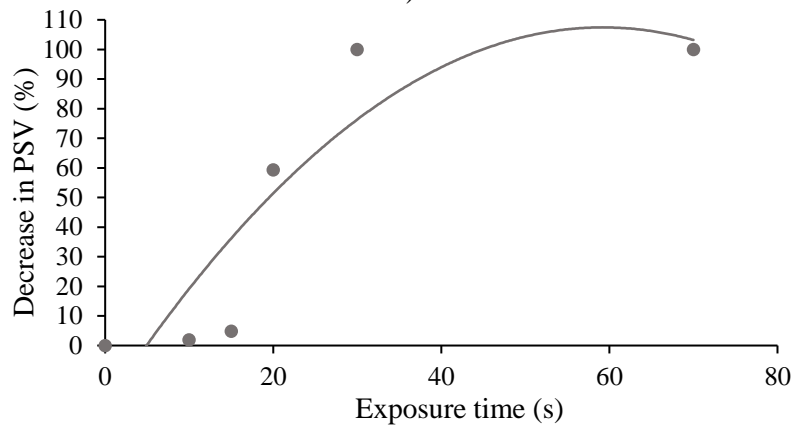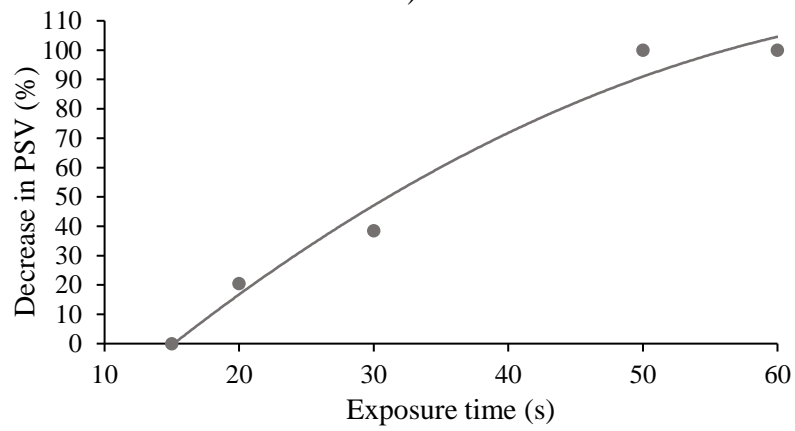
Figure 69. Magnitude of mean pulse sound velocity (PSV) decrease vs. exposure time to a) 5 kW, b) 10 kW, and c) 15 kW microwave power for granite.

4.2.5 K_{IC}

For kimberlite samples, the results show that increasing the exposure time decreased the K_{IC} of the samples (Figure 70).
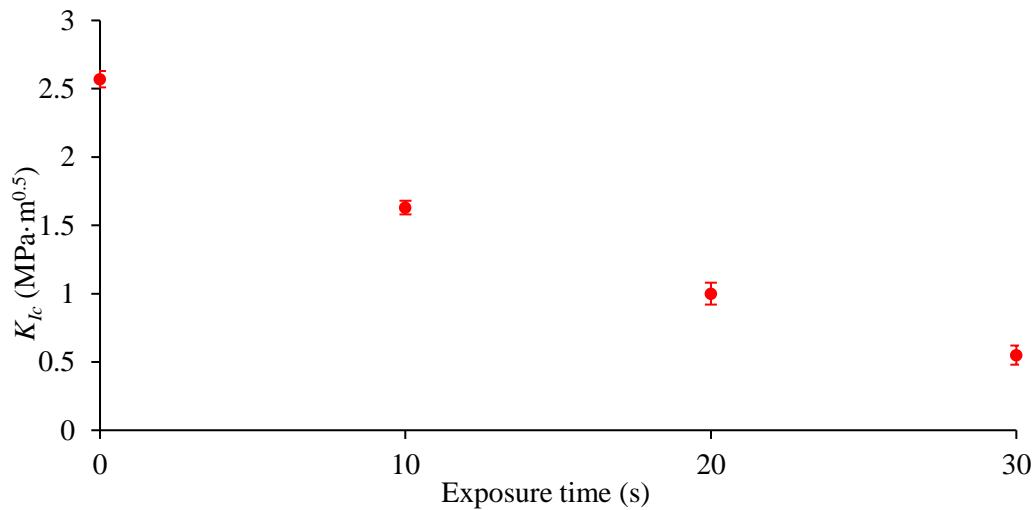
Figure 70. Mean (±SD) stress intensity factor (K_{IC}) of 63-mm diameter kimberlite discs cut before treatment at 3 kW power for 10, 20, or 30 s at a distance of 15 mm from the horn antenna.

The mean K_{IC} of basalt discs did not differ with disc diameter, but the variation around the mean was lower at 70 mm diameter than at 50 mm diameter (Figure 71). The 70 mm diameter was considered optimal in terms of variation and material consumption for testing.
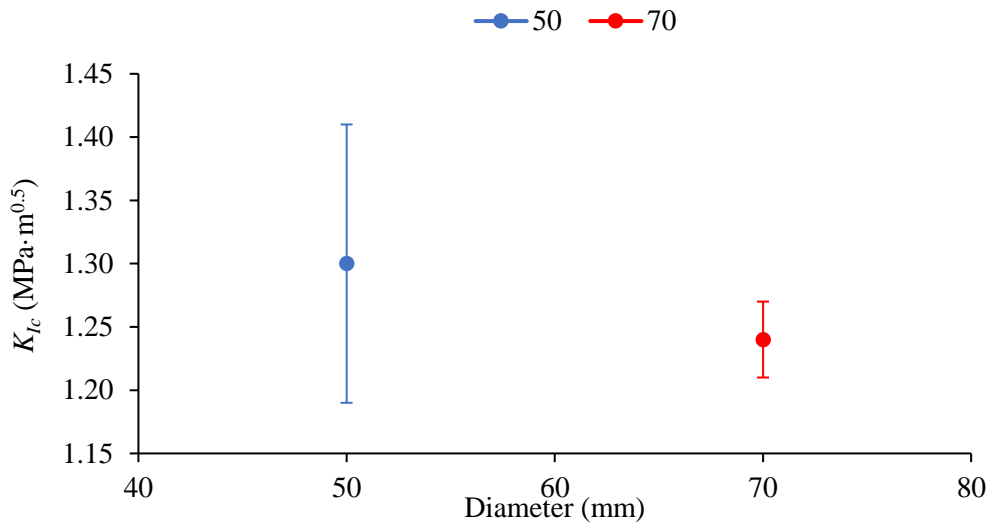
Figure 71. Stress intensity factor under (K_{IC}) vs. diameter of untreated basalt discs.

Based on the HOME data in section 4.4, the direction of sample cutting was determined for basalt discs. For the 50 mm diameter discs, a non-uniform heating line was created in the middle of the disc by microwave irradiation (Figure 72 a), which will cause a non-uniform effect on sample strength at different locations. Cutting the sample on the heating line affected K_{IC} more than cutting the sample perpendicular to the heating line (Figure 72 b).
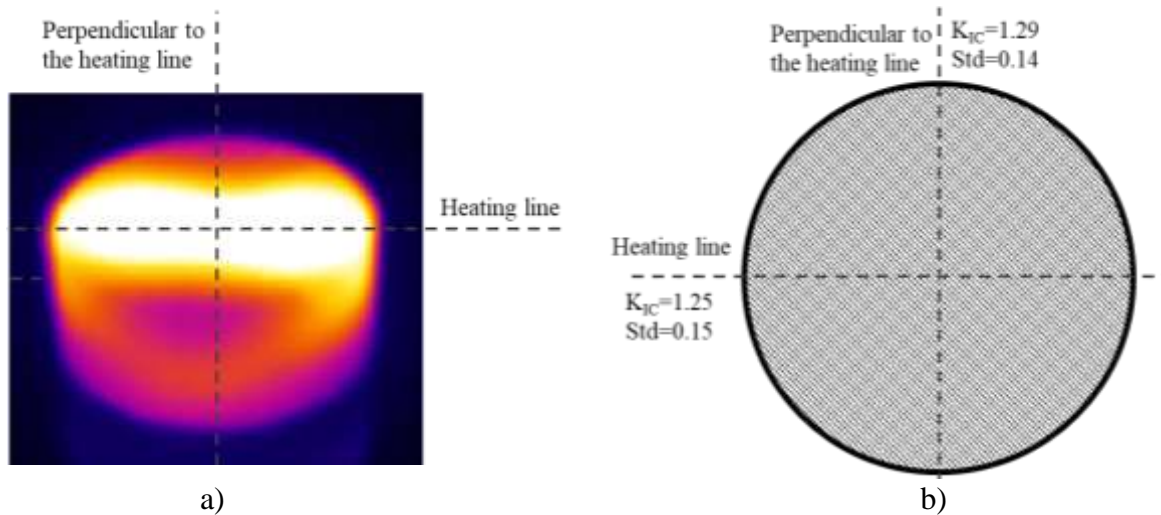
Figure 72. Effect on the stress intensity factor (K_{IC}) of 50-mm diameter basalt discs of cutting on and perpendicular to the heating line

Cutting the 50 mm basalt discs before microwave treatment enhanced the effect of irradiation on K_{IC} relative to than cutting the sample after microwave treatment (Figure 73).

96
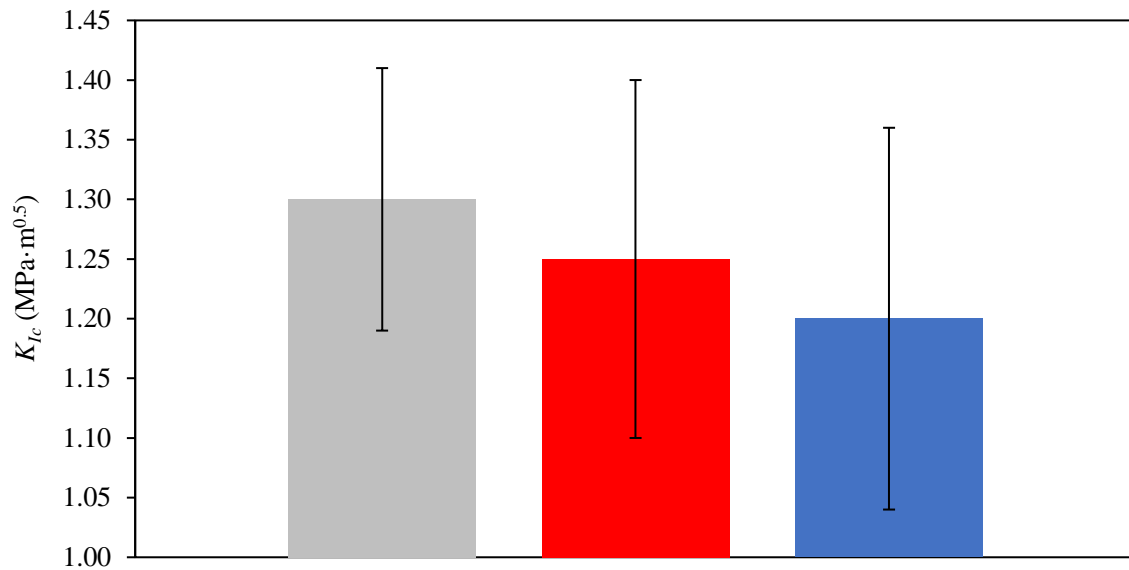
Figure 73. Mean (±SD) stress intensity factor (K_{IC}) of 50-mm diameter basalt discs untreated (grey), cut after treatment (red), and cut before treatment (blue) at 3 kW power for 4 s at a distance of 15 mm from the horn antenna.

Since the variation around the mean was higher for 50 mm diameter and one exposure time was used (4 s), the exposure was not considered for 50 mm diameter and the work was continued on 70-mm diameter.

For 70-mm diameter basalt discs, increasing the exposure time from 10 to 30 s decreased the K_{IC} (Figure 74). Cutting the samples before microwave treatment enhanced the effect of the treatment on K_{IC} relative to cutting the discs after treatment. This is that cutting the sample into discs and creating the notch using the saw will cause the cracks, especially around the notch; and then the sample will be exposed to microwave irradiation which will cause more cracks leading the sample to be more weak.
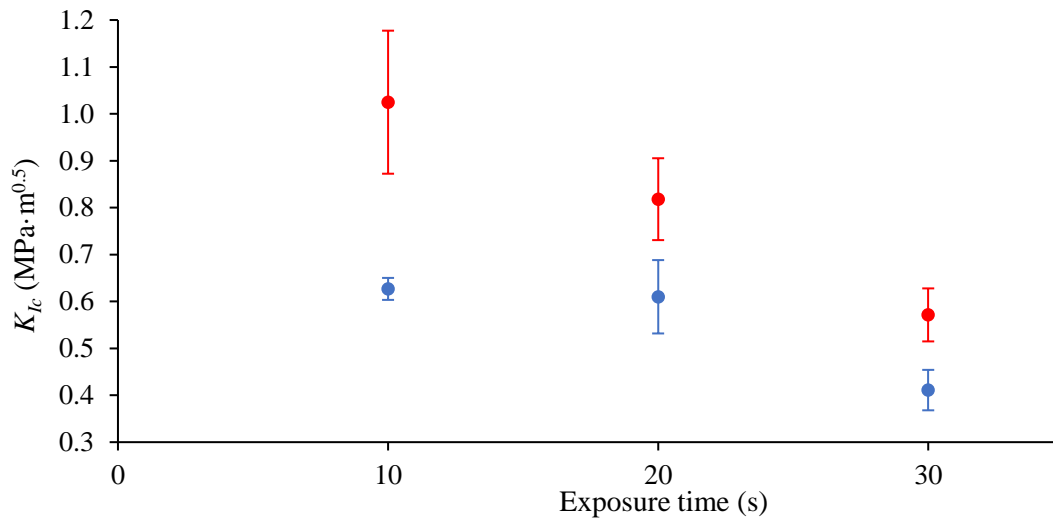
Figure 74. Mean (±SD) stress intensity factor (K_{IC}) of 70-mm diameter basalt discs cut after treatment (red) and cut before treatment (blue) at 3 kW power for 10, 20, or 30 s at a distance of 15 mm from the horn antenna.

Although increasing the exposure time enhanced the strength reduction of K_{IC} of basalt discs, this increase was not energy efficient: the WOME decreased with increasing exposure time (Figure 75). The highest WOME (2.32%/kWh/t) was achieved by cutting the sample before and testing after microwave treatment.
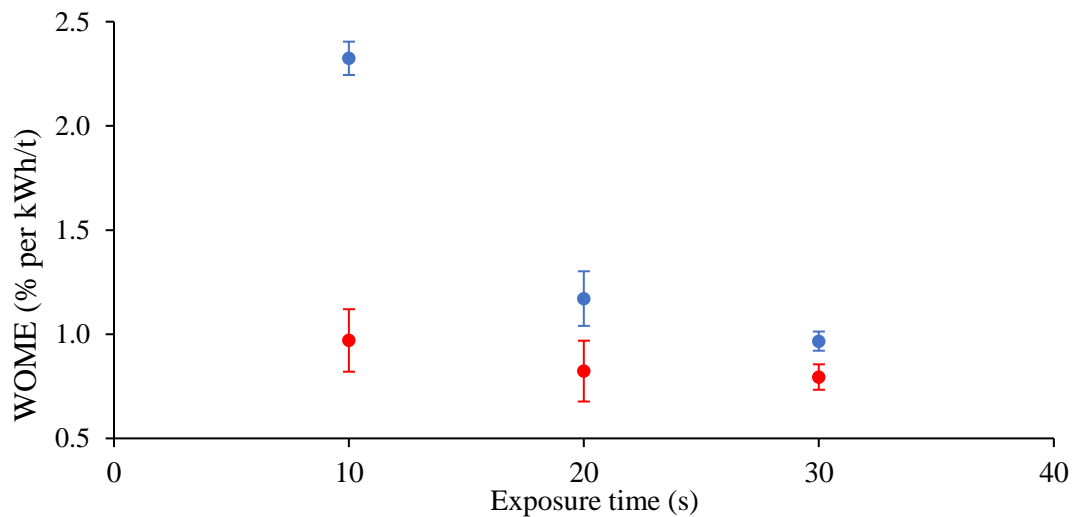
Figure 75. Mean (±SD) Weakening Over Microwave Energy (WOME) of 70-mm diameter basalt discs cut after treatment (red) and cut before treatment (blue) at 3 kW power for 10, 20, or 30 s at a distance of 15 mm from the horn antenna

4.3 Ramp-up time

Half of the microwave energy was absorbed by the water as heat; the remainder was rejected into the cooling loop of the microwave system. Energy absorption linearly increased with microwave time at a rate that increased with power level from 5 to 15 kW (Figure 76). The ramp-up time can be calculated from the linear relationship to microwave power shown in Figure 77. These data are useful for precisely calculating energy input.
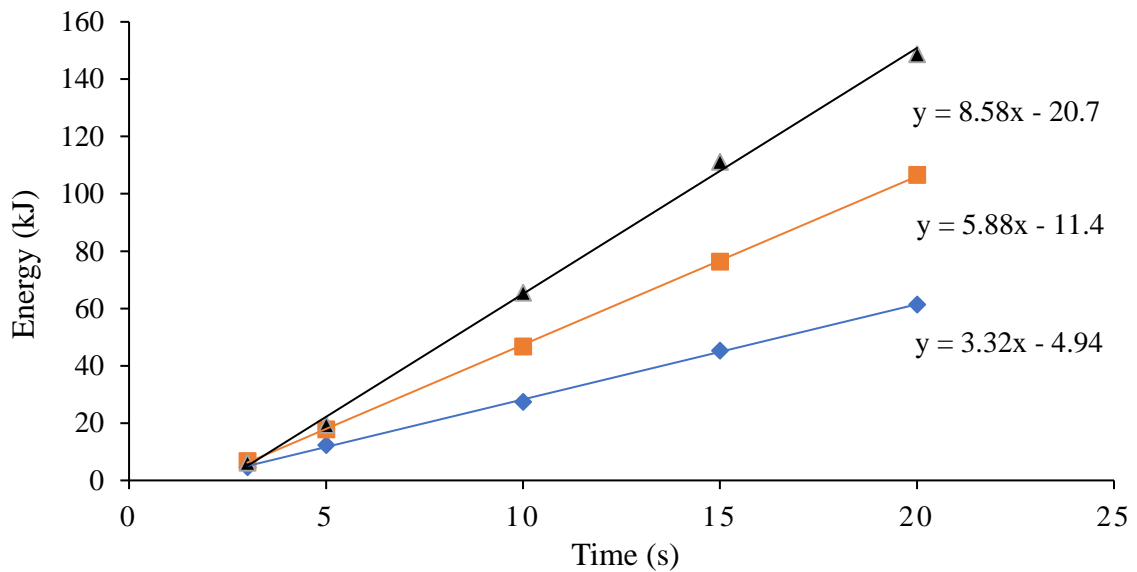
Figure 76. Heat energy absorbed by 1 L of water vs. exposure time to 5 (blue), 10 (orange), or 15 kW (black) microwave power.
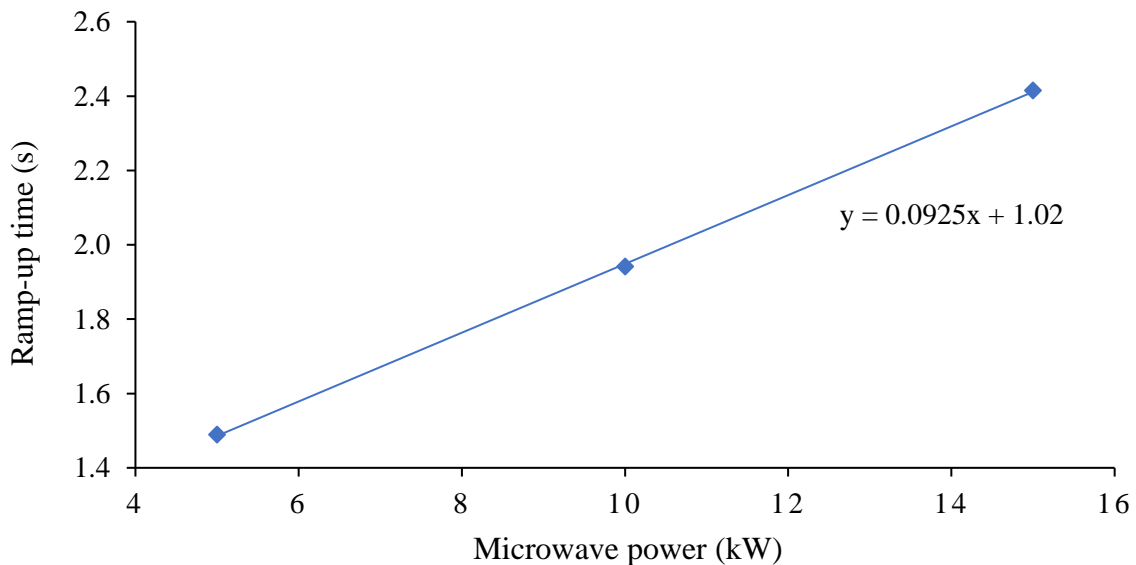
Figure 77. Ramp-up time vs. microwave power level.

4.4 Energy absorption behavior in single-mode cavity

The HOME decreased with the distance from the horn antenna for single, vertical, 50×100 mm basalt cylinders from a peak of 13.85% at 15 mm distance (the focal point of EM waves) to 4.06% at 160 cm (Figure 78).
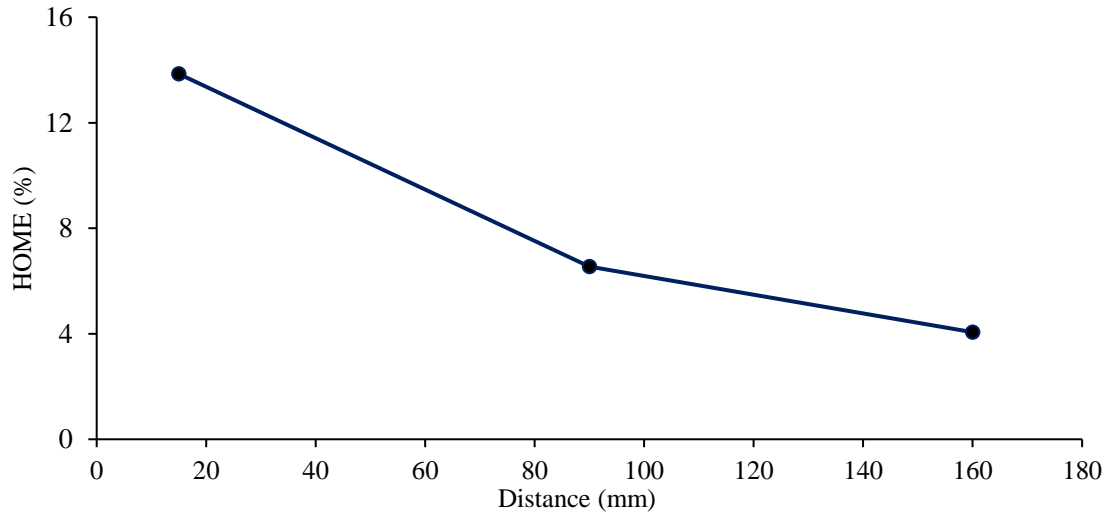
Figure 78. Heat Over Microwave Efficiency (HOME) of single, vertical basalt cylinders vs. distance from the horn antenna.

For single, horizontal, 50×100 mm basalt cylinders, the HOME also decreased with the distance from the horn antenna in the single-mode cavity, (Figure 79). The maximum HOME was lower (8.28%) and closer to the antenna (10 mm) than that observed for the vertical orientation.
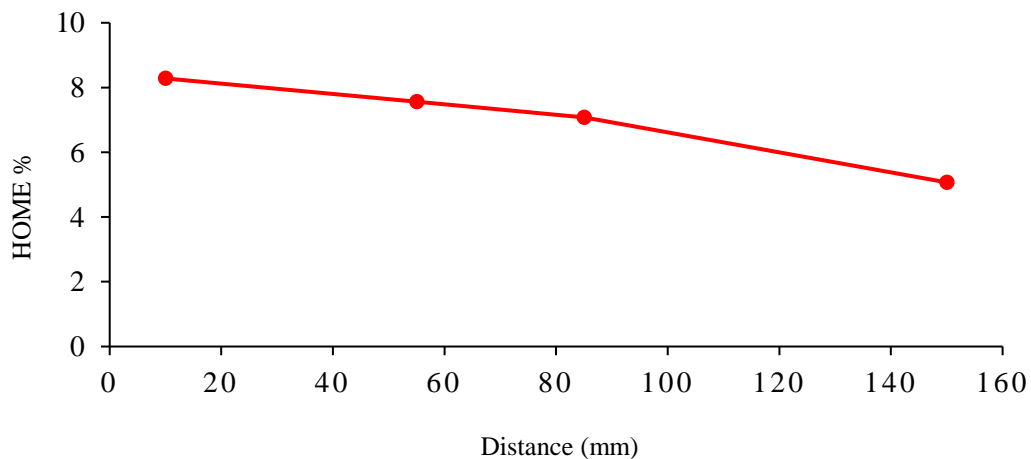
Figure 79. Heat Over Microwave Efficiency (HOME) of single, horizontal basalt cylinders vs. distance from the horn antenna.

The maximum HOME was (38.8%) for two samples and (39.4%) for three vertical cylindrical basalt samples at 15 mm distance from the horn antenna in the single-mode microwave cavity (Figure 80). This illustrates a notable boost in HOME value, demonstrating that increasing the number of the treated samples resulted in increasing the HOME value.
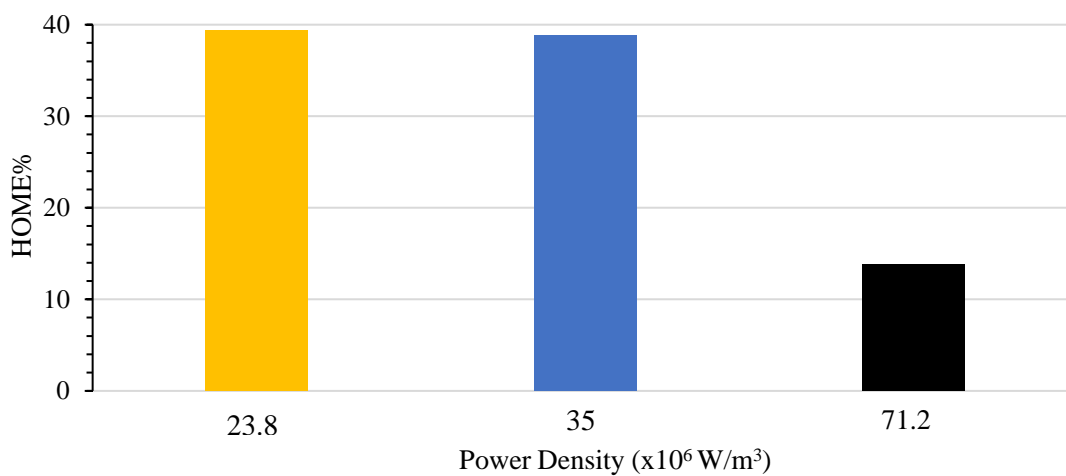
Figure 80. The comparison of HOME for one sample (black), two samples (blue) and three samples (yellow) within a Single-mode cavity

For basalt discs, the mean HOME only differed between 50 and70 mm discs at a distance of 95 mm from the horn antenna (Figure 81). When the sample was placed closer to the horn antenna, the energy absorption was higher than at greater distances. The highest recorded value was at a 15 mm distance from the horn antenna. As a result, the 15 mm distance was chosen as the most suitable distance for the MW treatment. At 55 mm HOME decreased for 50 and70 mm discs and at a distance of 95 mm from the horn antenna, HOME increased for both discs. Due to the complexity of placing the samples at a 95 mm distance from the antenna, it was decided that for the microwave treatment experiments, the sample should be placed at a 15 mm distance.

Changing the sample size not only changes the maximum and minimum values of the energy absorption but also highly affects the locations at which these optimum values are achieved. This HOME change is a result of the electric field distribution within the cavity and the sample.
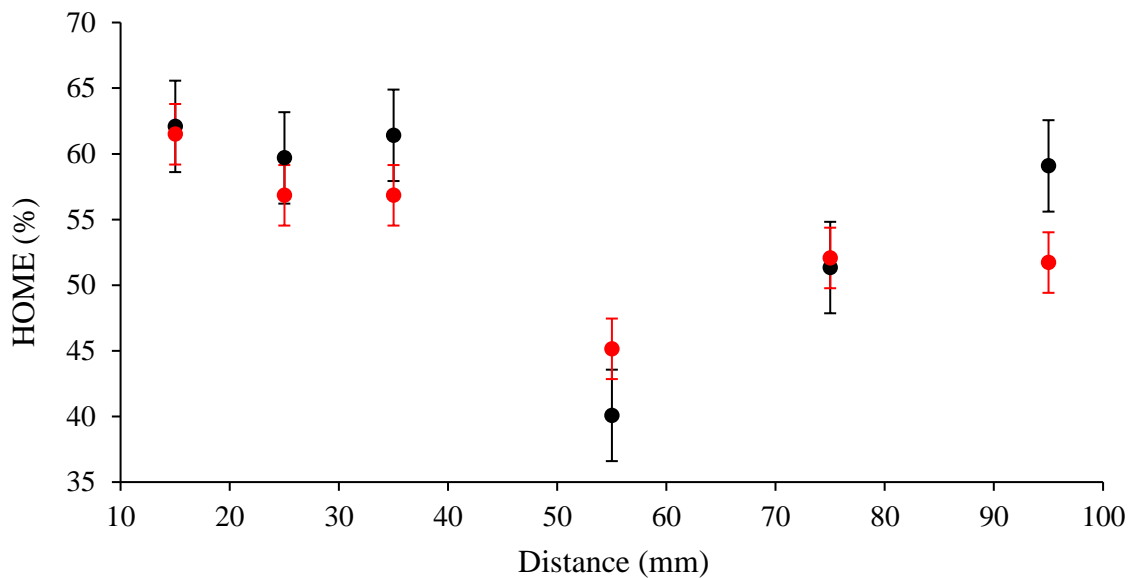
Figure 81. Mean (± SD) Heat Over Microwave Efficiency (HOME) of 50 mm (black) and 70 mm (red) diameter basalt discs vs. distance from the horn antenna.

The temperature distribution on the surface of basalt discs after microwave treatment was affected by disc diameter and distance from the horn antenna. At all distances, the 50 mm disc top surface (Figure 82) was hotter than the 70 mm disc top surface (Figure 83). At 15 mm, the temperature distribution was asymmetrical for the 50 mm disc (Figure 82) and approximately symmetrical for the 70 mm disc. This is due to electric field distribution inside the cavity. The heating pattern in the sample significantly depends on the geometry of the sample and its location in the cavity. Figure 82 and Figure 83 support this claim by showing how significantly the temperature distribution within the samples changes based on their size and distance from the antenna.
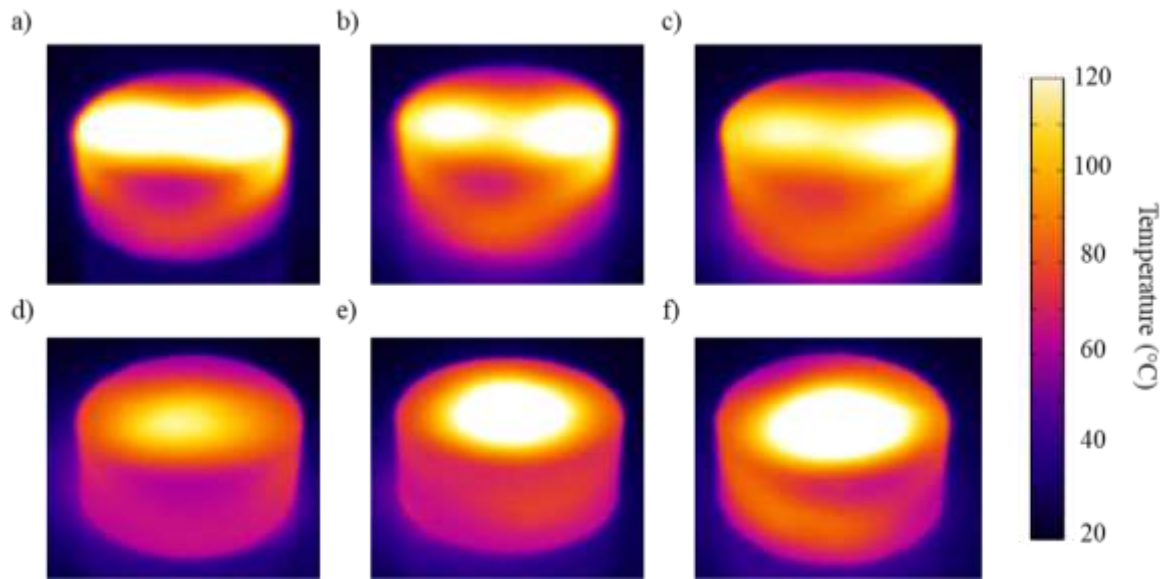
Figure 82. Heat distribution on the surface of 50-mm diameter basalt discs the samples at: a) 15 cm, b) 25 cm, c) 35 cm, d) 55 cm, e) 75 cm, and f) 95 cm from the horn antenna.
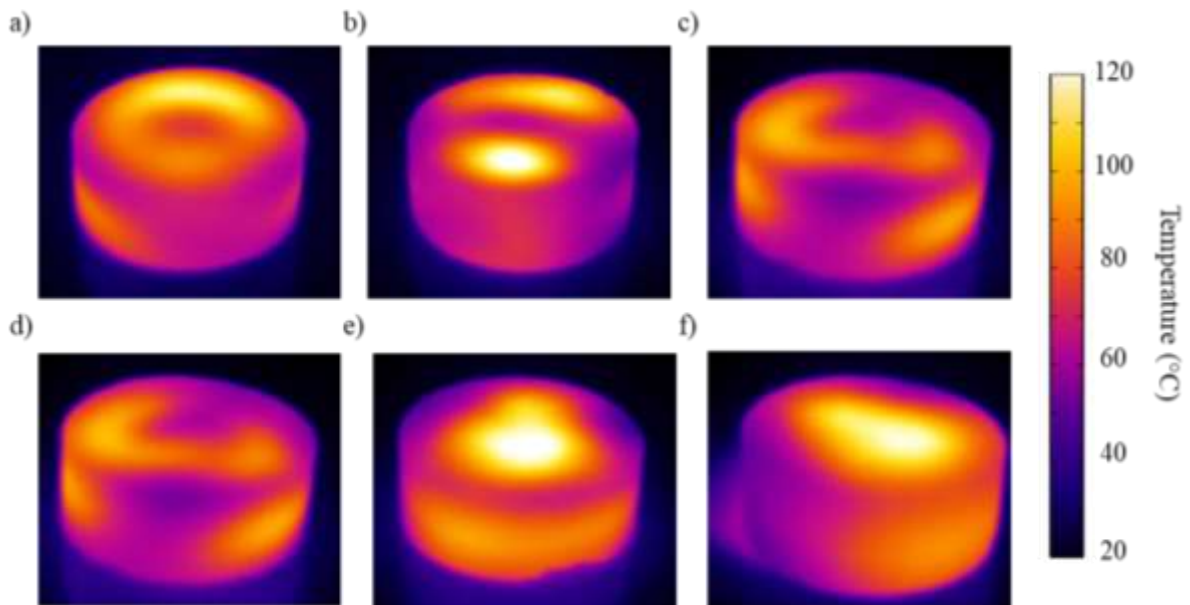
Figure 83. Heat distribution on the surface of 70-mm diameter basalt discs the samples at: a) 15 cm, b) 25 cm, c) 35 cm, d) 55 cm, e) 75 cm, and f) 95 cm from the horn antenna.

In field conditions, microwaves irradiate a rock face over a finite area. Slab-shaped rock samples better represent a rock face because they have a larger surface area relative to thickness than cylindrical or disc-shaped samples. For 20×15×10 cm (L×W×H) basalt slabs, the HOME increased with distance from the horn antenna from 17 to 55 mm (40.27%) and then decreased again at 95 mm (Figure 84). Alejano et al. (2014) found that 40×40×2 cm (L×W×H) basalt slabs subjected to 3 kW power at 2.45 GHz frequency for 120 s had the highest surface

temperatures in closest proximity to the horn antenna, and surface macrocrack density increased with temperature. Again, changing the sample size not only changes the maximum and minimum values of the energy absorption but also highly affects the locations at which these optimum values are achieved.
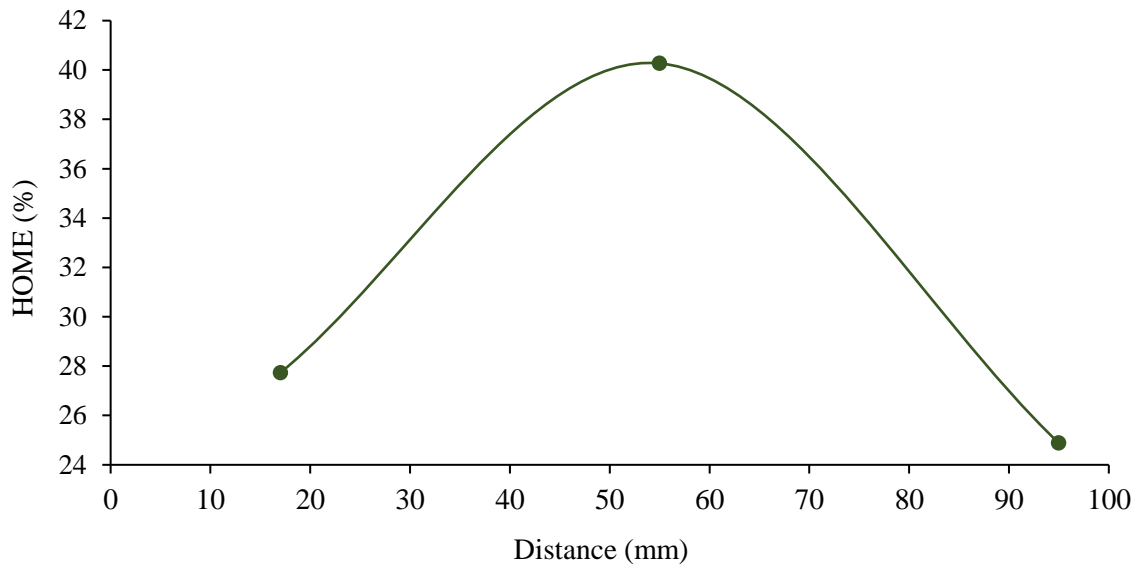
Figure 84. Heat Over Microwave Efficiency (HOME) of basalt slab vs. distance from the horn antenna.

4.5 WOME analysis

Figure 85 compares the wakening effects of microwave irradiation on basalt slabs treated in the single-mode and multi-mode cavity settings. The magnitude of WOME for UCS-sized and cubical basalt samples exposed to microwaves in a multi-mode cavity (Lu et al., 2019a; Lu et al., 2019b) does not exceed 0.53% despite the increase in power density to values as high as 48×10^6 W/m^3. The failure of cubical basalt samples in responding to power density increases signifies the importance of both geometrical considerations and energy in attaining a better microwave-induced weakening effect. The results of UCS tests performed on microwave-treated cylindrical basalt samples were almost similar to cubical basalt samples, where The magnitude of WOME for UCS-sized was 0.43% at a power density of 30.6×10^6 W/m^3. Basalt

slabs treated in a single-mode cavity setting demonstrate a substantially enhanced rate of strength decay and a severe extent of microwave-induced damage. The magnitude of WOME increased with increasing the power density to reach 5.27% at 55.3 x10^6 W/m^3. Values of WOME in a single-mode cavity setting indicate the significance of the HOME value (Figure 84) in achieving better strength reduction. It can be seen that the adjustment of the heating scenario has resulted in up to 10 times higher magnitude of WOME for the samples treated at the same power density level.

Figure 86 indicates a decrease in the induced microwave energy of basalt slabs exposed to microwaves in a single-mode cavity setting compared to the microwave-treated cylindrical and cubical basalt samples in a multi-mode set-up, lowering it to values as low as 15.7 kWh/t. The results showed that the damage in the samples was achieved at the lower energy input of 15.7 kWh/t, resulting in a higher WOME up to 5.98%. It can be concluded that the geometrical considerations of the samples, microwave setups and the single-mode cavity are ways to improve WOME. WOME of 40 – 50 (% per kWhr/t) is the expected value for future work to be achieved, so microwave technology could be feasible for practical applications (Hassani et al., 2020).
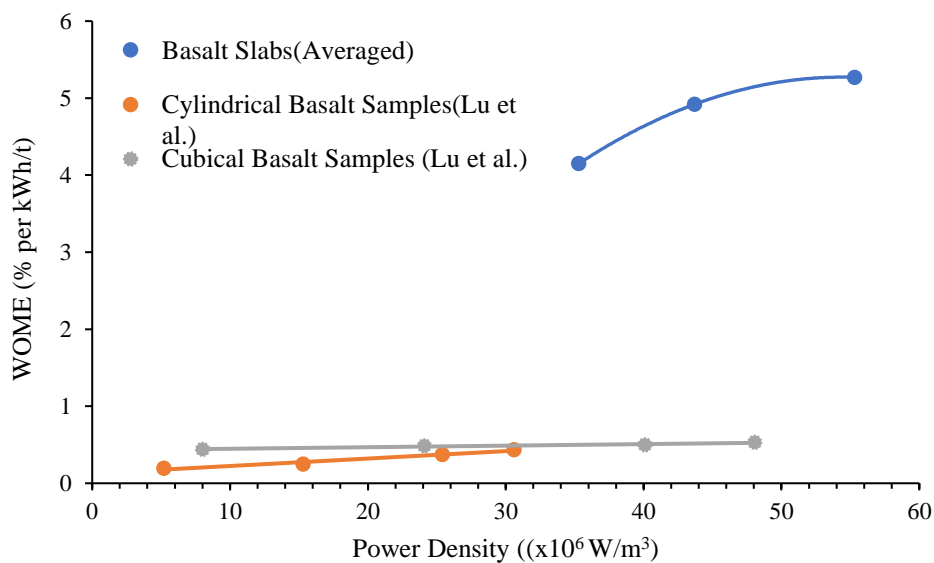
105

Figure 86. The magnitude of WOME for basalt slabs treated in a single-mode cavity setting compared to the results of microwave exposure of UCS-sized and cubical basalt samples in the published literature

4.6 Quenching effect on strength reduction after microwave treatment

The mean BTS of untreated 50 mm diameter $\times$25 mm high basalt discs was 13.01 MPa (Figure 87). After microwave treatment at 15 kW power for 5 s in the single-mode cavity followed by rapid- and air-cooling, the mean BTS was 30% (9.07 MPa) and 45% lower (7.12 MPa), respectively. Thus, cooling basalt samples for a longer time led to a stronger decrease in BTS.
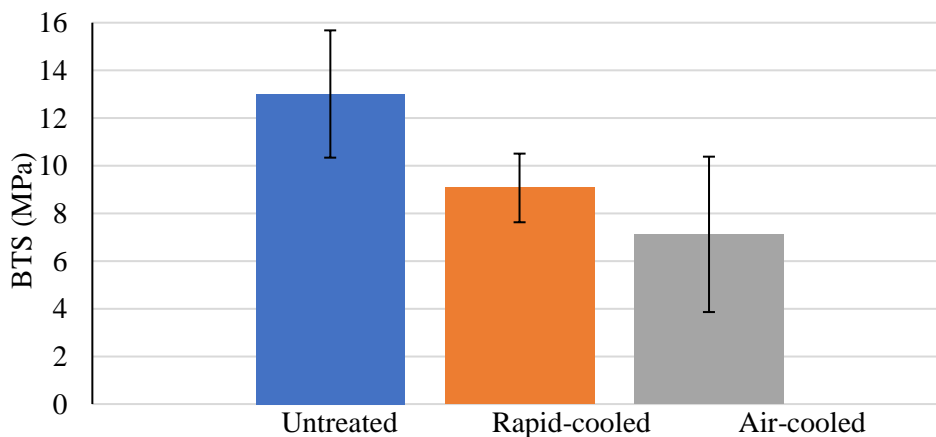
Figure 87. Mean (±SD) Brazilian tensile strength (BTS) of untreated, microwave-treated and rapidly cooled, and microwave-treated and air-cooled basalt discs

Chapter 5 Conclusions

This thesis investigated kimberlite (VK, HK, and TK) and granite and limestone and basalt. Core samples from the Victor mine in northern Ontario and Gahcho Kue mine in the Northwest Territories were evaluated for RQD, specific gravity, porosity, specific heat capacity, and dielectric properties—using the coaxial probe technique—to provide insights into each rock type's ability to absorb microwave irradiation. The core samples were cut into cylindrical and disc shapes and the ends of the samples were flattened for the microwave tests.

The UCS, BTS, CAI, and pulse sound velocity were investigated before and after treatment in a multi-mode microwave cavity at various exposure times and power levels (2–14 kW). The thermal profiles and the time required for each sample to reach a maximum temperature (not more than 500°C) were determined.

A single-mode cavity was used to analyze the efficiency of microwave energy, specifically, the HOME (% of the energy absorbed normalized to microwave energy input) and the WOME (% fracture toughness reduction normalized to microwave energy input). The ramp-up time of the system was determined. The effect of distance from the horn antenna on the HOME was studied by using different numbers (1–3), shapes (cylinders, discs, and slabs), and orientations of basalt samples. Finally, the effect of rapid or slow cooling on rock strength reduction was quantified. The highest energy absorption was achieved at a 15 mm distance from the horn antenna.

Mode I fracture toughness (K_{IC}) was tested on VK and basalt discs using the NSCB method before and after microwave treatment at 3 kW power and exposure times ranging from 4 to 30 s. The K_{IC} decreased with increasing exposure time and when the samples were cut before treatment. Thermal imaging linked temperature contours on the sample surface to the K_{IC}.

Microwave treatment was shown to be a promising technique that combines microwave irradiation and mechanical breakage. It has the potential to facilitate continuous mining and improve the production rate while reducing costs.

5.1 Conclusions

The key findings of this thesis research can be summarized as follows:

- The dielectric constants of HK and TK indicate that they should be the ablest to absorb microwave irradiation, whereas granite would be the least.

- The loss tangents and loss factors of VK, HK, and TK indicate that they should have a stronger ability to dissipate microwave energy than granite or limestone.

- The low loss tangent of limestone meant that, although it did not readily absorb microwave irradiation, it also did not readily dissipate heat energy; thus, it retained heat better than HK, VK, or granite

- UCS and BTS decreased with exposure time in a multi-mode cavity at each power level, and the rate of decline increased with power level from 5 to 15 kW. The linear relationships could be used to predict strength reduction.

- The rate of the decline in UCS differed among rock types.
  - VK: 17% reduction after 115 s at 5 kW power; 47% reduction after 30 s at 10 kW; and 100% reduction (i.e., sample broke) after 25 s at 15 kW.
  - HK: 51% reduction after 45 s at 5 kW; 32% reduction after 20 s at 10 kW; 100% reduction after 40 s at 15 kW.
  - TK: 59% reduction after 45 s at 5 kW; 66% reduction after 45 s at 10 kW.
  - Granite: 35% reduction after 60 s at 5 kW; 100% reduction 50 s at 10 kW, and 100% reduction after 30 s at 15 kW.
  - Limestone: 56% reduction after 45 s at 5 kW; 59% reduction after 45 s at 10 kW.

- The rate of the decline in BTS differed among rock types.

  - VK: 59% reduction after 60 s at 3 kW.

  - HK: 60% reduction after 150 s at 3 kW.

  - TK: 48% reduction after 90 s at 3 kW.

  - Granite: 14% reduction after 60 s at 3 kW.

  - Limestone 28% reduction after 90 s at 3 kW.

- Microwave irradiation in a multi-mode cavity had no detectable effect on the abrasivity of any rock type.

- The pulse sound velocity for VK, HK, and granite decreased after microwave treatment in a multi-mode cavity due to the formation of cracks. TK and limestone were not tested.

- The maximum HOME for single, vertical and horizontal basalt cylinders was observed at 15 and 10 mm from the horn antenna in a single-mode cavity, respectively.

- For basalt discs, the maximum HOME was achieved at 15 mm.

- The maximum HOME for single basalt slabs was observed at 55 mm from the horn antenna.

- The HOME increased with the increasing number of cylindrical samples from one to three.

- The WOME for Basalt slabs treated in a single-mode cavity setting demonstrated a substantial strength reduction as a result of microwave-induced damage. The magnitude of WOME increased with increasing the power density to reach 5.27% at 55.3 $\times 10^6$ W/m^3.

- The results showed that the damage in the Basalt slabs samples was achieved at the lower energy input of 15.7 kWh/t, resulting in a higher WOME up to 5.98%.

- Cooling basalt discs more slowly enhanced BTS reduction.

- The fracture toughness of VK and basalt decreased before microwave treatment.

  o The K_{IC} of kimberlite decreased with increasing the exposure time.

  o 70-mm diameter basalt discs provided the best results with an acceptable range of error.

- For 50-mm diameter basalt discs, the temperature distribution on the surface after irradiation was non-uniform and had a readily demarcated heating line. Cutting the discs on the heating line led to a lower K_{IC} after microwave treatment.

- For 70-mm diameter discs, the temperature distribution on the surface was symmetrical to asymmetrical.

- Increasing the exposure time was not energy efficient: the WOME decreased with increasing exposure time.

- The highest WOME (2.32%/kWh/t) was achieved by cutting the sample before microwave treatment at a 15 mm distance.

6. Future work

This research provides promising insights into the application of microwaves to assist rock breakage technologies. Additionally, microwave irradiation of hard rocks could be an attractive approach to improve rock excavation efficiency. The following are recommendations for future work:

- To use these data for the numerical model development for the eventual design

- Investigate the impact of microwaves on mineral processing (crushing and grinding), especially of kimberlite rocks.

- Conduct single- and multi-mode tests at very high-power levels and short exposure time using different types of materials and rocks.

- Work to increase the energy efficiency of microwave-assisted rock breakage by establishing more efficient microwave setups.

- Conduct a study on the economic analysis of using microwave-assisted rock excavation and comminution in mining and mineral processing operations.

- Conduct CAI on broken samples before and after microwave treatment.

Bibliography

ASTM D7012-04, 2004. Standard Test Method for Compressive Strength and Elastic Moduli of Intact Rock Core Specimens under Varying States of Stress and Temperatures. ASTM International, West Conshohocken, PA, USA.

ASTM D3967-05, 2005. Standard Test Method for Splitting Tensile Strength of Intact Rock Core Specimens. ASTM International, West Conshohocken, PA, USA.

ASTM D7625-10, 2010. Standard Test Method for Laboratory Determination of Abrasiveness of Rock Using the CERCHAR Method. ASTM International, West Conshohocken, PA, USA.

ASTM D6473-15, 2015. Standard Test Method for Specific Gravity and Absorption of Rock for Erosion Control. ASTM International, West Conshohocken, PA, USA.

ASTM C20-00(2015), 2015. Standard Test Methods for Apparent Porosity, Water Absorption, Apparent Specific Gravity, and Bulk Density of Burned Refractory Brick and Shapes by Boiling Water. ASTM International, West Conshohocken, PA, USA.

ASTM D4611-16, 2016. Standard Test Method for the Specific Heat of Rock and Soil. ASTM International, West Conshohocken, PA, USA.

ASTM D6032/D6032m-17, 2017. Standard Test Method for Determining Rock Quality Designation (RQD) of Rock Core. ASTM International, West Conshohocken, PA, USA.

Alejano, R., Perucho, Á., Olalla, C ., Jiménez, R., 2014. Rock Engineering and Rock Mechanics: Structures in and on Rock Masses. Crc Press, Boca Raton,FL.

Ali, A. Y., Bradshaw, S. M., 2009. Quantifying damage around grain boundaries in microwave treated ores. Chemical Engineering and Processing: Process Intensification 48 (11-12), 1566-1573.

Ali, A. Y., Bradshaw, S. M., 2010. Bonded-particle modelling of microwave-induced damage in ore particles. Minerals Engineering 23 (10),780-790.

Ali, A. Y., Bradshaw, S. M., 2011. Confined particle bed breakage of microwave treated and untreated ores. Minerals Engineering 24 (14), 1625-1630.

Aliha, M. R. M., Hosseinpour, G. R., Ayatollahi, M. R., 2013. Application of cracked triangular specimen subjected to three-point bending for investigating fracture behavior of rock materials. Rock mechanics and rock engineering, 46(5), 1023-1034.

Atkinson, C., Smelser, R. E., Sanchez, J. O., 1982. Combined mode fracture via the cracked Brazilian disk test. International Journal of Fracture 18 (4), 279-291.

Ayatollahi, M. R., Aliha, M. R. M., 2007. Fracture toughness study for a brittle rock subjected to mixed mode I/II loading. International Journal of Rock Mechanics and Mining Sciences 44 (4), 617-624.

Babu, M. K., krishnaiah, O.V., 2003. Studies on abrasive waterjet machining of black granite through design of experiments. Experimental Techniques 27(5) 49-54.

Backers, T., 2005. Fracture toughness determination and micromechanics of rock under mode I and mode II loading. Doctoral dissertation, GeoForschungsZentrum Potsdam.

Barani, K., Koleini, S.M. J., Rezai, B., Khodadadi, A., 2012. Effect of sample geometry and placement on iron ore processing by microwave. Advanced Materials Research 488, 841-846.

Barani, K., Koleini, S. M. J., Rezaei, B., 2011. Magnetic properties of an iron ore sample after microwave heating. Separation and Purification Technology 76(3),331-336.

Barker, C., Timmerman, K., 1981. Water jet drilling of long horizontal holes in coal beds. In Proc. First US Water Jet Symposium 7(8), 1-9.

Begley, S., 2010. Electromagnetic properties of materials: Characterization at microwave frequencies and beyond. presented at the Agilent Webinar.

Berryman, A. K., Smith, B. H. S., Jellicoe, B. C., 2004. Geology and diamond distribution of the 140/141 kimberlite, Fort à la Corne, central Saskatchewan, Canada. Lithos 76 (1-4), 99-114.

Bilen, C., 2021. Microwave assisted limestone grinding. Particulate Science and Technology 40(2), 151-164.

Bilgin, N., Dincer, T., Copur, H., 2002. The performance prediction of impact hammers from Schmidt hammer rebound values in Istanbul metro tunnel drivages. Tunnelling and Underground Space Technology 17(3), 237-247.

Bluhm, H., Frey, W., Giese, H., Schultheiss, C.,Strassner, R., 2000. Application of pulsed HV discharges to material fragmentation and recycling. IEEE Transactions on Dielectrics and Electrical Insulation 7(5) 625-636.

Brace, W. F., Bombolakis, E. G., 1963. A note on brittle crack growth in compression. Journal of Geophysical Research 68 (12), 3709-3713.

Bush, A. J., 1976. Experimentally determined stress-intensity factors for single-edge-crack round bars loaded in bending. Experimental Mechanics 16 (7), 249-257.

Callister, JR., W. D., Rethwisch, D. G., 2020. Fundamentals of materials science and engineering: an integrated approach. John Wiley & Sons.

Chandrasekaran, S., Ramanathan, S., basak, T., 2012. Microwave material processing—a review. AIChE Journal 58(2), 330-363.

Chen, C.H., Chen, C.S., Wu, J.H., 2008. Fracture toughness analysis on cracked ring disks of anisotropic rock. Rock Mechanics and Rock Engineering 41(4), 539-562.

Chen, F., Sun, Z., Xu, J., 2001. Mode I fracture analysis of the double edge cracked Brazilian disk using a weight function method. International journal of rock mechanics and mining sciences (1997) 38 (3), 475-479.

Chen, T. T., Dutrizac, J. E., Haque, K. E., Wyslouzil, W., Kashyap, S., 1984. The relative

transparency of minerals to microwave radiation. Canadian Metallurgical Quarterly, 23(3), 349–351.

Chong, K. P., Kuruppu, M. D., 1984. New specimen for fracture toughness determination for rock and other materials. International Journal of Fracture 26 (2), R59-R62.

Clerjon, S., Damez, J.L., 2009. Microwave sensing for an objective evaluation of meat ageing. Journal of Food Engineering 94(3-4), 379-389.

Cook, N. G. W., Harvey, V. R., 1974. An appraisal of rock excavation by mechanical, hydraulic, thermal and electromagnetic means. In Advances in Rock Mechanics: Proc. of the 3rd Inter. Congress on Rock Mechanics pp1-7.

Council, N. R., 1994. Drilling and excavation technologies for the future. National Academies Press.

Crow, S.C., 1974. The effect of porosity on hydraulic rock cutting. International Journal of Rock Mechanics and Mining Sciences & Geomechanics Abstracts 11(3), 103-105.

Crow, S. C., 1973. A theory of hydraulic rock cutting. International Journal of Rock Mechanics and Mining Sciences & Geomechanics Abstracts 10 (6), 567-584.

Didenko, A. N., Zverev, B. V., Prokopenko, A. V., 2005. Microwave fracturing and grinding of solid rocks by example of kimberlite. Physics-Doklady 50 (7), 349-350.

Didenko, A. N., Prokopenko, A.V., 2009. Kimberlite fracture by prompt microwave-heating. In 2009 19th International Crimean Conference Microwave & Telecommunication Technology, IEEE, 855-856.

Edwards, C., 2004. The Cigar Lake project- Mining, ore handling and milling. Canadian Mining and Metallurgical Bulletin 97 (1078), 105-114.

Farmer, I., Attewell, P., 1965. Rock penetration by high velocity water jet: A review of the general problem and an experimental study. International Journal of Rock Mechanics and Mining Sciences & Geomechanics Abstract 2(2), 135-153.

Field, M., Scott Smith B. H., 1999. Contrasting geology and near-surface emplacement of

 kimberlite pipes in southern Africa and Canada. Proceedings of the 7th international

 kimberlite conference 1, 214-237.

Fitzgibbon, K. E., Veasey, T. J., 1990. Thermally assisted liberation - a review. Minerals

 Engineering 3(1-2),181-185.

Ford, J., Pei, D. C. T.,1967. High temperature chemical processing via microwave absorption.

 Journal of Microwave Power 2 (2), 61-64.

Fowell, R. J., Hudson, J. A., Xu, C., Zhao, X., 1995. Suggested method for determining mode

 I fracture toughness using cracked chevron notched Brazilian disc (CCNBD)

 specimens. International Journal of Rock Mechanics and Mining Sciences and

 Geomechanics Abstracts 7 (32), 322A.

Gabriel, C., Gabriel, S.H., Grant, E.H., Grant, E.S. J., Hastead, B., Michael, P., Mingos, D.,

 1998. Dielectric parameters relevant to microwave dielectric heating.Chemmical

 Society Reviews 27 (3), 213 - 223

Gahan, B. C., 2002. Laser drilling: Understanding laser/rock interaction fundamentals. Gas

 Tips 8, 4-8.

Godio, A., Dall'ara, A., 2012. Sonic log for rock mass properties evaluation ahead of the

 tunnel face—a case study in the alpine region. Journal of Applied Geophysics 87,71-

 80.

Goodfellow, P. R., 1992. The influence of microstructural rock properties on water jet-

 assisted cutting.

Bäckblom, G., Forssberg, Eric., Haugen, S., Johansson, J., Naarttijärvi, T., Öhlander, B.,
 2010. Mifu | Smart Mine of The Future Conceptual Study, 1-36

Griffith, A. A., 1921. VI. The phenomena of rupture and flow in solids. Philosophical

 transactions of the royal society of london. Series A, containing papers of a

 mathematical or physical character 221(582-593), 163-198.

Griffiths, D. J., 1999. Introduction to elementary particles. 3rd ed. Upper Saddle River, NJ: Prentice Hall.

Grundas, S., 2011. Advances in induction and microwave heating of mineral and organic materials.

Guo, H., Aziz, N. I., Schmidt, L. C., 1993. Rock fracture-toughness determination by the Brazilian test. Engineering Geology 33 (3), 177-188.

Gupta, M., Leong, E. W. W., 2008. Microwaves and metals. John Wiley & Sons. (Asia) Pte. Ltd.

Gushchin, V. V., Kuznetsov, V V., Chernikov, V. A., Merzon, A. G., Protasov, Y. I., Vartanov, G. A., 1979. Driving horizontal workings by means of an entry drifting machine with electrothermomechanical cutting. Soviet Mining 15 (2), 133-137.

Gushchin, V. V., Rzhevskii, V. V., Kuznetsov, V. V., Protasov, Y.I., Yurchenko, N.N., 1973. Driving of workings by a cutter-loader with electrothermal rock breaking. Soviet Mining 9 (6), 618-622.

Gwarek, W., Celuch-Marcysiak, M., 2004. A review of microwave power applications in industry and research. In: Proceeding of the 15th International Conference on Microwaves Radar and Wireless Communications (MIKON-2004). Institute of Electrical and Electronic Engineers, Warsaw, Poland, pp. 843-848

Haeri, H., Sarfarazi, V., Yazdani, M., Shemirani, A. B., Hedayat, A., 2018. Experimental and numerical investigation of the center-cracked horseshoe disk method for determining the mode I fracture toughness of rock-like material. Rock Mechanics and Rock Engineering 51(1), 173-185.

Hagan, P.C., 1992. The cuttability of rock using a high pressure water jet. Proceeding of the

    Western Australia conference on mining geomechanics. The University of New

    South Wales (UNSW), Sydney, Australia, 8- 10.

Haque, K. E., 1999. Microwave energy for mineral treatment processes—a brief review.

    International Journal of Mineral Processing 57(1), 1-24.

Hartlieb, P,. Grafe, B., 2017. Experimental study on microwave assisted hard rock cutting of

    granite. BHM Berg-und Hüttenmännische Monatshefte162 (2) 77-81.

Hartlieb, P., Grafe, B., Shepel, T., Malovyk, A., Akbari, B., 2017. Experimental study on

    artificially induced crack patterns and their consequences on mechanical excavation

    processes. International Journal of Rock Mechanics and Mining Sciences 100, 160-

    169.

Hartlieb, P., Leindl, M., Kuchar, F,. Antretter, T., Moser, P., 2012. Damage of basalt induced

    by microwave irradiation. Minerals Engineering 31, 82-89.

Hartlieb, P., Toifl, M., Kuchar, F., Meisels, R., Antretter, T., 2016. Thermo-physical

    properties of selected hard rocks and their relation to microwave-assisted

    comminution. Minerals Engineering 91, 34-41.

Hassani, F., 2010a. Review of Explosive-Free Rock Breakage (EFRB) technologies.

    McGill University, Montreal, Canada.

Hassani, F., Nekoovaght, P., 2011. The development of microwave assisted machineries to

    break hard rocks. In: Proceedings of the 28th International Symposium on

    Automation and Robotics in Construction (ISARC). Seoul, South Korea, pp. 678–

    684.

Hassani, F., Nekoovaght, P.M., Radziszewski, P., Waters, K.E., 2011. Microwave assisted

    mechanical rock breaking. In: Proceedings of the 12th ISRM international congress

on rock mechanics. Beijing, China: International Society for Rock Mechanics, 2075-80.

Hassani, F., Nekoovaght, P. M., Gharib, N., 2016. The influence of microwave irradiation on rocks for microwave-assisted underground excavation. Journal of Rock Mechanics and Geotechnical Engineering 8 (1), 1-15.

Hassani, F., Radziszewski, P., Ouellet, J., Nokken, M., Nekoovaght, P., 2008. Microwave Assisted Drilling And Its Influence On Rock Breakage A Review. ISRM International Symposium-5th Asian Rock Mechanics Symposium 1, 87-104.

Hassani, F., Shadi, A., Rafezi, H., Sasmito, A. P., Ghoreishi-Madiseh, S. Ali., 2020. Energy analysis of the effectiveness of MW-assisted fragmentation. Minerals Engineering 159, 106642

Hetman, C. M., Smith, B. S., Paul, J. L., Winter, F., 2004. Geology of the Gahcho Kue kimberlite pipes, NWT, Canada: root to diatreme magmatic transition zones. lithos, 76 (1-4), 51-74.

Hill, J. M., Marchant, T. R., 1996. Modelling microwave heating. Applied Mathematical Modelling 20(1), 3-15.

Von Hippel, A. R., 1954. Dielectrics and waves. John Wiley & Sons, New York.

Hoekstra, P., 1976. Rock, Frozen Soil and Ice Breakage by High-frequency Electromagnetic Radiation: a Review. Department of Defense, Department of the Army, Corps of Engineers, Cold Regions Research and Engineering Laboratory.

Iqbal, M. J., Mohanty, B., 2007. Experimental calibration of ISRM suggested fracture toughness measurement techniques in selected brittle rocks. Rock Mechanics and Rock Engineering 40 (5), 453 - 475.

Irwin, G. R., 1957. Analysis of stresses and strains near the end of a crack transversing a plate. Trans. ASME, Ser. E, J. Appl. Mech. 24, 361-364.

Jansen, D., Hutchins, D., Young, R., 1991. Acoustic imaging of thermally fractured rock. In IEEE 1991 Ultrasonics Symposium, pp. 695-698.

Jerby, E., Dikhtyar, V., Aktushev, O., Grosglick, U., 2002. The Microwave Drill. Science, 298 (5593), 587-589

Jerby, E., Nerovny, Y., Meir, Y., Korin, O., Peleg, R.,Shamir, Y., 2018. A silent microwave drill for deep holes in concrete. IEEE Transactions on Microwave Theory and Techniques, 66 (1), 522-529.

Jha, S. N., Narsaiah, K., Basediya, A. L., Sharma, R., Jaiswal, P., Kumar, R., Bhardwaj, R. 2011. Measurement techniques and application of electrical properties for nondestructive quality evaluation of foods—a review. Journal of food science and technology 48 (4), 387-411.

Jin, L., 2015. The impact of water on heat distribution and mechanical properties of basalt after microwave treatment. Department of Mining and Materials Engineering.McGill University, Montreal, Quebec, Canada.

Jones, D. A., Kingman, S. W., Whittles, D. N., Lowndes, I.S., 2005. Understanding microwave assisted breakage. Minerals Engineering 18 (7), 659-669.

Jones, D. S., 1964. The theory of electromagnetism. Pergamon Press, Oxford, UK.

Kahraman, S., Canpolat, A. N., Fener, M., 2020a. The influence of microwave treatment on the compressive and tensile strength of igneous rocks. International Journal of Rock Mechanics and Mining Sciences 129, 104303.

Kahraman, S., Canpolat, A. N., Fener, M., Kilic, C.O., 2020b. The assessment of the factors affecting the microwave heating of magmatic rocks. Geomechanics and Geophysics for Geo-Energy and Geo-Resources 6 (4), 1-16.

Khan, M. T., Ali, S. M., 2012. A brief review of measuring techniques for characterization of dielectric materials. International Journal of Information Technology and Electrical Engineering 1(1).

Kingman, S. W., 2009. Pre-treatment of multi-phase materials using high field strength electromagnetic waves. U.S. Patent 7,476,829. Washington, DC: U.S. Patent and Trademark Office.

Kingman, S. W., Jackson, K., Bradshaw, S. M., Rowson, N.A., Greenwood, R., 2004a. An investigation into the influence of microwave treatment on mineral ore comminution. Powder Technology 146 (3) 176-184.

Kingman, S. W., Jackson, K., Cumbane, A., Bradshaw, S.M., Rowson, N. A., Greenwood, R., 2004b. Recent developments in microwave-assisted comminution. International Journal of Mineral Processing 74 (1-4), 71-83.

Kingman, S. W., Vorster, W. A., Rowson, N. A., 2000. The Influence of Mineralogy on Microwave Assisted Grinding. Minerals Engineering 13(3),313-327.

Kobusheshe, J., 2010. Microwave enhanced processing of ores. Doctoral Dissertation, University of Nottingham.

Koiwa, T., Shiratori, Y., Takahashi, H., Matsumoto, S., 1975. Rock breaking by microwave radiation-effects of local heating and thermal fracture. Ministry of Transport; Nagase, Yokosuka, Japan: 181-209.

Kumar, P., Sahoo, B.K., De, S., Kar, D.D., Chakraborty, S. Meikap, B.C., 2010. Iron ore grindability improvement by microwave pre-treatment. Journal of industrial and engineering chemistry 16(5), 805-812.

Kuruppu, M. D., 1997. Fracture toughness measurement using chevron notched semi-circular bend specimen. International Journal of Fracture 86 (4), L33-L38.

Kuruppu, M.D., Obara, Y., Ayatollahi, M. R., Chong, K.P., Funatsu, T., 2014. ISRM-suggested method for determining the mode I static fracture toughness using semi-circular bend specimen. Rock Mechanics and Rock Engineering 47(1), 267-274.

Li, X., Wang, S., Xu, Y., Xia, K., Lu., G. 2020. Effect of microwave irradiation on dynamic mode-I fracture parameters of Barre granite. Engineering Fracture Mechanics 1- 224: 106748.

Lindroth, D. P., Berglund, W. R., Morrell, R. J., Blair, J.R.,1993. Microwave assisted drilling in hard rock. Tunnels & Tunnelling International 25 (6), 24-27.

Lindroth, D. P., Morrell, R. J., Blair, J. R., 1991. Microwave assisted hard rock cutting (No. US 5003144). National Energy Technology Laboratory, Pittsburgh, PA, and Morgantown, WV.

Lovás, M., Kováčová, M., Dimitrakis, G., Čuvanová, S., Znamenáčková, I., Jakabský, Š., 2010. Modeling of microwave heating of andesite and minerals. International Journal of Heat and Mass Transfer 53(17-18), 3387-3393.

Lu, G-M., Feng, X-T., Li, Y-H., Hassani, F., Zhang, X., 2019a. Experimental Investigation on the Effects of Microwave Treatment on Basalt Heating, Mechanical Strength, and Fragmentation. Rock Mechanics and Rock Engineering 52(8), 2535-2549.

Lu, G-M., Feng, X-T., Li, Y-H., Zhang, X., 2019b. The microwave-induced fracturing of hard rock. Rock Mechanics and Rock Engineering 52(9), 3017-3032.

Lu, G-M., Li, Y-H., Hassani, F., Zhang, X., 2017. The influence of microwave irradiation on thermal properties of main rock-forming minerals. Applied Thermal Engineering 112, 1523-1532.

Lu, G., Feng, X., Li, Y., Zhang, X., 2020. Influence of microwave treatment on mechanical behaviour of compact basalts under different confining pressures. Journal of Rock Mechanics and Geotechnical Engineering 12 (2), 213-222.

Maurer, W. C., 1968. Novel Drilling Techniques. Pergamon Press, New York ISBN: 0-87814-117-0

Meredith, R. J., 1998. Engineers＇handbook of industrial microwave heating (Issue 25). Institution of Electrical Engineers.

Metaxas, A.C., Meridith, R. J., 1983. Industrial Microwave Heating. Peter Peregrinus; London, UK.

Mooney, W. D., 1992. Multigeneric origin of crustal reflectivity: a review of seismic reflection profiling of the continental lower crust and Moho. Continental lower crust pp. 45-79.

Murová, I., Lovás, M., Jakabský, Š., 2000. The influence of microwave radiation on the failure of rocks. Acta Montanistica Slovaca 5 (3), 283-285.

Murray, C., Courtley, S., Howlett, P., 1994. Developments in rock-breaking techniques. Tunnelling and Underground Space Technology 9 (2), 225-231.

Natanzi, A. S., laefer, D. F., 2014. Using chemicals as demolition agents near historic structures. In 9th International Conference on Structural Analysis of Historical Constructions, Mexico City, Mexico, 14-17 October, 2014.

Nejati, H., Hassani, F., Radziszewski, P., 2012. Experimental investigation of fracture toughness reduction and fracture development in basalt specimens under microwave illumination. [M], Earth and Space 2012: Engineering, Science, Construction, and Operations in Challenging Environments: 325-334.

Nekoovaght Motlagh, P., 2009. An investigation on the influence of microwave energy on basic mechanical properties of hard rocks. Master thesis. Concordia University, Montreal.

Nekoovaght, P., Gharib, N., Hassani, F., 2014. Microwave assisted rock breakage for space

    mining. In: ASCE's Aerospace Division, the 14th Earth and Space Conference.

    St.Luis, USA, pp. 414-423.

Omran, M., Fabritius, T., Elmahdy, A. M., Abdel-Khalek, N.A., El-Aref, M., Elmanawi,

    A.E.H., 2014. Effect of microwave pre-treatment on the magnetic properties of iron

    ore and its implications on magnetic separation. Separation and Purification

    Technology 136,223-232.

Osepchuk, J., M., 1984. A history of microwave heating applications. IEEE Transactions on

    Microwave Theory and Techniques 32(9),1200-1224.

Ouchterlony, F., 1981. Extension of the compliance and stress intensity formulas for the

    single edge crack round bar in bending. Fracture Mechanics for Ceramics, Rocks,

    and Concrete. ASTM Compass STP745 pp. 237–256.

Ouchterlony, F., 1988. Suggested methods for determining the fracture toughness of rock.

    International Journal of Rock Mechanics and Mining Sciences 25 (2), 71-96.

Ouchterlony, F., 1989. On the background to the formulae and accuracy of rock fracture

    toughness measurements using ISRM standard core specimens. International Journal

    of Rock Mechanics and Mining Sciences & Geomechanics Abstracts 26 (1),13-23.

Ouellet, J., Radziszewski, P., Raghavan, V., Satish, H., Hassani, F., 2013. Electromagnetic

    energy assisted drilling system and method . United States Patent 8,550,182.

Peinsitt, T., Kuchar, F., Hartlieb, P., Moser, P., Kargl, H., Restner, U., Sifferlinger, N., 2010.

    Microwave heating of dry and water saturated basalt, granite and sandstone.

    International Journal of Mining and Mineral Engineering 2 (1), 18-29.

Perez, N., 2004. Plastic Fracture Mechanics. Fracture Mechanics, Springer, Boston, MA, pp.

    147-172.

Pickles, J., 2008. Representations in an electronic age: Geography, GIS, and democracy. Praxis (e) Press.

Prokopenko, A., 2011. Microwave Heating for Emolliating and Fracture of Rocks. INTECH Open Access Publisher, London, UK.

Protasov, Y. I., Chernikov, V.A., Kuznetsov, V. V., Merzon, A. G., Retinskii, V. S., 1984. A study of electrothermomechanical destruction of hard rocks with a rotary heading machine. Journal of Mining Science 20(6), 462-467.

Rostami, J., 2011. Mechanical rock breaking. SME mining engineering handbook 415-434.

Santamarina, J. C., 1989. Rock excavation with microwaves: a literature review. Foundation Engineering: Current Principles and Practices. ASCE, Evanston, Illinois, United States 459-473.

Sarkar, C., Heaman, L. M., Pearson, D. G., 2015. Duration and periodicity of kimberlite volcanic activity in the Lac de Gras kimberlite field, Canada and some recommendations for kimberlite geochronology. Lithos 218, 155-166.

Satish, H., 2005. Exploring microwave assisted rock breakage for possible space mining applications. Master of Engineering. McGill University, Montreal.

Satish, H., Ouellet, J., Raghavan, V., Radziszewski, P., 2006. Investigating microwave assisted rock breakage for possible space mining applications. Mining Technology 115 (1), 34-40.

Scott, G., 2006. Microwave pretreatment of a low grade copper ore to enhance milling performance and liberation. Stellenbosch, South Africa: Department of process Engineering, University of Stellenbosch; MS Thesis.

Shiryaev, A. M., Kotkis, A. M., 1983. Methods for determining fracture toughness of brittle porous materials. INDUST. LAB. 48 (9), 917-918.

Shyam, A., Lara-curzio, E., 2006. The double-torsion testing technique for determination of fracture toughness and slow crack growth behavior of materials: a review. Journal of materials science 41 (13), 4093-4104.

Sikong, L., Bunsin, T., 2009. Mechanical property and cutting rate of microwave treated granite rock. Song klanakarin journal of science and Technology 31(4) 447-452.

Singh, S. P., 1998. Non-explosive applications of the PCF concept for underground excavation. Tunnelling and Underground Space Technology 13 (3) 305-311.

Singh, T. N., Singh, V., 2005. An intelligent approach to prediction and control ground vibration in mines. Geotechnical and Geological Engineering 23, 249-262.

Smith, B. H. S., 2008. Canadian kimberlites: geological characteristics relevant to emplacement. Journal of Volcanology and Geothermal Research 174(1-3), 9-19.

Sparks, R. S. J., 2013. Kimberlite volcanism. Annual Review of Earth Planetary Sciences 41, 497-528.

Steneck, N. H., Cook, H. J., Vander, A. J., Kane, G. L., 1980. The origins of US safety standards for microwave radiation. Science 208(4449), 1230-1237.

Sun, J., Wang, W., Yue, Q., 2016. Review on Microwave-Matter Interaction Fundamentals and Efficient Microwave-Associated Heating Strategies. Materials 9 (4), 231.

Suresh, S., 1998. Fatigue of materials. Cambridge university press.

Szendi-Horvath, G., 1980. Fracture toughness determination of brittle materials using small to extremely small specimens. Engineering Fracture Mechanics, 13 (4), 955-961.

Szwedzicki, T., 2003. Rock mass behaviour prior to failure. International Journal of Rock Mechanics and Mining Sciences 40 (4), 573-584.

Takahashi, H., koiwa, T., Miyazaki, S., Kihara, S., Matsumoto, S., 1979. Rock excavation by microwave - Capability of high power microwave rock breaker (100kW, 200kW) for

rock excavation. Port and Airport. Port and Airport Research Institute, Nagase, Yokosuka, Japan.

Takahashi, T., 2004. ISRM suggested methods for land geophysics in rock engineering. International journal of rock mechanics and mining sciences 41(6), 885-914.

Teimoori, K., 2021. Multiphysics Study of Microwave Irradiation For Rock Pre-Conditioning and Breakage.

Thiercelin, M., Roegiers, J.C., 1988. Fracture toughness determination with the modified ring test. In: Proceedings of the international symposium on engineering in complex rock formations, Beijing. pp. 284-290.

Toifl, M., Hartlieb, P., Meisels, R., Antretter, T., Kuchar, F., 2017. Numerical study of the influence of irradiation parameters on the microwave-induced stresses in granite. Minerals Engineering 103-104, 78-92.

Toifl, M., Meisels, R., Hartlieb, P., Kuchar, F., Antretter, T., 2016. 3D numerical study on microwave induced stresses in inhomogeneous hard rocks. Minerals Engineering 90, 29-42.

Tutluoglu, L., Keles, C., 2011. Mode I fracture toughness determination with straight notched disk bending method. International Journal of Rock Mechanics and Mining Sciences 48 (8), 1248-1261.

Tutluoglu, L., Keles, C., 2012. Effects of geometric factors on mode I fracture toughness for modified ring tests. International Journal of Rock Mechanics and Mining Sciences 51, 149-161.

Ulaby, F. T., Bengal, T.H., Dobson, M.C., East, J.R., Garvin, J.B., Evans, D.L., 1990. Microwave dielectric properties of dry rocks. IEEE Transactions on Geoscience and Remote Sensing, 28(3), 325-336.

Venkatesh, M. S., Raghavan, G. S. V., 2005. An overview of dielectric properties measuring techniques. Canadian biosystems engineering 47 (7), 15-30.

Walkiewicz, J. W., Clark, A. E., Mcgill, S. L., 1991. Microwave-assisted grinding. IEEE Transactions on industry applications 27(2), 239-243.

Wang, Q.Z., Xing, L., 1999. Determination of fracture toughness KIC by using the flattened Brazilian disk specimen for rocks. Engineering Fracture Mechanics 64 (2), 193-201.

Wang, Q. Z., Zhang, S., Xie, H. P., 2010. Rock dynamic fracture toughness tested with holed-cracked flattened Brazilian discs diametrically impacted by SHPB and its size effect. Experimental Mechanics 50 (7), 877-885.

Webb, K. J., Smith, B. H. S., Paul, J. L., Hetman, C.M., 2004. Geology of the Victor Kimberlite, Attawapiskat, Northern Ontario, Canada: cross-cutting and nested craters. Lithos 76 (1-4), 29-50.

Wee, F. H., Soh, P. J., Suhaizal, A. H. M., Nornikman, H., Ezanuddin, A.A.M., 2009. Free space measurement technique on dielectric properties of agricultural residues at microwave frequencies. In: International Microwave and Optoelectronics Conference (IMOC 2009), pp. 183-187.

Wei, M. D., Dai, F., Xu, N. W., Xu, Y., Xia, K., 2015. Three-dimensional numerical evaluation of the progressive fracture mechanism of cracked chevron notched semi-circular bend rock specimens. Engineering Fracture Mechanics 134, 286-303.

Wei, M. D., Dai, F., Liu, Y., Xu, N.W., Zhao, T. 2018. An experimental and theoretical comparison of CCNBD and CCNSCB specimens for determining mode I fracture toughness of rocks. Fatigue & Fracture of Engineering Materials & Structures 41(5) 1002-1018.

West, G., 1989. Rock abrasiveness testing for tunnelling. International Journal of Rock Mechanics and Mining Science and Geomechanic Abs, 26(2), 151-160.

Whittles, D. N., Kingman, S. W., Reddish, D. J., 2003. Application of numerical modelling for prediction of the influence of power density on microwave-assisted breakage. International Journal of Mineral Processing 68(1-4), 71-91.

Wijk, G., 1992. A model of tunnel boring machine performance. Geotechnical and Geological Engineering 10 (1), 19-40.

Wilhelm, K., E., E., 1937. Apparatus for the generation of short electromagnetic waves. U.S. Patent 2,094,602.

Willis, R., Ashworth, S., 2002. Technology and knowledge transfer-good practice guidelines. Journal of the Southern African Institute of Mining and Metallurgy 102(5), 269-273.

Womack, J. P., Jones, D. T., 1997. Lean thinking—banish waste and create wealth in your corporation. Journal of the Operational Research Society 48(11), 1148-1148

Xiaohong, L., Jiansheng, W., Yiyu, L., Lin, Y., Huiming, K., 2000. Experimental investigation of hard rock cutting with collimated abrasive water jets. International Journal of Rock Mechanics and Mining Sciences 37 (7), 1143-1148.

Yang, X., Zhu, H., Zhou, X., Nie, A., 2020. Experimental investigation on the evolution of structure and mechanical properties of basalt induced by microwave irradiation. RSC Advances 10 (54),32723-32729.

Yuan, Y., Shao, Z., Qiao. R., Fei, X., Cheng, J., 2020. Thermal response and crack propagation of mineral components in olivine basalt under microwave irradiation. Arabian Journal of Geosciences 13(14), 1-11.

Zeng, J., Hu, Q., Chen, Y., Shu, X., Chen, S., He, L., Tang, H., Lu, X.,2019. Experimental investigation on structural evolution of granite at high temperature induced by microwave irradiation. Mineralogy and Petrology 113(6), 745-754.

Zheng, Y., 2017. Fracturing of hard rocks by microwave treatment and potential applications in mechanised tunnelling (Doctoral dissertation, Monash University).

Zheng, Y.L., Zhang, Q.B., Zhao, J., 2016. Challenges and opportunities of using tunnel boring machines in mining. Tunneling and Underground Space Technology 57, 287-299.

Zheng, Y., Zhao. X., Zhao, Q., Li, J., Zhang, Q. 2020. Dielectric properties of hard rock minerals and implications for microwave-assisted rock fracturing. Geomechanics and Geophysics for Geo-Energy and Geo-Resources 6 (1), 1-17.

Znamenácková, I., Lovás, M., HÁJEK, M., Jakabský, Š., 2003. Melting of andesite in a microwave oven. Journal of Mining and Metallurg, Section B: Metallurgy 39 (3-4), 549-557.

Appendix A: Photographs of As-Received Drill Core Samples

Drill Core ID	Box No.	Photograph
V-17-653	2	
V-17-653	4	
V-17-659	47	
V-17-659	48	
V-17-661	14	
V-17-661	15	
V-17-661	47	
V-17-661	48	
V-17-662	8	
V-17-662	9	
V-17-662	56	
V-17-662	57	

Drill Core ID	Box No.	Photograph
V-14-588	41	
V-14-588	42	
V-14-588	43	
V-14-590	3	
V-14-590	4	
V-14-590	5	
V-14-590	11	
V-14-590	12	
V-14-590	51	
V-14-590	52	
MPV-06-249	2	
MPV-06-249	3	
MPV-06-249	4	

Drill Core ID	Box No.	Photograph
MPV-06-249	12	
MPV-06-249	13	
MPV-06-249	14	
MPV-06-249	15	
MPV-06-249	16	
MPV-06-249	87	
MPV-07-297	10	
MPV-07-297	11	
MPV-07-297	19	
MPV-07-297	20	
MPV-07-297	21	
MPV-07-297	23	
MPV-07-297	24	

Drill Core ID	Box No.	Photograph
MPV-07-297	25	
MPV-07-298	3	
MPV-07-298	4	
MPV-07-298	5	
MPV-07-298	7	
MPV-07-298	8	
MPV-07-298	9	
MPV-07-298	11	
MPV-07-298	12	
MPV-07-298	22	
MPV-07-298	23	
MPV-07-298	30	

Appendix B: Rock Quality Designation (RQD) of Drill Cores

Drill Core ID	Box No.	Rock Type	RQD (%)	RQD (%; mean ± standard deviation)	Quality Description
V-17-653	2	VK	95.51	90.25±6.83	Excellent
V-17-653	4		94.89		
V-17-659	47		93.68		
V-17-659	48		92.02		
V-17-661	14		80.59		
V-17-661	15		95.63		
V-17-661	47		93.23		
V-17-661	48		93.64		
V-17-662	8		78.28		
V-17-662	9		78.66		
V-17-662	56		91.27		
V-17-662	57		95.57		
V-14-588	41	Limestone	88.38	74.82±11.62	Fair
V-14-588	42		59.30		
V-14-588	43		74.48		
V-14-590	3		59.63		
V-14-590	4		75.82		
V-14-590	5		92.07		
V-14-590	11		88.09		
V-14-590	12		66.67		
V-14-590	51		72.78		
V-14-590	52		70.99		
MPV-06-249	2	Granite	94.63	87.07±7.39	Good
MPV-06-249	3		91.72		
MPV-06-249	4		82.96		
MPV-06-249	11		84.29		
MPV-06-249	12		73.57		
MPV-06-249	13		87.70		
MPV-06-249	14		77.78		
MPV-06-249	15		96.3		
MPV-06-249	16		89.29		

Drill Core ID	Box No.	Rock Type	RQD (%)	RQD (%; mean ± standard deviation)	Quality Description
MPV-06-249	87		92.5		
MPV-07-297	10	TK	68.57	71.44±10.63	Fair
MPV-07-297	11		76.37		
MPV-07-297	19		78.26		
MPV-07-297	20		87.47		
MPV-07-297	21		54.37		
MPV-07-297	23		71.18		
MPV-07-297	24		59.46		
MPV-07-297	25		75.85		
MPV-07-298	3	HK	58.25	63.48±11.87	Fair
MPV-07-298	4		80.98		
MPV-07-298	5		64.65		
MPV-07-298	7		63.33		
MPV-07-298	8		50.48		
MPV-07-298	9		44.59		
MPV-07-298	11		52.05		
MPV-07-298	12		62.80		
MPV-07-298	22		67.46		
MPV-07-298	23		81.53		
MPV-07-298	30		72.13		

Appendix C: Specific Gravity of Drill Cores

Drill Core ID	Box No.	Rock Type	Specific Gravity (unitless)	Specific Gravity (mean ± standard deviation)
V-17-653	2	VK	2.32	2.53±0.11
V-17-653	4		2.50	
V-17-659	47		2.64	
V-17-659	48		2.63	
V-17-661	14		2.49	
V-17-661	15		2.49	
V-17-661	47		2.61	
V-17-661	48		2.62	
V-17-662	8		2.40	
V-17-662	9		2.43	
V-17-662	56		2.61	
V-17-662	57		2.61	
V-14-588	41	Limestone	2.43	2.56±0.11
V-14-588	42		2.73	
V-14-588	43		2.58	
V-14-590	3			
V-14-590	4		2.56	
V-14-590	5			
V-14-590	11			
V-14-590	12		2.49	
V-14-590	51			
V-14-590	52			
MPV-06-249	2	Granite	2.67	2.66±0.05
MPV-06-249	3		2.65	
MPV-06-249	4		2.65	
MPV-06-249	11		2.65	
MPV-06-249	12		2.62	
MPV-06-249	13		2.80	
MPV-06-249	14		2.67	
MPV-06-249	15		2.65	

Drill Core ID	Box No.	Rock Type	Specific Gravity (unitless)	Specific Gravity (mean ± standard deviation)
MPV-06-249	16		2.64	
MPV-06-249	87		2.60	
MPV-07-297	10	TK kimberlite	2.37	2.51±0.15
MPV-07-297	11		2.54	
MPV-07-297	19		2.59	
MPV-07-297	20		2.63	
MPV-07-297	21		2.64	
MPV-07-297	23		2.66	
MPV-07-297	24		2.24	
MPV-07-297	25		2.40	
MPV-07-298	3	HK kimberlite	2.55	2.52±0.10
MPV-07-298	4		2.55	
MPV-07-298	5		2.53	
MPV-07-298	7		2.43	
MPV-07-298	8		2.47	
MPV-07-298	9		2.47	
MPV-07-298	11		2.33	
MPV-07-298	12		2.45	
MPV-07-298	22		2.63	
MPV-07-298	23		2.63	
MPV-07-298	30		2.67	

Appendix D: Porosity of Drill Cores

Drill Core ID	Box No.	Rock Type	Porosity (%)	Porosity (%; mean ± standard deviation)
V-17-653	2	VK	13.47	5.61±4.39
V-17-653	4		4.79	
V-17-659	47		2.13	
V-17-659	48		0.74	
V-17-661	14		7.97	
V-17-661	15		6.03	
V-17-661	47		0.80	
V-17-661	48		1.29	
V-17-662	8		12.34	
V-17-662	9		9.41	
V-17-662	56		5.27	
V-17-662	57		3.13	
V-14-588	41	Limestone	12.06	6.11±3.26
V-14-588	42		11.34	
V-14-588	43		5.32	
V-14-590	3		5.78	
V-14-590	4		5.47	
V-14-590	5		6.22	
V-14-590	11		4.31	
V-14-590	12		5.87	
V-14-590	51		2.78	
V-14-590	52		1.95	
MPV-06-249	2	Granite	0.25	0.13±0.08
MPV-06-249	3		0.15	
MPV-06-249	4		0.13	
MPV-06-249	11		0.08	
MPV-06-249	12		0.09	
MPV-06-249	13		0.02	
MPV-06-249	14		0.05	
MPV-06-249	15		0.10	
MPV-06-249	16		0.17	

Drill Core ID	Box No.	Rock Type	Porosity (%)	Porosity (%; mean ± standard deviation)
MPV-06-249	87		0.25	
MPV-07-297	10	TK kimberlite	Cannot be tested	0.68±0.23
MPV-07-297	11		Cannot be tested	
MPV-07-297	19		0.78	
MPV-07-297	20		0.42	
MPV-07-297	21		0.84	
MPV-07-297	23		Cannot be tested	
MPV-07-297	24		Cannot be tested	
MPV-07-297	25		Cannot be tested	
MPV-07-298	3	HK kimberlite	0.51	3.49±3.11
MPV-07-298	4		1.83	
MPV-07-298	5		1.76	
MPV-07-298	7		5.37	
MPV-07-298	8		2.66	
MPV-07-298	9		7.43	
MPV-07-298	11		9.29	
MPV-07-298	12		6.58	
MPV-07-298	22		0.88	
MPV-07-298	23		0.54	
MPV-07-298	30		1.58	

Appendix E: Specific Heat of Drill Cores

Drill Core ID	Box No.	Rock Type	Specific heat capacity (J/g/°C)	Specific heat capacity (J/g/°C; mean± standard deviation)
V-17-653	2	VK	0.94	0.88±0.07
V-17-653	4		0.97	
V-17-659	47		0.75	
V-17-659	48		0.85	
V-17-661	14		0.89	
V-17-661	15		0.89	
V-17-661	47		0.87	
V-17-661	48		0.90	
V-17-662	8		0.96	
V-17-662	9		0.91	
V-17-662	56		0.82	
V-17-662	57		0.76	
V-14-588	41	Limestone	0.90	0.81±0.06
V-14-588	42		0.87	
V-14-588	43		0.77	
V-14-590	3		0.88	
V-14-590	4		0.81	
V-14-590	5		0.85	
V-14-590	11		0.73	
V-14-590	12		0.80	
V-14-590	51		0.79	
V-14-590	52		0.74	
MPV-06-249	2	Granite	0.67	0.64±0.05
MPV-06-249	3		0.67	
MPV-06-249	4		0.68	
MPV-06-249	11		0.71	
MPV-06-249	12		0.65	
MPV-06-249	13		0.65	
MPV-06-249	14		0.58	
MPV-06-249	15		0.62	
MPV-06-249	16		0.66	

Drill Core ID	Box No.	Rock Type	Specific heat capacity (J/g/°C)	Specific heat capacity (J/g/°C; mean± standard deviation)
MPV-06-249	87		0.56	
MPV-07-297	10	TK	Cannot be tested	0.82±0.11
MPV-07-297	11		Cannot be tested	
MPV-07-297	19		0.89	
MPV-07-297	20		0.91	
MPV-07-297	21		0.81	
MPV-07-297	23		0.68	
MPV-07-297	24		Cannot be tested	
MPV-07-297	25		Cannot be tested	
MPV-07-298	3	HK	0.94	0.94±0.05
MPV-07-298	4		0.95	
MPV-07-298	5		1.00	
MPV-07-298	7		0.98	
MPV-07-298	8		0.96	
MPV-07-298	9		1.01	
MPV-07-298	11		0.92	
MPV-07-298	12		0.92	
MPV-07-298	22		0.89	
MPV-07-298	23		0.85	
MPV-07-298	30		0.88	